CHEMICAL ENGINEERING SCIENCE
GENIE CHIMIQUE

VOL. 11 1959 No. 3

Liquid metal irrigation of a packed bed

N. A. WARNER

School of Metallurgy, The University of New South Wales, P.O. Box 1, Kensington, New South Wales, Australia

(*Received* 25 *August* 1958; *in revised form* 11 *May* 1959)

VOL. 11 959/60

Abstract—Liquid hold-up and gas phase pressure drop data are reported for mercury irrigation of a packed bed of ½ in. steel raschig rings with countercurrent flow of hydrogen and nitrogen.

The static hold-up of mercury was found to decrease slightly with increasing liquid rates. This effect, not observed in aqueous or organic liquid irrigations, is attributed to an increased mobility of the liquid in the bed because of the greater energy associated with the flow of dense media such as a liquid metal.

When nitrogen was the gas phase, the static hold-ups, dynamic hold-ups and irrigated liquid specific surfaces are all larger than those observed under comparable conditions with hydrogen as the gas phase. This is considered to be due to the greater interfacial tension of mercury and nitrogen.

An empirical correlation is developed between the liquid hold-up, gas phase pressure drop, gas mass flow rate and gas density. It is suggested that this type of correlation would be of value for estimating the hold-up of molten metal or slag in high temperature systems, where direct measurement would be difficult, but where a room temperature analogue could be readily constructed.

Résumé—Des données concernant le *hold-up* d'un liquide et la chute de pression dans la phase gazeuse sont relevées dans le cas de l'irrigation par du mercure d'un lit de garnissage d'anneaux de Raschig en acier d'½ in., avec un écoulement à contre courant d'hydrogène et d'azote.

Le *hold-up* statique du mercure décroît lentement avec les vitesses croissantes du liquide. Cet effet n'est pas observé dans des irrigations aqueuses ou de liquides organiques ; il est attribué à une mobilité accrue du liquide dans le lit, due à une énergie plus grande associée à l'écoulement du milieu dense tel celui d'un métal liquide.

Quand l'azote est la phase gazeuse les *hold-ups* statiques et dynamiques, les surfaces spécifiques irriguées par le liquide sont toutes plus grandes que celles observées observées avec l'hydrogène comme phase gazeuse, dans des conditions comparables. Ceci serait dû à la plus grande tension interfaciale du mercure et de l'azote.

Une corrélation empirique est développée entre le *hold-up* liquide, la chute de pression dans la phase gazeuse, la vitesse de l'écoulement massique du gaz et la densité du gaz. Il est suggéré que ce type de corrélation sera de valeur pour l'estimation du *hold-up* du métal fondu, ou d'un laitier dans des systèmes à haute température où une mesure directe est difficile, mais où un analogue à la température ambiante peut être rapidement construit.

Zusammenfassung—Der Flüssigkeitsinhalt und der gasseitige Druckabfall für die Berieselung eines Festbettes aus 6,5 mm-Raschigringen aus Stahl mit Quecksilber wird angegeben, wenn Wasserstoff oder Stickstoff entgegenströmen.

Der statische Flüssigkeitsinhalt an Quecksilber fiel etwas ab mit steigendem Flüssigkeitsstrom, wie es bisher bei wässerigen oder organischen Berieselungsflüssigkeiten nicht beobachtet wurde. Die Ursache dieses Effekts ist die grössere Beweglichkeit der Flüssigkeit in dem Bett wegen der höheren Energie, die mit der Strömung einer Flüssigkeit hoher Dichte, wie hier eines flüssigen Metalls, verbunden ist.

Bei Stickstoff als strömendem Gas waren der statische und der dynamische Flüssigkeitsinhalt und die berieselte spezifische flüssige Oberfläche grösser als es unter vergleichbaren Bedingungen bei Wasserstoff beobachtet wurde. Die Ursache wird in der grösseren Grenzflächenspannung zwischen Quecksilber und Stickstoff gesehen.

Es wurde eine empirische Beziehung zwischen dem Flüssigkeitsinhalt, dem gasseitigen Druckabfall, dem Gasstrom und der Gasdichte entwickelt. Eine solche Beziehung kann für die Abschätzung des Flüssigkeitsinhalts bei geschmolzenem Metall oder Schlacke in Hochtemperatursystemen von Bedeutung sein, bei denen direkte Messungen schwierig, ein Analogieversuch bei Raumtemperatur aber leicht durchzuführen ist.

INTRODUCTION

MOLTEN METAL or slag irrigation of fixed beds under non-wetting conditions occurs frequently in pyrometallurgical operations. An analysis of such irrigations, for the purpose of evaluating heat and mass transfer rates, requires information on the volume of liquid in the bed, the liquid surface area and the condition of the liquid hold-up under operative conditions.

To give an insight into the flow of molten slag over coke, countercurrent to a gas, GARDNER [1] measured pressure drops and hold-ups for water irrigating a packed coke bed under non-wetting conditions and indicated that the data were to enable interpretation of future heat and mass transfer studies on the molten slag system.

A similar motive prompted this investigation, as information was required to analyse mass transfer data obtained when molten lead was the irrigating liquid phase and nitrogen containing zinc vapour at an elevated temperature was the countercurrent gas phase.

To simulate the flow of molten lead over the packing of an absorption column, mercury was used as the liquid phase with hydrogen and nitrogen as the countercurrent flowing gas phase.

Although these studies were primarily aimed at evaluating the dynamics of molten lead flow over a packed bed, by studing the mercury irrigation of the same packing material, it is considered that the discussions have general application to other liquid metal or heavy media irrigations.

THEORETICAL ASPECTS

(i) *Fluid flow through fixed beds*

Single phase fluid flow through packed columns has been reviewed by ERGUN [2].

The equation developed by ERGUN [2] on the basis of numerous previous reported data for fluid flow in granular beds was

$$\frac{\Delta P}{L} g_c = 150 \frac{(1-\epsilon)^2}{\epsilon^3} \frac{\mu U}{D_p{}^2} + 1{\cdot}75 \frac{1-\epsilon}{\epsilon^3} \frac{U^2 \rho}{D_p} \quad (1)$$

i.e. the pressure losses are caused by simultaneous kinetic and viscous energy losses. The first term on the R.H.S. of equation (1), representing the viscous energy loss, is the most important factor at low flow rates and of little significance at high flow rates, whereas the second term in the right-hand side of equation (1), representing the kinetic energy losses, is the most significant at high flow rates and of little importance at very low flow rates. As the gas flows involved in this investigation were fairly high, the viscous energy losses could be assumed negligible compared to kinetic energy losses, and the form of equation (1) simplified:

$$\frac{\Delta P}{L} g_c = a' \rho U^2 \quad (2)$$

ERGUN [2] assigned a value of $1{\cdot}75 \left[(1-\epsilon)/\epsilon^3\right]\left[1/D_p\right]$ for the term a', for the single fluid phase flow through a packed bed. Under the conditions of these studies, the bed porosity ϵ altered according to the hold-up of liquid in the packing as also did the size parameter D_p. The

term a' in this investigation was therefore considered to be some function of the total hold-up of the liquid in the packing, and the true velocity (V) was used rather than the superficial velocity (U) in the modified equation (3).

$$\frac{\Delta P}{x\,(h_T)} = x'\,(\rho V^2) \tag{3}$$

The method originally proposed by BLAKE [3] and used subsequently by CARMAN [4] for correlating pressure drop data in packed beds, by an approach analogous to the established procedure of plotting the friction factor as a function of Reynolds number for fluid friction in pipe systems, was modified by MOTT [5] to allow a more direct comparison to be made between porous media and pipe flow. The forms proposed by MOTT are presented in equations (4), (5), (6), (7).

$$\mathrm{R}_e = \frac{4U\rho}{\mu S} \tag{4}$$

or

$$\mathrm{R}_e = \frac{4V\rho\epsilon}{\mu S} \tag{5}$$

$$f = \frac{\Delta P\, 2g\, \epsilon^3}{LS\,\rho\, U^2} \tag{6}$$

or

$$f = \frac{\Delta P\, 2g\, \epsilon}{LS\,\rho\, V^2} \tag{7}$$

As suggested by GARDNER [1] the types of correlation, employing the surface area per unit packed volume, are suitable for examination of flow when the packing is irrigated, as they allow the total surface area exposed to the gas flow to be estimated from a measurement of the gas phase pressure drop. The unknown S can be found by cover plotting the data on a previously determined correlation in which the dry surface area is known. Such an evaluation of the irrigated total specific surface would be useful for establishing the correct gas phase Reynolds number, but in itself it does not indicate the contribution to the specific surface, which is due to the liquid phase, as the specific surface obtained by such a procedure represents both solid and liquid surface presented to the gas flow.

(ii) *Liquid hold-up in packed beds*

The void space in the packing, which is occupied by liquid under operating conditions, must be taken into consideration when the bed porosity is determined. The total volume of liquid in the packed bed under operating conditions is known as the total hold-up. The total hold-up (h_T) is considered to be the sum of the static hold-up (h_S) and the dynamic hold-up (h_D). The static hold-up is defined as the liquid in the packing which does not drain from the packing when the liquid supply to the column is discontinued. The dynamic hold-up represents the liquid which will drain from the packing when the liquid supply is cut off. The relation between the three hold-ups is given by equation (8).

$$h_T = h_S + h_D \tag{8}$$

Several investigators have measured or estimated liquid hold-ups. Two extensive studies were reported by ELGIN and WEISS [6] and JESSER and ELGIN [7] but there was no complete analysis of the three different types of hold-up for packed columns, until the recent work of SHULMAN *et al.* [8] and GARDNER [1].

These investigators postulated that the total hold-up may be divided into two parts. One part of the hold-up was considered to be due to accumulated semi-stagnant liquid, residing at places which have a natural retentive effect upon the liquid, such as points of contact between the packing elements. This liquid was considered to be semi-stagnant but not entirely at rest, the flow being so slow that its volume was governed by other effects such as the surface tension of the liquid. SHULMAN *et al.* [8] considered this component of the hold-up to be equal to the static hold-up. GARDNER [1] recognized the existence of further terms contributing to the semi-stagnant component. A small quantity was added to the static hold-up to allow for liquid passing in and out of the sites of static hold-up and a further allowance was made for the pressure drop across the bed creating new sites of semi-stagnant liquid.

The flowing part of the hold-up was considered to be the dynamic hold-up. GARDNER [1] developed an empirical expression allowing the

flowing part of the hold-up to be analysed in a logical form.

GARDNER [1] and SULMAN *et al.* [8] both reported the static hold-up as being independent of the gas and liquid rate. The static hold-up was found to be a function of the physical properties of the packing surface.

In the past, it had been assumed that the dynamic hold-up was independent of gas rate up to the flooding point and so dynamic hold-ups in some of earlier studies were determined at zero gas rate. However, both SHULMAN *et al.* [8] and GARDNER [1] showed that this was not the case, as the dynamic hold-up was found to increase with increase in gas rate, even before the loading point was reached. In the non-wetting case, it was suggested that the effect of gas rate on the dynamic hold-up was that the liquid was retarded by frictional effects or that it was dispersed into a larger number of thinner trickles.

Besides allowing the bed porosity to be evaluated, hold-up studies are also important in the interpretation of mass transfer data, because of the different significance, which can be attached to the components of the total liquid hold-up, in so far as their being effective, in the mass transfer process. This very important aspect was discussed in detail by SHULMAN *et al.* [9], when the effective interfacial area, as distinct from the total interfacial area, was analysed.

EXPERIMENTAL

Apparatus and procedure

A small glass column was packed to a height of 1·75 ft with $\frac{1}{4}$ in. steel raschig rings. The volume of rings in the column was obtained by weighing the rings prior to their addition to the column. The volume of the packed height of the empty glass column was determined by addition of a tared quantity of water. The relevant dimensions of the column are given in Table 1 and a line diagram of the experimental apparatus is shown in Fig. 1.

The mercury feed to the column was from a head tank through a pipe provided with both a plug cock and a needle valve. The needle valve was used for flow control and the plug cock served as the quick acting valve required for measuring the mercury hold-up. The mercury flow rate was

Table 1. *Dimensions of packed column*

Column diameter	= 1·75 in.
Free cross-sectional area	= 0·01665 ft^2
Packed height	= 1·75 ft
Volume of rings	= 231 ml
Volume of empty bed	= 826 ml
Dry bed porosity	= 0·72
Irrigated bed porosity	= (595-h_T)/826
Packing material	= $\frac{1}{4}$ in. × $\frac{1}{4}$ in. × 20 gauge steel raschig rings

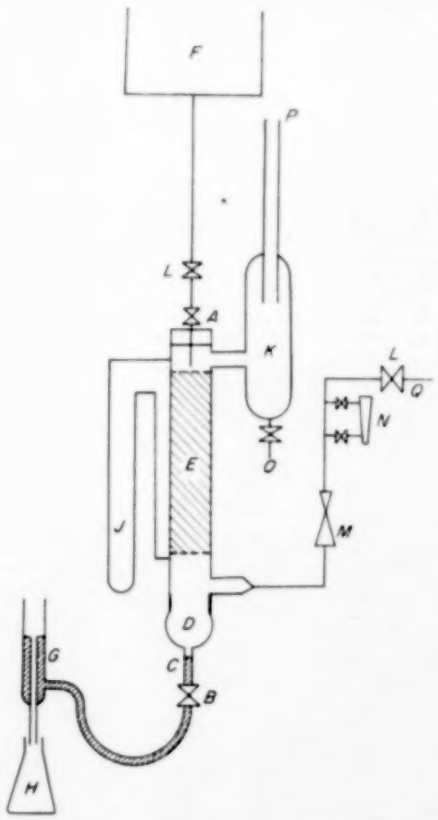

FIG. 1. Diagram of apparatus.
A–Stockcock on inlet liquid. B–Stopcock on outlet liquid. C–Liquid run-off tube. D–Storage bowl. E–Raschig ring packing. F–Mercury head tank. G–Variable lute. H–Receiving vessel. J–Manometer. K–Mercury entrainment trap. L–Needle control valve. M–Venturi meter. N–Rotameter. O–Drainage cock. P–Exhaust to atmosphere. Q–Compressed gas connexion.

Table 2. Pressure drop and hold-up for mercury irrigation

Mercury rate (lb/min)	*Static hold-up* h_S (ml)	*Dynamic hold-up* h_D (ml)	*Gas hold-up* h_G (ml)	*Total hold-up* h_T (ml)	*Bed porosity* ϵ	*Gauge pressure at base of column* (cm Hg)	*True gas velocity* V_g (ft/sec)	*Pressure drop across bed* ΔP (cm H_2O)
			Nitrogen gas phase					
1·50	112·9	9·5	31·5	153·9	0·538	15·0	15·2	160·5
18·09	101·2	120	5	226·2	0·456	14·5	12·3	171·4
5·16	108·6	24	8	140·6	0·553	7·1	10·8	74·8
10·00	100·2	60	5	165·2	0·525	9·1	11·1	102·0
18·84	92·9	82	1	175·9	0·513	4·8	7·9	59·8
5·34	103·2	31	0·5	134·7	0·559	4·3	8·1	46·2
2·41	105·5	24	0·5	130·0	0·565	4·1	7·9	40·8
10·56	97·2	77·5	10	184·7	0·502	14·5	14·3	168·6
14·41	96·2	50·5	0	146·7	0·546	0	2·2	6·8
6·44	103·2	45	16·5	164·7	0·525	12·7	14·0	146·2
3·06	103·2	22·5	13·5	139·2	0·556	10·4	13·0	110·2
6·89	93·9	36	5	134·9	0·559	8·9	12·0	97·9
12·56	100·2	92	10	202·2	0·483	15·5	14·1	187·7
2·59	98·2	16	12	126·2	0·570	8·9	12·2	92·5
3·22	101·2	22	39	162·2	0·528	19·1	15·7	201·3
15·75	96·2	58	0	154·2	0·538	0	2·22	6·8
3·28	105·5	16	0	121·5	0·575	0	2·08	4·1
5·16	102·2	21	0	123·2	0·574	0	2·08	4·1
16·88	85·5	61	0	146·5	0·546	0	0·92	1·1
8·34	91·9	30	0	121·9	0·575	0	0·87	0·9
3·62	96·2	14	0	110·2	0·588	0	0·85	0·7
14·31	90·8	52·5	0	143·3	0·552	0	3·93	16·1
4·72	98·2	22	0	120·2	0·578	0	3·76	12·2
2·03	100·2	10	0	110·2	0·588	0	3·68	10·7
			Hydrogen gas phase					
15·56	85·3	83	9	177·3	0·510	12·4	47·5	149·5
8·06	87·5	35	9	131·5	0·542	7·9	42·8	88·3
17·06	85·5	62	4	151·3	0·586	4·3	31·0	50·3
3·84	91·9	18	3	112·9	0·586	2·8	28·2	35·3
8·00	91·9	29	5	125·9	0·570	3·3	29·0	38·0
14·84	88·8	51	0	139·8	0·554	1·8	19·6	23·1
7·94	92·9	26	1	119·9	0·578	1·8	18·7	17·7
6·03	96·2	20	1	117·2	0·581	1·8	19·0	20·4
18·34	87·5	55·5	0	134·0	0·552	1·0	14·2	14·2
10·84	89·8	36	0	125·8	0·570	0·8	13·6	11·7
5·25	90·8	19·5	0	110·3	0·588	0·8	13·2	9·7
20·47	80·5	66	0	146·5	0·546	0	3·14	1·5
3·41	88·8	13	0	101·8	0·598	0	2·86	0·8
8·97	87·5	29	0	116·5	0·582	0	2·94	1·1
18·78	87·5	69	0	156·5	0·534	0	5·46	3·6
8·09	91·9	27	0	118·9	0·578	0	5·05	2·5
6·69	92·9	23	0	115·9	0·582	0	5·15	2·4
13·59	89·8	46	0	135·8	0·558	0	7·70	5·5
6·28	90·8	23	0	113·8	0·585	0	7·33	4·9
2·78	98·2	13	0	111·2	0·587	0	7·30	4·5

VOL. 11 959/60

obtained by weighing the discharge from the column.

Nitrogen or hydrogen were metered to the column by a venturi meter for the higher flow rates and a rotameter for the lower flows. The gas was admitted at the bottom of the column with manometer tappings located above and below the packed bed. The pressure drop across the bed was measured using a simple manometer.

The base of the glass column was provided with a bowl of sufficient storage capacity to collect the mercury hold-up when the supply to the column was cut off.

The experimental technique was as follows:

(a) When steady state conditions at the desired gas and mercury flow rates were reached, the variable lute was adjusted so that the level of the liquid in the run-off tube was at the calibration mark and the pressure drop across the bed was recorded.

(b) Stockcocks A and B were then closed simultaneously, but the gas supply to the column was left unaltered.

(c) The liquid which drained from the packing, the dynamic hold-up, was determined by opening stopcock B and draining off the mercury into the receiver H, until the liquid level in the run-off tube was again at the calibration mark.

(d) The stopcock B was closed once this level had been reached and the gas supply to the column was then turned off. At very high gas flow rates, a further quantity of mercury drained from the column, which was measured in the same way as the dynamic hold-up. This contribution to the total hold-up was termed the "gas hold-up."

(e) The static hold-up was determined by weighing the column at the conclusion of each run and subtracting the weight of the column before irrigation.

Experimental results

Using the foregoing procedures, the pressure drops and hold-ups for mercury irrigation of the packing with hydrogen and nitrogen flow were determined and the results presented in Table 2. The mercury hold-ups in the absence of gas flow but with hydrogen and nitrogen atmospheres are given in Table 3.

Pressure drops were also measured across a previously mercury irrigated bed and across the dry packing before irrigation and are shown in Tables 4 and 5 respectively.

As all data were obtained under approximately the same ambient conditions, a constant temperature of 20°C was used throughout in evaluating the physical properties of the gas phases. The true gas velocity takes into account the actual void space in the bed under the operating conditions and the density evaluated at the mean pressure in the bed.

DISCUSSION

(i) *Static hold-up*

Previous investigators, who have reported static hold up data in aqueous and organic liquid systems, have observed the static hold-up as being constant for the particular liquid and packing. However, the results of this investigation show that the liquid metal irrigation rate has a slight but definite effect on the static hold-up, in that the static hold-up decreases with increased liquid rate. This effect can be seen in Fig. 2. Although the liquid rate effects the static hold-up, no consistent effect could be attributed to the gas flow rate although the results at zero gas flow rate do appear slightly higher than the other data.

The other interesting feature of Fig. 2 is that the static hold-up for nitrogen is displaced above the hydrogen data. This effect is thought to be due to a difference in interfacial tension between the mercury and the two gases. PERRY [9] gives the interfacial tension of mercury and nitrogen as higher than the interfacial tension of mercury and hydrogen, being 496 dynes/cm and 470 dynes/cm at 15°C and 19°C respectively. The increase of static hold-up with an increase in surface tension is consistent with the finding of SHULMAN *et al.* [10], who studied a surface tension range of 23 to 86 dynes/cm by the addition of wetting agents to water.

A probable explanation of the observed effect

VOL 11 1959/

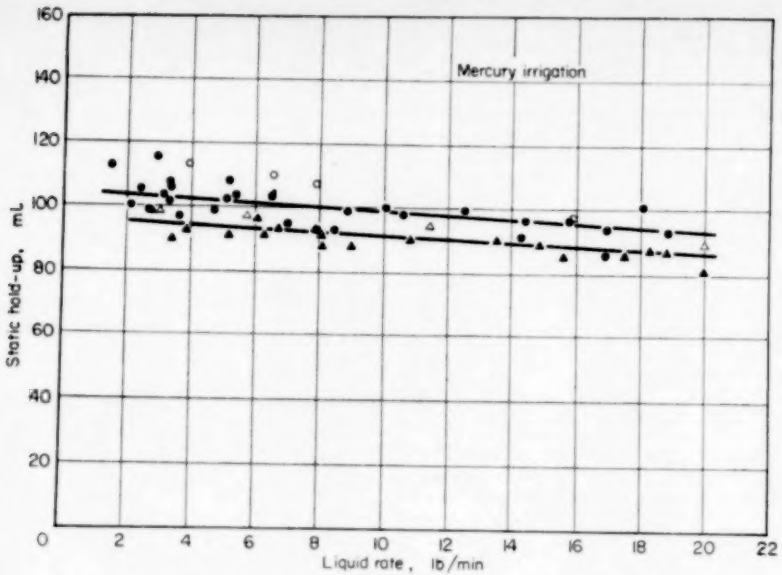

FIG. 2. Mercury irrigation static hold-up.

○ Nitrogen atmosphere, no flow.
● Nitrogen flow.
△ Hydrogen atmosphere, no flow.
▲ Hydrogen flow.

which the liquid rate had on the static hold-up in this investigation is that liquid metals or other density liquids possess much greater kinetic energies than water when irrigating a packing, and therefore the possibility of dispersing or "knocking-on" semi-stagnant pockets of liquid is much greater and this effect increases with increase liquid rate. The significance of this would be that the semi-stagnant pockets of liquid, observed in packings irrigated with water, would be very much more mobile in the case of a dense liquid irrigating the packing. Under these conditions, the whole concept of effective interfacial area in mass transfer would have to be reviewed, as the increased mobility of the dense liquids could well result in the static hold-up being almost as effective as the recognized flowing component, the dynamic hold-up.

(ii) *Dynamic hold-up*

The dynamic hold-up for mercury irrigating the packing is not purely a function of liquid rate, and therefore supports the recent results of GARDNER [1] and SHULMAN *et al.* [8], who showed that the earlier practice of assuming

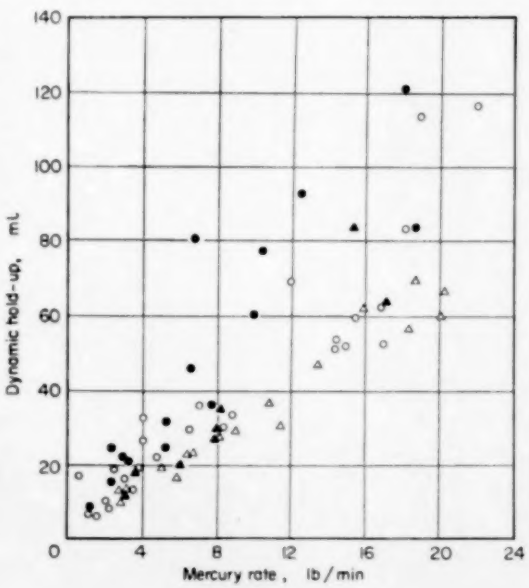

FIG. 3. Mercury irrigation dynamic hold-up.

○ Nitrogen absence of gas hold-up
● Nitrogen presence of gas hold-up.
△ Hydrogen absence of gas hold-up.
▲ Hydrogen presence of gas hold-up.

the dynamic hold-up to be solely related to the liquid rate was incorrect.

Table 3. Mercury hold-up in absence of gas flow

Mercury rate (lb/min)	*Static hold-up* h_S (ml)	*Dynamic hold-up* h_D (ml)	*Total hold-up* h_T (ml)
	Hydrogen atmosphere		
20·09	89·8	59	148·8
11·41	92·9	30	122·9
5·69	96·2	16	112·2
3·69	98·2	10·5	108·7
	Nitrogen atmosphere		
15·88	98·2	61	159·2
7·84	106·5	36	142·5
6·47	109·6	28·5	138·1
3·91	112·9	19	131·9

Table 4. Pressure drop across previously mercury-irrigated column

Previous irrigation $h_T = 98$ ml *and* $\epsilon = 0{\cdot}60$

Gauge pressure at base of column (cm Hg)	*True gas velocity* V_g (ft/sec)	*Pressure drop across bed* ΔP (cm H_2O)
	Hydrogen gas phase	
0	4·83	2·0
0·3	7·11	4·2
0·5	9·50	7·2
0·8	13·8	11·0
1·3	17·3	16·1
1·5	21·4	24·8
2·5	28·1	33·3
3·3	32·1	45·6
4·3	37·8	56·6
4·3	42·4	67·5
	Nitrogen gas phase	
0	0·83	0·7
0	1·39	1·7
0	1·99	3·5
0·3	2·70	6·0
0·5	3·58	9·4
0·8	5·40	14·1
1·0	6·88	24·3
2·5	8·73	34·0
5·1	12·20	66·6

Fig. 3 is a plot of dynamic hold-up versus the mercury irrigation rate. The dynamic hold-up is clearly dependent on other factors besides the liquid rate. Increased gas rates, in general, increased the dynamic hold-up. The reasons for this were outlined by GARDNER [1]. The high gas rates correspond to the points in Fig. 3 in which there was a "gas hold-up." The dynamic hold-up plotted is the liquid which drained from the packing before the gas flow was reduced and therefore excludes any "gas hold-up" contribution.

Table 5. Pressure drop across column before irrigation $\epsilon = 0{\cdot}72$

Gauge pressure at base of column (cm Hg)	*True gas velocity* V_g (ft/sec)	*Pressure drop across bed* ΔP (cm H_2O)
	Nitrogen gas phase	
2·3	7·4	20·4
5·3	10·5	42·1
8·9	12·6	70·7
1·3	5·7	13·3
0·8	5·0	10·3
0·8	4·5	8·4
0·3	3·0	5·6
0·3	2·3	3·7
0	1·7	2·3
0	1·2	1·3
	Hydrogen gas phase	
0	2·4	0·7
0	4·1	1·5
0	6·0	2·5
0	8·6	4·1
0·3	11·3	6·3
0·8	14·3	9·5
1·3	17·1	12·1
1·8	23·2	19·6
2·8	28·3	26·8
3·8	32·2	33·2
4·8	38·8	44·5

(iii) ***Reynolds number—friction factor correlation***

The experimental data of this investigation were analysed according to the method of GARDNER [1] to see if the total specific surface could be readily obtained, thus allowing the correct Reynolds number to be assigned to the gas phase.

VOL 11 1959/

As the specific surface appears in the denominator of both the Reynolds number and the friction factor, the most convenient method of evaluating the specific surface is to assign a value of unity to the dry packing, thus enabling the irrigated specific surface to be calculated as a ratio of the dry surface of the packing, which may be calculated, if the loss of area at the points of contact is neglected. The calculation is essentially a trial and error process of substituting values of the ratio of irrigated specific surface to the dry specific surface until the irrigated experimental point cover plots the curve representing the dry data, which is used as the datum for all calculations.

The curve representing the dry data, in which the specific surface is taken to be unity, is obtained by substituting $S = 1$ into equations (7) and (5) to obtain

$$\frac{\Delta P\, 2g\, \epsilon}{L\, \rho\, V_g^2} \quad \text{and} \quad \frac{4 V_g\, \rho\, \epsilon}{\mu}$$

as the functions to be plotted.

The data for zero mercury flow rate, but previously irrigated packing, were also calculated in the same form, as it was expected that the two sets of data would only vary by a constant ratio and would, therefore, plot parallel to each other on a log–log graph. The logarithmic plot of

$$\frac{\Delta P\, 2g\, \epsilon}{L\, V_g^2\, \rho} \quad \text{versus} \quad \frac{4 V_g\, \rho\, \epsilon}{\mu}$$

is shown in Fig. 4 in which the solid line is fitted to the experimental results.

The unexpected feature of Fig. 4 is that the specific surface of the dry and previously irrigated packing is the same. For both cases a single line represents all the data plotted. The conclusion may be reached for this particular instance, where the previous irrigation was such that a total hold-up of 98 ml remained in the packing, that the increase in surface area due to the presence of the liquid hold-up is exactly compensated by the decrease in the surface area of the dry packing exposed to gas flow.

The full line in Fig. 4 was then used as the datum line for evaluation of the irrigated specific surfaces. Values of

$$\frac{\Delta P\, 2g\, \epsilon}{V_g^2\, \rho\, L} \quad \text{and} \quad \frac{4 V_g\, \rho\, \epsilon}{\mu}$$

were calculated for all the irrigated data, and the results plotted on a log–log graph, in which

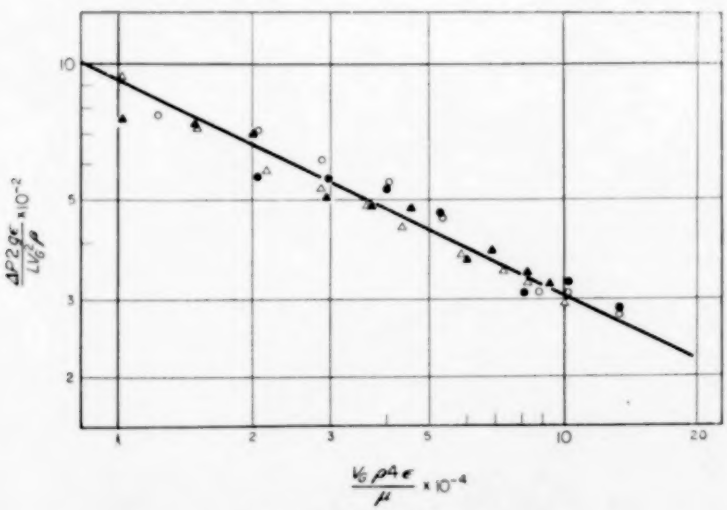

Fig. 4. Dry and previously irrigated packing.

○ Nitrogen before irrigation.
△ Hydrogen before irrigation.
● Nitrogen zero Hg rate
▲ Hydrogen zero Hg rate

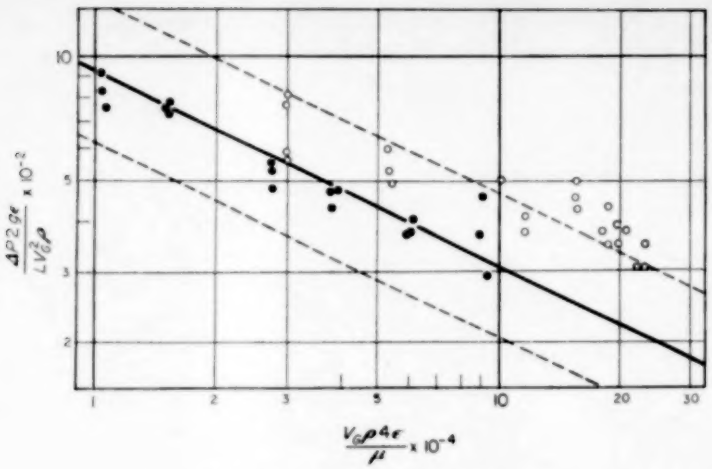

FIG. 5. Mercury irrigated data.
○ Nitrogen Hg irrigated. ● Hydrogen Hg irrigated.

the full line of Fig. 4 is drawn as the datum line as shown in Fig. 5.

Fig. 5 displays an unusual characteristic in that the hydrogen data, except for the highest Reynolds numbers, where "gas hold-up" effects were operative, exhibit specific surface of the same order or perhaps slightly less than the dry packing, whereas the nitrogen data suggests that the irrigated specific surfaces are quite significantly higher than the dry packing specific surface.

However, the data for the lowest nitrogen gas rate investigated, which are not plotted in Fig. 5, showed a reversal in trend, as the irrigated specific surfaces were less than the dry packing specific surface. As the pressure drops were measured with a simple manometer the error involved in the measurement of the pressure drops at low gas rates was such that the low gas rate data were of doubtful accuracy. Hence, it was decided not to plot these points but to record that they showed a reversal of trend. To be consistent all other pressure drops less than 1·5 cm H_2O were also not plotted.

A possible explanation of the significantly higher specific surfaces of the nitrogen data, even at gas rates where there was no "gas hold-up," is that differences in interfacial tension are the cause of the observed behaviour. Thus it would appear that, when nitrogen is the gas phase, the static hold-up and the specific surface for mercury irrigation are greater than the corresponding values for hydrogen as the gas phase, because of the higher interfacial tension of nitrogen with mercury.

In cases where there is a "gas hold-up," the specific surface would be expected to be somewhat greater than the other data. The group of points in Fig. 5 for values of

$$\frac{4 V_g \rho \epsilon}{\mu} \times 10^{-4}$$

greater than 15 for nitrogen are cases in which there were appreciable gas hold-ups.

The two broken lines drawn parallel to the datum line in Fig. 5 represent specific surfaces 30 per cent above and below the dry packing specific surface. The only data which show specific surfaces significantly outside these limits are the nitrogen data, in which the gas hold-up has increased the specific surface.

(iv) *The relation between total hold-up and pressure drop*

The type of correlation suggested by equation (3) appeared to be satisfactory for analysing the data,

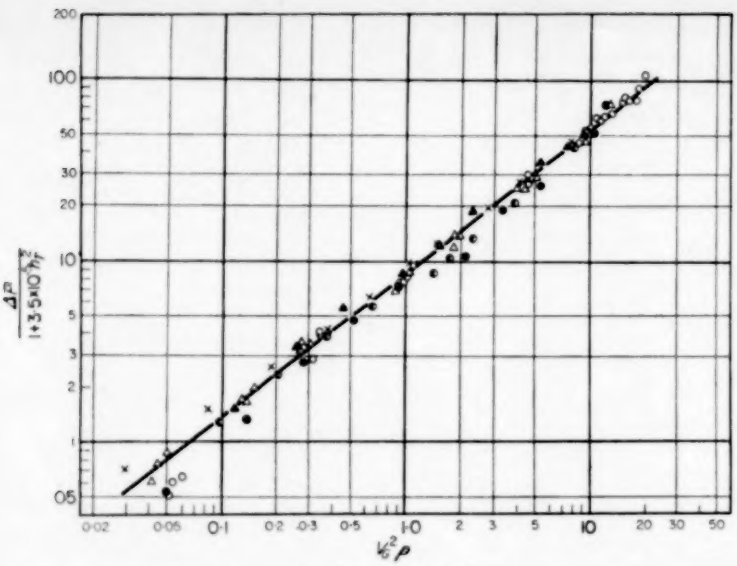

FIG. 6. Empirical correlation of all data.

○ Nitrogen Hg irrigated.
△ Hydrogen Hg irrigated
● Nitrogen zero Hg rate.
▲ Hydrogen zero Hg rate.
◐ Nitrogen before irrigation.
× Hydrogen before irrigation.

i.e. $$\frac{\Delta P}{x\,(h_T)} = x'\,(V_g^2\,\rho) \qquad (3)$$

Let $\Delta P = \Delta P_\circ\ [x\,(h_T)]$, for a given value of $(V_g^2\,\rho)$

i.e. $$x\,(h_T) = \frac{\Delta P}{\Delta P_\circ} \qquad (9)$$

if $x\,(h_T) = a + bh_T^c$, where a, b, c are constants.

Since $\Delta P = \Delta P_\circ$, when $h_T = 0$

$$x\,(h_T) = 1 + bh_T^c \qquad (10)$$

The constants b and c were determined by fitting an equation to the curve obtained when selected values of $x\,(h_T)$, calculated from equation (9), were plotted against h_T. Using this procedure the form of $x\,(h_T)$ given in equation (11) was obtained.

$$x\,(h_T) = 1 + 3{\cdot}5 \times 10^{-5}\,h_T^2) \qquad (11)$$

All the data of this investigation could be empirically correlated by a straight line on a log–log plot of

$$\frac{\Delta P}{(1 + 3{\cdot}5 \times 10^{-5}\,h_T^2}$$

versus $V_g^2\,\rho$ as shown in Fig. 6.

The correlation shown in Fig. 6 was developed for mercury irrigation, dry packing and previously mercury-irrigated packing. However, it seemed reasonable to expect the same correlation to be applicable to other liquid phases besides mercury. Tests were therefore undertaken on the same packing with water irrigation at various liquid and gas flow rates. The packing was then treated with paraffin wax to make it non-wetting to water and similar tests under non-wetting conditions were made.

The correlation developed from the mercury studies applied reasonably well to the water irrigated data, and hence the proposed correlation appears to be satisfactory, at least as a first approximation, for estimating the liquid hold-up on the same packing for any liquid system, by measuring the gas phase pressure drop, the mass flow rate and the density.

The other important feature of the correlation developed is that the state of the irrigating liquid, whether at rest as in the previously irrigated data or under actual irrigation, appears to make little difference to its applicability.

The correlation also holds equally well when the column is loaded, as the data in which there were appreciable "gas hold-ups" in the bed are represented by the same line as obtained for the column below the loading point. This is considered to be indicative of the close inter-relationship of pressure drop and hold-up, as most other forms of analysis show anomalies above the loading point.

Estimation of liquid hold-ups

Although SHULMAN *et al.* [10] have investigated the properties of the liquid phase, which affect the hold-up of aqueous and organic systems, the extrapolation of their results to a liquid metal of vastly different physical properties would be unwise.

More work of a fundamental nature on the flow of liquid metals or similar dense media is required before a reliable assessment can be made of the exact effect which the physical properties of the liquid phase have on the liquid hold-up.

In the absence of such information, it is suggested that the empirical method just outlined could be used for estimating liquid hold-ups in beds when the experimental difficulty precludes direct measurement, as for example, in high temperature liquid metal or molten slag irrigations. If the empirical relationship between the total liquid hold-up and the gas phase pressure drop can be developed on a room temperature model of the system, the extension of the correlation to the high temperature system would enable the total hold-up at zero irrigation rate (i.e. the static hold-up) or the total hold-up with irrigation to be estimated from the observed gas phase pressure drop across the bed, the gas temperature and the gas mass flow rates. The dynamic hold-up under the particular conditions would then be the difference of these estimates.

Acknowledgements—The continued interest and support of Professor J. P. BAXTER, School of Chemical Engineering and Vice-Chancellor, N. S. W. University of Technology, and Dr. G. H. ROPER, School of Chemical Engineering, is gratefully acknowledged.

Thanks are also due to Mr. N. SALASOO and Mr. N. KENNON for assistance in collecting the experimental data.

NOMENCLATURE

D_p	= characteristic dimension of the particle	ft
f	= Fanning friction factor	dimensionless
g	= acceleration due to gravity	ft/sec^2
g_c	= gravitational conversion factor	
h_D	= dynamic hold-up	ml
h_g	= gas hold-up	ml
h_s	= static hold-up	ml
h_T	= total hold-up	ml
L	= length of packed bed	ft
ΔP	= pressure drop across packed bed, lb/ft^2 in equations (1, 2, 6, 7), but for convenience in the dimensional equation (3) and the empirical correlation of Fig. 6	cm H_2O
$\Delta P_\circ$	= pressure drop across the dry packed bed	cm H_2O
R_e	= Reynolds number	dimensionless
S	= surface area per unit packed volume of bed	ft^2/ft^3
U	= superficial fluid velocity	ft/sec
V	= true fluid velocity	ft/sec
V_g	= true gas velocity	ft/sec
ϵ	= fractional voids or bed porosity	
ρ	= fluid density	lb/ft^3
μ	= fluid viscosity	lb/ft sec
$\chi(h_T)$	= function of total liquid hold-up	
$\chi'(V_g^2\rho)$	= function of gas inertia.	

REFERENCES

[1] GARDNER G. C. *Chem. Engng. Sci.* 1956 **5** 101.
[2] ERGUN S. *Chem. Engng. Progr.* 1952 **48** 89.
[3] BLAKE F. C. *Trans. Amer. Inst. Chem. Engrs.* 1922 **14** 415.
[4] CARMAN P. C. *Trans. Inst. Chem. Engrs.* 1937 **15** 150.
[5] MOTT R. A. *Some Aspects of Fluid Flow* pp. 242-256. Edward Arnold, London 1950.
[6] ELGIN J. C. and WEISS F. B. *Industr. Engng. Chem.* 1939 **31** 435.
[7] JESSER B. W. and ELGIN J. C. *Trans. Amer. Inst. Chem. Engrs.* 1943 **34** 277.
[8] SHULMAN H. L., ULLRICH C. F. and WELLS N. *Amer. Inst. Chem. Engrs. J.* 1955 **1** 247.
[9] PERRY J. H. *Chemical Engineers Handbook* (3rd Edition). p. 363. McGraw-Hill, New York 1950.
[10] SHULMAN H. L., ULRICH C. F., WELLS N. and PROULX A. Z. *Amer. Inst. Chem. Engrs. J.* 1955 **1** 259.

VOL 11 1959

Chemical Engineering Science, 1959, Vol. 11, pp. 161 to 182. Pergamon Press Ltd., London. Printed in Great Britain

The absorption of zinc vapour in molten lead

Countercurrent absorption in a packed column

N. A. Warner

School of Metallurgy, The University of New South Wales, P.O. Box 1, Kensington, N.S.W., Australia

(*Received* 23 *August* 1958; *in revised form* 11 *May* 1959

VOL. 11 959/60

Abstract—Experiments are described in which nitrogen containing zinc vapour is countercurrently contacted with molten lead in a small column packed with ¾ in. mild steel raschig rings. The heights of overall gas phase transfer units for the absorption of zinc vapour in molten lead using this packing are reported for a range of gas and lead temperatures and flow rates.

It is suggested that the scrubbing of gases containing zinc vapour, as in the recently developed zinc blast furnace, should be considered as an absorption not a condensation. It it demonstrated in these studies that zinc vapour can be continuously removed from a gas phase by absorption in molten lead under conditions such that both the gas and lead temperatures are well above the zinc dew point of the gas mixture.

A fundamental equation, for analysing the absorption of zinc vapour in molten lead in terms of conventional gas absorption theories is derived using the additive diffusional resistance concepts. Room temperature analogues of the zinc absorption in molten lead packed column enable evaluation of the flow characteristics of the irrigating liquid lead and the mass transfer properties of the packing under non-wetting conditions.

For the experimental conditions of these studies, the absorption of zinc vapour in molten lead is shown to be controlled by the diffusional resistance in the gas phase and can therefore be compared with other gas phase controlled absorptions such as ammonia in water from a dilute ammonia–air mixture. To correlate zinc and ammonia absorption data, a new quantity, the effective hold-up ratio is introduced. The results of the zinc absorption studies suggest that the total liquid hold-up is effective in this process because of the mobility of the static hold-up, when a liquid metal irrigates a packed bed.

The successful correlation of both the ammonia absorption in water and the zinc absorption in lead data indicates that the absorption of a metallic vapour in a molten metal at an elevated temperature can be analysed according to conventional gas absorption theories and also shows the value of room temperature analogues for experimentally difficult high temperature mass transfer processes.

Résumé—L'auteur décrit des expériences dans lesquelles de l'azote contenant de la vapeur de zinc est mis en contact en contre-courant avec du plomb fondu, dans une petite colonne à garnissage contenant des anneaux raschig en acier doux d'¾ in. Les hauteurs d'unité de transfert de la phase gazeuse globale pour l'absorption de la vapeur de zinc sur du plomb fondu en utilisant ce garnissage sont données pour un intervalle des températures du gaz et du plomb et des vitesses d'écoulement.

L'auteur suggère que l'épuration de gaz contenant de la vapeur de zinc soit comme dans les hauts fourneaux à zinc récemment développés, considérée comme une absorption et non comme une condensation. Cette étude montre que la vapeur de zinc peut être continuellement éliminée d'une phase gaz par absorption par du plomb fondu dans des conditions telles que les températures aussi bien du gaz que du plomb soient bien au-dessus du point de rosée du zinc du mélange gazeux.

Une équation fondamentale est définie pour l'analyse de l'absorption de la vapeur de zinc par le plomb fondu en fonction des théories habituelles de l'absorption des gas, en utilisant les concepts supplémentaires de la résistance à la diffusion. Des analogues à une température ambiante pour l'absorption du zinc dans une colonne à garnissage par du plomb fondu permettent d'évaluer les caractéristiques d'écoulement du plomb liquide irrigant et les propriétés de transfert de masse du garnissage dans des conditions de non-mouillage.

Pour les conditions expérimentales, l'absorption de vapeur de zinc par du zinc fondu est réglée par la résistance à la diffusion dans la phase gaz et peut donc être comparée avec d'autres absorptions réglées par la phase gaz, telles que l'absorption de l'ammoniac par l'eau à partir d'un mélange dilué air–ammoniac. L'introduction d'une nouvelle quantité, le rapport de *hold-up* (rétention) effectif permet de coordonner les données d'absorption du zinc et de l'ammoniac. Les résultats des études sur l'absorption du zinc suggèrent que le *hold-up* liquide total est effectif dans ce procédé à cause de la mobilité du *hold-up* statique quand un métal à l'état liquide irrigue un lit de garnissage.

La concordance des données sur l'absorption de l'ammoniac par l'eau et sur l'absorption du zinc par le plomb montre que l'absorption d'une vapeur métallique à température élevée, peut être analysée d'après les théories ordinaires sur l'absorption des gaz, et donne la valeur des analogues à température ambiante pour les transferts de masse à température élevée dont l'expérimentation est difficile.

Zusammenfassung—Es werden Versuche beschrieben, in denen Zinkdampf enthaltender Stickstoff mit geschmolzenem Blei im Gegenstrom in Berührung gebacht wird in einer kleinen Kolonne, die mit 6,5 mm-Raschigringen aus Fluss-Stahl gefüllt ist. Die Gesamt-Übertragungshöhen der Gasphase für die Absorption von Zinkdampf in geschmolzenem Blei in dieser Packung werden für einen Bereich der Gasund Bleitemperaturen und Strömungsmengen mitgeteilt.

Es wird vorgeschlagen, die Reinigung des Zinkdampf enthaltenden Gases, wie in dem kürzlich entwickelten Zinkhochofen, als Absorption und nicht als Kondensation anzusehen. Die Untersuchungen zeigen, dass Zinkdampf kontinuierlich aus der Gasphase durch Absorption in geschmolzenem Blei entfernt werden kann, wenn Gas-und Bleitemperaturen deutlich über dem Taupunkt des Zinks liegen.

Unter Benutzung des Begriffs der additiven Diffusionswiderstände wird für die Absorption des Zinkdampfes in geschmolzenem Blei eine Grundgleichung in Ausdrücken der gewöhnlichen Absorptionstheorie abgeleitet. Analogieversuche bei Raumtemperatur in der gleichen Kolonne erlauben die Auswertung der Fliessgrössen des herabrieselnden flüssigen Bleis und der Stoffübertragungseigenschaften der Packung bei Nichtbenetzung.

Unter den experimentellen Bedingungen dieser Untersuchungen zeigt sich die Absorption von Zinkdampf in geschmolzenem Blei bestimmt durch den Diffusionswiderstand in der Gasphase. Sie kann daher etwa mit der Absorption von Ammoniak in Wasser aus einer verdünnten Ammoniak–Luft-Mischung verglichen werden. Zur Korrelation der Zink-und der Ammoniakabsorptionswerte wird eine neue Grösse, das Verhältnis der effektiven Flüssigkeitsinhalte, eingeführt. Die Ergebnisse der Untersuchungen über die Zinkabsorption zeigen, dass der gesamte Flüssigkeitsinhalt wirksam ist wegen der Beweglichkeit des statischen Flüssigkeitsinhalts, wenn ein flüssiges Metall ein Festbett berieselt.

Die erfolgreiche Korrelation der Ammoniakabsorption in Wasser und der Zinkabsorption in Blei zeigt, dass die gewöhnliche Absorptionstheorie auch für die Absorption eines Metalldampfes in geschmolzenem Metall bei erhöhten Temperaturen gültig ist; auch der Wert von Analogieversuchen bei Raumtemperatur für Stoffübertragungsprozesse bei experimentell schwierigen hohen Temperaturen wird nachgewiesen.

INTRODUCTION

THE development of the zinc blast furnace by the Imperial Smelting Corporation at Avonmouth, England, has been recently outlined by MORGAN [1]. The success of the new process depends primarily on the recovery of zinc from a gas phase containing a relatively low concentration of zinc vapour and a considerable amount of carbon dioxide. To prevent re-oxidation of the zinc vapour on cooling, the hot gases are shock-chilled by direct contacting with showers of molten lead. Continuous removal of both heat and zinc from the furnace gases is obtained by pumping molten lead through a scrubber and an external cooling and phase separating vessel, from which the liquid zinc produced is continuously withdrawn and the lead returned to the scrubber.

The data of Table 1 were given by MORGAN [1] for the countercurrent scrubbing of zinc blast furnace gases with cool liquid lead saturated with zinc.

Table 1. *Typical countercurrent scrubber operating conditions (based on figures by* MORGAN [1])

Gas phase	
5% Zn at 1,000°C to be cooled to 450°C	
Lead phase	
Circulation rate	= 420 ton/ton Zn produced
Inlet temp.	= 440°C
Inlet composition	= 2·02% Zn (Saturated)
Outlet temp.	= 570°C
Outlet composition	= 2·26% Zn
Saturation at outlet temp.	= 4·90% Zn

MORGAN [1] and the zinc blast furnace patent literature refer to the gas–liquid lead contacting stages as condensers. It is proposed that such a nomenclature overlooks the fundamental mechanism involved, as does the statement made by MORGAN [1] when describing these units:

> "Rapid cooling tends to promote fog formation but the seriousness of this aspect is reduced by (a) the high superheat of the gases, which have a dew point of about 650°C and leave the furnace at 900–1000°C: and (b) the presence of a rain of unsaturated lead in which droplets of zinc are formed, but are themselves scrubbed by the intense rain of lead."

This implies that discrete drops of zinc are formed in the contacting stage, because the gas temperature in the vicinity of the lead falls below the dew point and it is these droplets of zinc which are collected by the scrubbing action of the lead showers.

The transfer of zinc from the gas phase into the liquid lead is clearly a diffusion controlled mass transfer operation. The zinc must diffuse from the bulk of the furnace gases through the laminar gas film on the gas–liquid lead interface and must then diffuse into the bulk of the lead phase. Hence at no stage would the zinc be present in particulate form.

Zinc droplets would be formed in the bulk of the gas phase, only if the bulk gas temperature fell below the dew point of its zinc vapour content. As the dew point of the inlet gases is approximately 650°C, the gas inlet temperature 1,000°C and the outlet lead temperature 570°C, it is very difficult to conceive the bulk gas temperature as falling below the dew point, when the temperature drops associated with the transfer of heat from the hot gases to the cooler lead are taken into account and when it is realised that the zinc content of the gases will decrease approximately exponentially as the gas traverses the "condenser," with the corresponding decrease in the dew point temperature of the gas mixture. Local cooling and zinc mist formation at the lead surfaces would also be unlikely, because in the gas film surrounding the lead surfaces a large zinc partial pressure gradient would be expected at high rates of mass transfer.

A more appropriate nomenclature for the gas–liquid lead contacting stages would be to call these units "absorbers," as it would appear that the fundamental unit operation involved is basically gas absorption.

The aim of the present investigation was to study the mechanism of the absorption of zinc vapour in molten lead and to see if the conventional gas absorption theories, developed for non-metallic systems at or near room temperature, could be applied to the absorption of a metallic vapour in a liquid metal at an elevated temperature.

Metallic vapour–liquid metals systems have not previously been analysed from this point of view and thus there have been no similar investigations reported in the literature.

EXPERIMENTAL

When the experimental programme was initiated, the laboratory disk column, as introduced by STEPHENS and MORRIS [2], was considered to be the most desirable apparatus for studying the continuous countercurrent absorption of zinc vapour in molten lead. Because of difficulties associated with the flow of molten lead over the disks, this column proved unsuitable. A small packed column, whilst not possessing the advantage of known interfacial area, was finally chosen.

The guiding considerations in the design of the experimental apparatus were that the absorption would have to be carried out on a relatively small scale and that continuous operation of the apparatus for periods up to one day would be required to collect the necessary data.

Although the absorption column itself was only of a small size, the ancillary systems, essential to its operation, presented numerous design problems because of the high temperature of operation.

Basically the experimental apparatus consisted of a small packed column irrigated with molten lead and up which a stream of nitrogen and zinc vapour could be passed with provision for measuring the gas and lead phase temperatures, flow rates and zinc compositions. The essential components and layout of the apparatus are shown in Fig. 1.

Description of apparatus

(i) *Liquid lead system.* The molten lead supply to the column was from a large insulated tank containing a small submerged centrifugal pump and needle control valve and provided with an inert nitrogen atmosphere. Intermittent checks on the lead discharge rate into a casting wheel located at the bottom of the absorption column enabled control of the lead flow rate. The lead discharged from the pump into a $\frac{3}{8}$ in. O.D. 18 gauge stainless steel tube and was heated to the desired temperature as it went through this tube by passing a heavy electrical current through the pipe and its contents. Approximately 350 A were required to heat the lead to the column operating temperature. The heavy current source used was a 1000 A, 12·5 V Selenium Rectifier Plating Unit. The passage of heavy current through the tube also served to preheat the tube to above the melting point of lead, before the lead pump was switched on.

Direct heating by the passage of heavy current provided a very convenient method of keeping other components at the required temperature. The superheater and gas analysis sampling lines in the gas circulation system were kept well above the dew point of the zinc vapour by this method. The low voltage, high current electrical circuit used is shown in Fig. 2.

(ii) *Gas circulation system.* Nitrogen was used as carrier gas for the zinc vapour. The gas circuit operated on a closed system with two sliding vane rotary blowers in parallel providing the necessary boosting for recirculation. A wet gasholder filled with light oil was connected to the suction side of the boosters to maintain a positive pressure of 2 in. w.g. on the suction side of the system. The infiltration of air into the system through any leaks was thus prevented. Any leaks in the system were made up by supply of nitrogen from the gasholder. The nitrogen supply to the gasholder was by an automatic solenoid operated valve from a compressed nitrogen source.

(a) *Preheater.* To preheat the nitrogen to a temperature of approximately 600°C, a heater was constructed consisting essentially of a tube furnace inside which were six passes each 2 ft 6 in. long of $\frac{3}{8}$ in. O.D. stainless steel tube.

(b) *Carbonizer.* The commercial grade nitrogen make-up to the system was contaminated with oxygen and therefore a unit was designed, so that the oxygen content of the nitrogen was converted to carbon monoxide before passage to the zinc boiler. This was achieved by interposing, in the line between the preheater and the zinc boiler, a tube packed with carbon granules maintained at approximately 1,000°C. This unit was designated the carbonizer.

As the nitrogen was recycled, the problem of oxygen contamination would have been eliminated, if there were no leaks in the gas circulation system requiring make-up, because the removal of oxygen would have been substantially complete by gaseous oxidation of the zinc after one pass through the zinc boiler.

(c) *Zinc boiler.* Preheated nitrogen was passed over a crucible containing liquid zinc at or near the boiling point (906°C at 1 atm). This unit was termed the zinc boiler. The power input to the boiler determined the rate of vaporization to give the desired zinc partial pressure in the nitrogen stream.

Because of the high temperature service required and the extreme corrosive nature of liquid zinc at these temperatures, external heating of a metal boiler containing a crucible of zinc was precluded. The back pressure on the boiler was approximately 5 lb/in² gauge and therefore the boiler had to be contained in a metal vessel to prevent excessive leakage and to facilitate connexion to the other metallic components of

VOL 11 1959/

VOL. 11 959/60

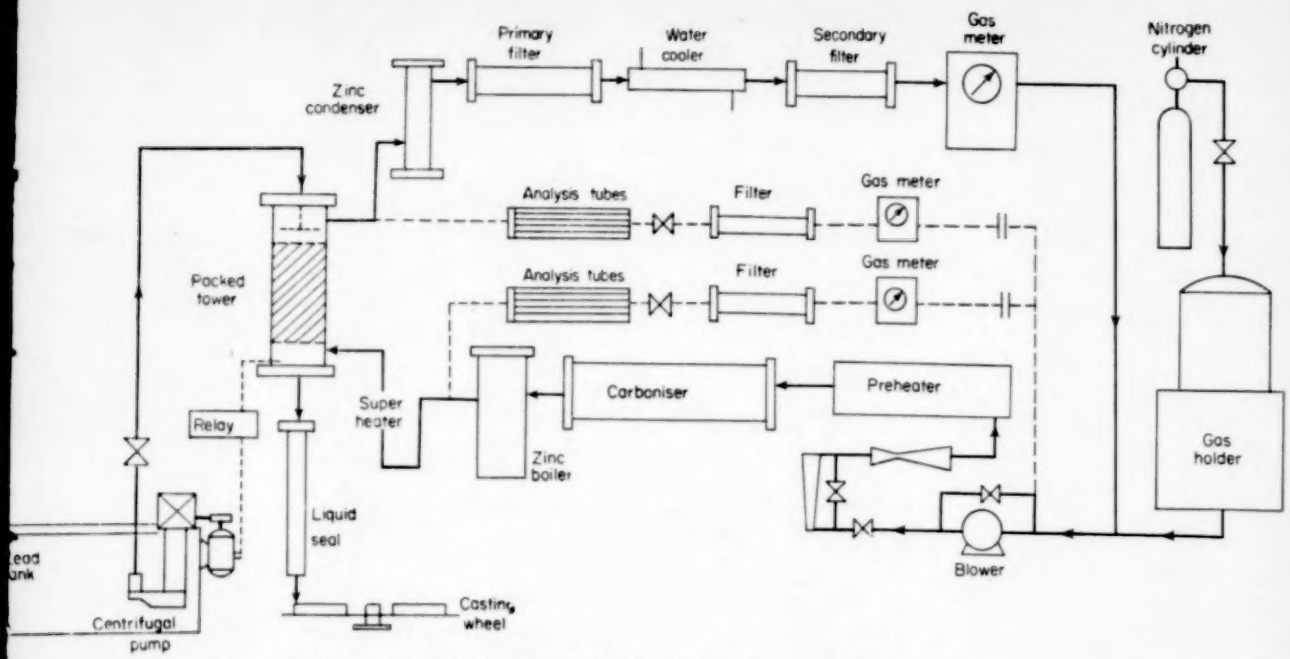

FIG. 1. Flow sheet of zinc absorption in molten lead apparatus.

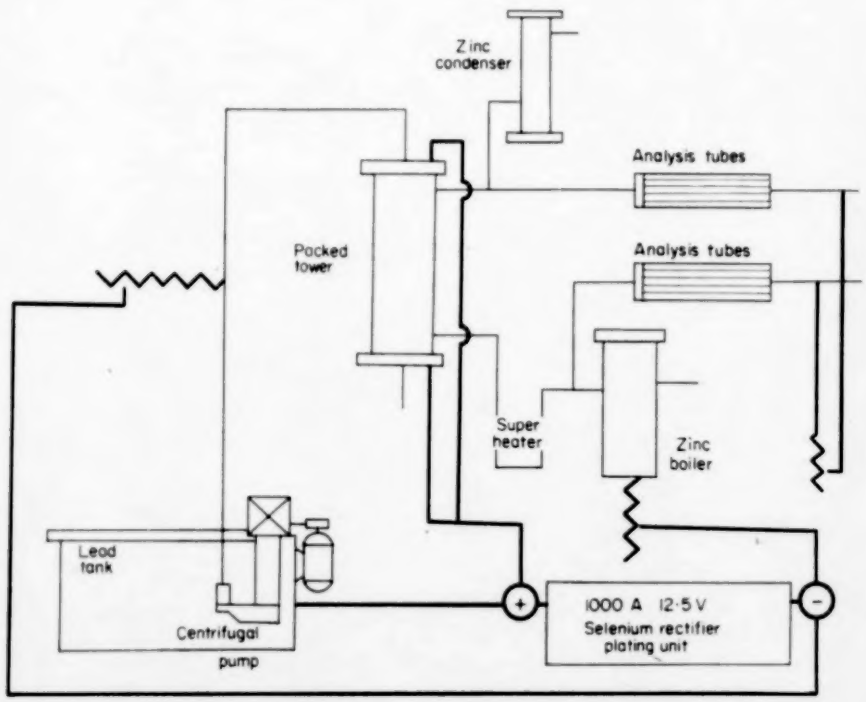

FIG. 2. Low voltage, heavy current electrical circuit.

the gas circulation system. The solution to these considerations was to build the furnace inside a mild steel vessel and to insulate the space between the furnace and the metal walls so that the metal wall temperature was below 600°C with the electric resistance furnace in the zinc containing atmosphere and under the pressure of the unit. The contructional details of the zinc boiler are shown in Fig. 3.

(d) *Superheater.* To ensure that there was no condensation of zinc in the gas line between the zinc boiler and the absorption column, a superheating section was installed to bring the gas temperature to 700–800°C before it entered the absorption column. For the mass flow rates required, the necessary superheating was obtained in a four foot length of ¼ in. O.D. stainless steel tube at 850°C set in between the boiler and the absorption column. A current of approximately 250 A was passed through this tube, to maintain the superheater tube at the required temperature.

(iii) *The packed absorption column.* The

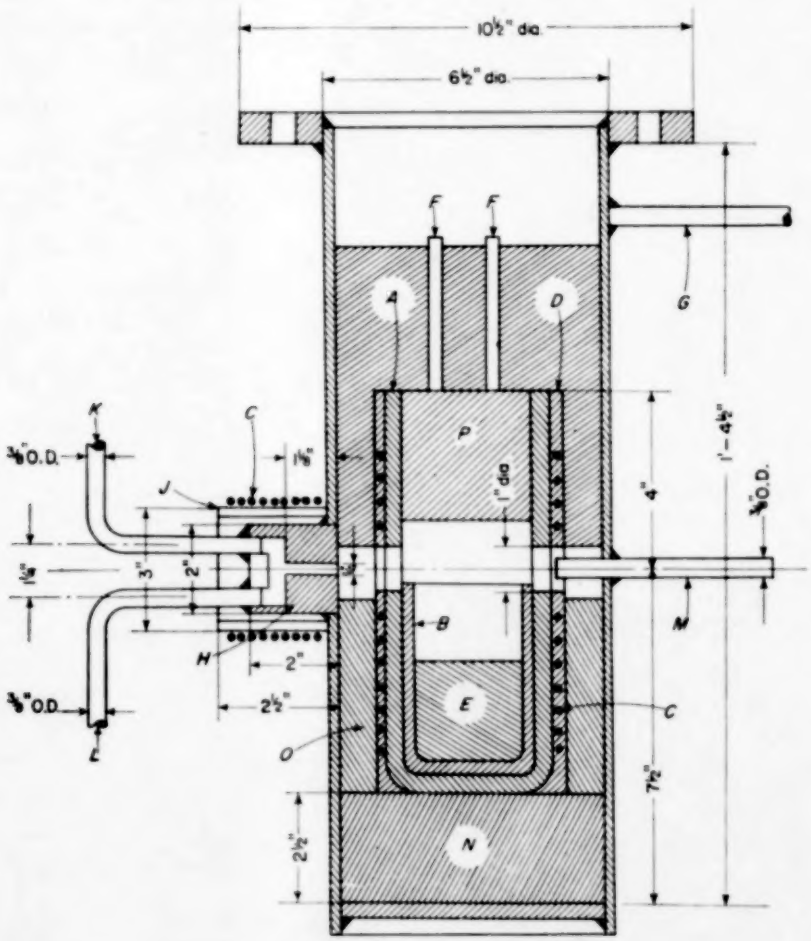

FIG. 3. The zinc boiler.

A–Morgan sillimanite crucible N3907. B–Morgan sillimanite crucible N1938. C–"Kanthal" resistance winding. D–Alumina cement. E–Zinc charge. F–Power input insulating tubes. G–Heavy current connexion. H–Outlet gas manifold. J–Silica tube. K–Inlet gas sampling line. L–Superheater. M–Gas inlet from carbonizer. N–Insulating brick. O–Vermiculite insulation. P–Steel wool.

principal dimensions of the packed column are summarized in Table 2.

The shell of the absorption column was fabricated from a 2 in. O.D. 10 gauge stainless steel tube. Details of the shell construction are shown in Fig. 4. The tower was packed to a height of 1·75 ft with ¼ in. mild steel raschig rings. The raschig rings were machined by

Table 2. Details of the packed column

Internal diameter	= 1·74 in.
Empty cross-sectional area	= 0·01654 ft²
Packing material	= ¼ in. × ¼ in. × 20 gauge steel raschig rings
Packed height	= 1·75 ft
Bed porosity (before irrigation)	= 0·72

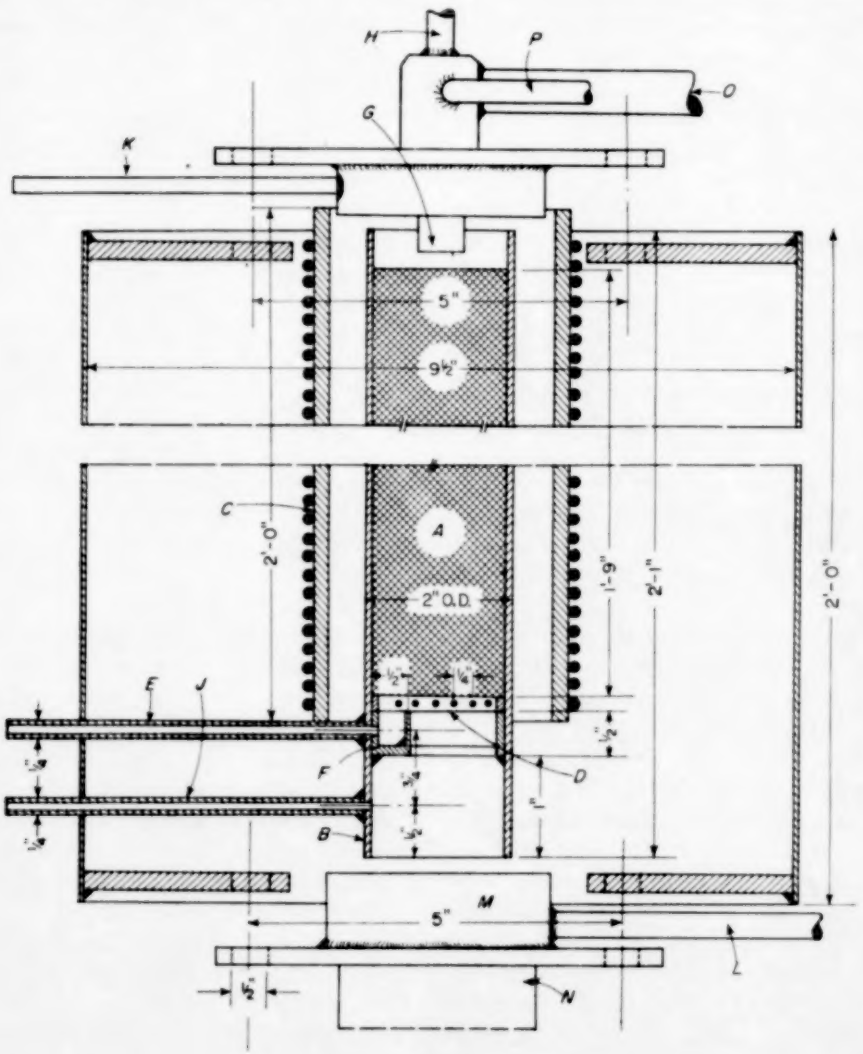

FIG. 4. The packed absorption column.

A–Packed bed ¼ in. M.S. raschig rings. B–Column shell. C–Column furnace. D–Packing support. E–Lead temperature probe. F–Lead collecting reservoir. G–Lead inlet nozzle. H–Lead inlet from pump. J–Gas inlet temperature probe. K–Gas outlet temperature probe. L–Gas inlet superheater. M–Inlet gas distributor. N–Liquid seal. O–Gas outlet from column. P–Outlet gas sampling line.

parting off $\frac{3}{4}$ in. lengths of $\frac{1}{4}$ in. O.D. 20 gauge mild steel tube. The weight of rings added to the column was recorded to allow calculation of the bed porosity.

Lead and gas temperature probe tubes were welded to the bottom section of the shell. Through these probe tubes, stainless steel thermowells made from 3·5 mm O.D. stainless steel tube were inserted into the lead and gas streams. The lead thermowell was located in a small reservoir placed directly under the packing support. Portion of the lead flowing down the column collected in this reservoir, thus enabling its temperature to be measured. The gas temperature thermowell was located directly beneath the reservoir and therefore contact with lead flowing in the column was precluded.

A manometer pressure tapping was located beside the gas temperature probe at the bottom of this column. This pressure tapping was also shielded from the lead flow by placing it directly underneath the reservoir used for measuring the lead temperature.

No connexions were made to the top section of the column shell to allow installation of a 2 kW (240 V) nichrome resistance furnace on a 3 in. silica tube around the column shell to balance the heat loss from the walls of the column.

The top gas temperature probe and the manometer pressure tapping were located in the sealing ring welded to the top cover plate of the column after the furnace was placed in position. The top lead temperature was measured by a thermowell located in the liquid lead feed nozzle.

To the top cover plate of the column were welded the lead inlet tube, the gas outlet and combined primary zinc condenser and entrained lead trap and the outlet gas analysis sampling line.

The bottom cover plate of the column contained the gas inlet distributor. The gas distribution to the bottom of the column was through $5 \times \frac{1}{4}$ in. diameter ports.

To prevent zinc condensation, additional heating was provided around the gas distributor at the bottom of the column by a coal gas burner formed in two semicircular sections so that the circumference of the distributor was evenly heated. A gas burner was also provided on the top cover plate.

The lead discharge pipe from the column was submerged in a reservoir of molten lead in which an overflow was positioned to allow continuous removal of the lead from the column. The liquid seal thus formed was capable of holding column pressures up to 5 lb/in² gauge. The overflow from the liquid seal was cast into ingots.

To prevent liquid lead from flowing back into the gas circulation system in the case of a blockage in the lead discharge from the column, a relay device was installed in the absorption column to interlock lead level in the column to the centrifugal pump. Once the lead inside the column built up to a dangerous level, the lead pump automatically cut off. A 32 V probe was located inside the absorption column. Once contact was made between the insulated probe and the wall of the column by liquid lead, a change-over type electromagnetic relay de-energized the coil of an electromagnetic contactor, which cut off the supply of current to the motor driving the pump. The contactor was also arranged with thermal overload protection for the motor.

Analytical procedures

(a) *Gas phase zinc analysis system.* The nitrogen containing zinc vapour was analysed for its zinc content before and after leaving the absorption column. Samples of gas were drawn off from the inlet and outlet gas streams by piping sample lines to the suction side of the gas boosters.

The sample of gas for analysis on the inlet side of the absorption column was taken from the outlet manifold of the zinc boiler. The sample of gas for outlet zinc analysis was taken directly from the top cover plate of the absorption column. Both inlet and outlet sample lines were of $\frac{3}{8}$ in. O.D. stainless steel tube connected electrically together in series. The lines formed the circuit for the passage of the heavy current (approximately 250 A) used for keeping them above the dew point of the zinc vapour. Temperature control of the lines was by insertion of the required resistance in series with the circuit.

VOL 11 1959

The sample lines were connected by " ermeto " couplings to removeable stainless steel headers inside resistance furnaces also maintained well above the dew point of the zinc vapour. Connected to the headers and protruding out of the analysis furnaces were welded $\frac{3}{8}$ in. O.D. stainless steel tubes, each containing (at the cold end) a small glass wool filter unit for collecting the condensed zinc formed, as the gas cooled inside these tubes. These filter units were connected by detachable $\frac{1}{4}$ in. O.D. copper tubes to a manifold provided with a plug cock for each tube, allowing a sample to be drawn through the desired analysis tube. Interposed between the manifolds and the blower were 30 ft^3/hr oil filled gas meters on both the inlet and outlet analysis systems. Orifice meters were located on the outlet of the gas meters to enable the rate of sampling during a run to be observed and controlled at the desired rate.

Provision was made in the construction of the analysis headers for installing seven tubes in both the inlet and outlet analysis headers. The inlet and outlet analysis headers were identical. Stainless steel all welded construction was used throughout, to enable the tubes to be leached with nitric acid and to prevent undue oxidation at the high temperatures used. At the conclusion of the experimental run on the apparatus, the headers were removed from the furnaces, the zinc leached out of each tube individually with hot 5 N HNO_3 and determined volumetrically using sodium versenate.

(*b*) *Chemical analysis.* After an initial separation of lead by a two stage precipitation with sulphuric acid, the zinc in the lead effluent from the column was determined volumetrically using the disodium salt of ethylenediamine tetracetic acid (sodium versenate) under buffered conditions at pH 10 with Eriochrome Black T as the indicator. Complete separation of lead and zinc was not required initially as the small amount of lead remaining in solution was titrated with sodium versenate with the zinc ions complexed by cyanide addition. Once the lead end point was reached, the addition of formaldehyde destroyed the zinc complex rendering the zinc available for titration with sodium versenate.

The method outlined was checked with synthetic mixtures of lead nitrate containing small known amounts of zinc and was found reliable.

A primary separation of lead and zinc was not required in the gas phase zinc analysis. Because of the low lead partial pressures, the zinc collected in the analysis tubes was only slightly contaminated with lead and hence it was possible to titrate this lead directly, whilst the zinc was in the cyanide complex, before releasing the zinc for titration.

Operating procedure

The gas circulation system was purged with the blowers on, until the residual oxygen in the system was less than 0·5 per cent, before the power to the various furnaces in the circuit was turned on. Complete oxygen at this stage was considered unnecessary, as also was the use of special oxygen-free nitrogen. As the nitrogen in the system was recycled, the final removal of oxygen from the system relied on the reaction with the hot charcoal bed in the carbonizer and also on reaction of any CO_2 or O_2 with the zinc vapour formed later when the zinc boiler had reached operating temperature. The gas in the system, under the final operating conditions, was therefore considered to be oxygen free, as the only make-up to the system was to allow for leaks and this small make-up passed through the carbonizer before entering the zinc boiler and the absorption column.

When the gas circulation system had reached steady state conditions for the column temperatures required, the lead pump was switched on and the flow adjusted by the submerged needle valve. After 10 to 30 minutes of pumping, the column temperatures became fairly steady and the run was commenced. (Minimum number of phase throughputs before run, liquid lead = 25, gas = 500). For a period of 10 to 30 min, depending on the lead flow rate, the following run procedure was followed:

(i) All the lead was collected and weighed.
(ii) The total gas flow over the test period was read from the gas meter.
(iii) The inlet and outlet analysis samples were drawn through the appropriate

analysis tubes, tagged for the particular run and the sample volumes noted.

(iv) The rate of sample withdrawal was noted by observing the orifice meters on both the inlet and outlet analysis systems.

(v) The pressure at the base of the column was read. For the lower gas throughputs, it was sometimes necessary to increase the column pressure by slightly closing a valve on the gas line before the meter, to allow analysis samples to be drawn off at the desired rate.

(vi) The rotameter reading and pressure at the blower were noted.

(vii) The pressure drop across the packed column was measured.

(viii) Samples of lead for analysis were obtained by directly collecting the discharge from the liquid seal in a steel crucible approximately $1\frac{1}{4}$ in. high $\times$ $\frac{3}{4}$ in. diameter. Usually six samples were obtained evenly spread over the test period.

(ix) The total time of the test period was noted and the duration of the run marked on the chart of the sixteen point temperature recorder which recorded all relevant operating temperatures.

Although the gas analysis system was designed to allow seven runs on the apparatus before removal of the analysis headers for zinc analysis, it was found that only three runs could be made during a one day campaign. The usual procedure was to allow the gas system to cool down overnight, with the nitrogen still connected to the gasholder, after the completion of three runs, and to repeat the procedure the following day for the remaining three runs, before dismantling the gas analysis headers for analysis. The remaining gas analysis tube in the inlet and outlet assemblies, not used in the series of runs, served as a blank in the zinc analysis.

Experimental results

The experimental data obtained using the foregoing procedures are tabulated in Table 3. Runs 4B, 4C and 4D were discarded because of a leak discovered at the conclusion of the experiments in the inlet analysis tube No. 4. This leak was not present in Run 4A, as the analysis tubes used in the A series of runs were replaced at the conclusion of this series by modified forms to enable easier dismantling. Run 1D was discarded because the automatic cut-off on the lead pump was actuated during this run and therefore a complete series of data was not obtained.

For series A, the gas inlet zinc mole fraction was calculated from the experimentally determined gas outlet and lead analyses, assuming a zinc balance of 100 per cent. For Series B, C and D, the gas inlet mole fraction was obtained by chemical analysis. The reason for this difference was that in Series A, the first set of runs on the apparatus, the experimental procedure was different to the later runs in that inlet gas was not analysed during the test period but measured directly after the test. This procedure was later considered unwise, as operating conditions tended to alter and therefore the early procedure did not give a true indication of conditions during the test period.

The outlet lead was analysed for zinc in Series A and B. This enabled a check to be made on the accuracy of the analytical procedures including the efficiency of the zinc traps and the gas and lead flow systems, by calculating zinc mass balances for these runs. A zinc balance could not be established on Runs 1A and 2A because initial experimental difficulties in these two runs prevented samples of the inlet gas being taken.

The zinc mass balances for Series A and B are shown in Table 3. These results clearly indicate the reliability of the experimental data, particularly when the experimental difficulties associated with the investigation are considered.

As a result of the excellent zinc mass balances obtained, the time consuming zinc analysis of the outlet lead was not undertaken for Series C and D. In these series, the inlet zinc concentration in the lead and the inlet and outlet gas phase zinc compositions were determined experimentally. The zinc in the outlet lead was calculated assuming a zinc mass balance of 100 per cent. Although the outlet lead was analysed in Series B, the values tabulated in Tables 3 were also calculated assuming 100 per cent zinc balance, as the gas

VOL 11 1959/

VOL. 11 59/60

Table 3. Experimental results – countercurrent absorption of zinc vapour in molten lead

	Run	Temperatures (°C)				Flow rates (lb mole/hr)		Mole fraction Zn in Pb		Gaseous zinc mole fraction		Total pressure in column (mm Hg)	Inlet zinc partial pressure (mm Hg)	Pressure drop across column (cm H_2O)	Zinc mass balance (%) $\left(\frac{\text{Zn absorbed in Pb}}{\text{Zn removed from gas}}\right)$	Estimated total hold-up of molten lead (ml)
		Gas in	Gas out	Lead in	Lead out	Lead	Gas	Inlet $x_2 \times 10^5$	Outlet $x_1 \times 10^5$	Inlet $y_1 \times 10^4$	Outlet $y_2 \times 10^5$					
Series A	1A	620	590	510	620	3·04	0·158	4·9	92·3	181·6	35·5	841	15·3	15·4	—	185
	2A	645	570	530	715	1·73	0·089	4·9	96·8	188·7	6·5	800	15·1	6·9	—	190
	3A	700	550	460	665	1·86	0·138	4·9	79·5	108·2	11·8	836	9·0	14·0	82	190
	4A	655	525	425	565	2·92	0·132	4·9	56·3	126·3	17·5	836	10·6	16·0	84	215
	5A	620	505	400	495	5·65	0·132	4·9	38·3	165·8	14·7	841	13·9	27·7	90	270
	6A	655	510	450	595	2·03	0·138	4·9	128·0	190·3	12·9	836	15·9	14·5	87	200
Series B	1B	730	550	460	675	1·75	0·268	4·9	18·6	11·0	20·9	887	0·98	50·1	103	215
	2B	710	510	445	635	2·29	0·253	4·9	19·8	14·6	11·4	892	1·30	48·3	99	225
	3B	725	520	455	650	1·91	0·204	4·9	39·0	32·7	8·1	876	2·86	31·0	92	215
	5B	685	525	480	605	1.46	0·0219	5·5	29·3	161·0	15·4	826	13·30	1·9	100	280
	6B	665	510	460	565	2·31	0·0438	5·5	35·3	158·0	10·0	841	13·30	4·2	91	255
Series C	1C	760	685	650	765	2·30	0·147	10·5	12·5	5·53	22·4	863	0·48	20·7	—	215
	2C	720	630	560	660	4·26	0·145	10·5	11·9	5·45	12·3	873	0·48	36·2	—	275
	3C	735	670	720	735	0·83	0·148	10·5	19·2	6·71	18·3	863	0·58	17·2	—	195
	5C	740	640	610	715	2·45	0·0577	10·5	11·3	4·64	11·5	842	0·39	7·2	—	260
	6C	750	635	550	705	3·90	0·0598	10·5	11·2	5·88	10·8	842	0·50	—	—	—
Series D	2D	740	650	610	760	2·62	0·147	5·8	43·9	74·5	65·0	910	6·78	20·8	—	225
	3D	700	600	515	635	4·92	0·140	5·8	29·4	90·0	70·5	930	8·37	50·0	—	315
	5D	700	610	530	640	4·42	0·0496	5·8	16·2	95·5	25·6	868	8·30	6·6	—	280
	6D	700	625	635	710	1·77	0·0450	5·8	25·9	81·5	23·1	878	7·16	4·4	—	250

phase analyses were considered more reliable than the determinations of zinc in the outlet lead.

Evaluation of over-all transfer units

By definition, for dilute systems "the number of over-all gas phase transfer units" (N_{OG}) is given by equation (1):

$$N_{OG} = \int_{y_2}^{y_1} \frac{dy}{y - y_e} \qquad (1)$$

For a particular absorption column of packed height Z, the number of transfer units and the height of a transfer unit are related:

$$Z = H_{OG} \cdot N_{OG} \qquad (2)$$

If the equilibrium line is linear, N_{OG} can be calculated from the terminal concentrations:

$$N_{OG} = \frac{y_1 - y_2}{(y - y_e)_{L.M.}} \qquad (3)$$

and if $y_e = 0$

$$N_{OG} = \ln\left(\frac{y_1}{y_2}\right) \qquad (4)$$

For the small column used in this investigation experimental difficulty precluded direct measurement of the terms required to rigorously evaluate equation (1); only the terminal values were measured and the intermediate conditions evaluated using two assumptions.

An exponential decrease of the gas phase zinc concentration from the bottom to the top of the column was assumed. As the equilibrium zinc partial pressures for the alloys formed in these studies were usually small, the assumption made was unlikely to introduce any serious error.

The second assumption made was that the lead temperature was linearly related to the position in the column. As the exit lead temperature was in no case greater than 1·35 times the inlet temperature, the more straightforward linear relationship was used rather than an exponential.

Under the conditions of this investigation, only a slight error was introduced if N_{OG} was evaluated by equation (3), using the terminal conditions only. As the difference between the two methods of evaluating N_{OG} was small, the simpler procedure was used throughout to evaluate N_{OG} and hence H_{OG}. The values of N_{OG} and H_{OG} obtained using equation (3) are given in Table 4. The equilibrium zinc partial pressures used in the calculations were based on the free energy change equations of KELLEY [3] and LUMSDEN [4], respectively, for the vapour pressure of pure zinc and the zinc activity coefficient in lead–zinc alloys.

Table 4. Calculated values of N_{OG} and H_{OG}

Series A						
Run	1A	2A	3A	4A	5A	6A
N_{OG}	3·95	5·71	4·62	4·33	4·72	5·03
H_{OG} (ft)	0·45	0·31	0·39	0·41	0·38	0·35
Series B						
Run	1B	2B	3B	4B	5B	6B
N_{OG}	1·67	2·56	3·70	—	4·65	5·06
H_{OG} (ft)	1·07	0·70	0·48	—	0·38	0·35
Series C						
Run	1C	2C	3C	4C	5C	6C
N_{OG}	1·15	1·58	1·78	—	1·65	1·86
H_{OG} (ft)	1·55	1·13	1·00	—	1·09	0·96
Series D						
Run	1D	2D	3D	4D	5D	6D
N_{OG}	—	2·58	2·57	—	3·65	3·66
H_{OG} (ft)	—	0·68	0·68	—	0·48	0·48

ADDITIVE DIFFUSIONAL RESISTANCE ANALYSIS

For the countercurrent absorption of zinc vapour in molten lead in a packed column, the temperature of the liquid lead changes appreciably as it flows through the absorption column, and the equilibrium conditions alter according to the position in the column because the zinc activity coefficient and the vapour pressure of pure zinc vary greatly with temperature.

As the absorptions of this investigation were carried out in very dilute alloys, Henry's law could be assumed to apply for each temperature level within the absorption column. Hence the equilibrium zinc partial pressure over the alloys formed by absorption, for a particular temperature, are linearly related to the zinc concentration in the liquid lead alloy; i.e. the mole fraction (y_e) of zinc in the gas phase, which is in equilibrium with a zinc mole fraction of (x) the liquid lead phase can be given by the following equations:

VOL 11 1959

$$p_{Zn} = x\,\gamma_{Zn}\,p^{\circ}_{Zn} \tag{5}$$

$$\therefore y_e = \frac{p^{\circ}_{Zn}\,\gamma_{Zn}}{P_T} \cdot x \tag{6}$$

The equilibrium conditions in a system in which molten lead is contacted with zinc vapour can therefore be represented, for the case of very dilute alloys, by a series of straight lines of slope $(p^{\circ}_{Zn}\,\gamma_{Zn})/P_T$ for each lead temperature. If the equilibrium conditions are considered in this light, the fundamental equation (7) can be derived for the absorption of zinc vapour in molten lead, using the additive diffusional resistance concepts.

$$Z = \frac{G_m}{P}\int_{y_2}^{y_1}\frac{dy}{K_g a\,(y-y_e)} = \frac{G_m}{P}\int_{y_2}^{y_1}\frac{dy}{k_g a\,(y-y_e)} + \\ + G_m\int_{y_2}^{y_1}\frac{(p^{\circ}_{Zn}\,\gamma_{Zn})\,dy}{P_T\,k_L a\,\rho_m\,(y-y_e)} \tag{7}$$

This equation can be simplified somewhat if the individual film coefficients are assumed constant throughout the column (strictly only correct for isothermal dilute systems) and the equation rewritten in terms of transfer units as shown in equation (8).

$$\therefore H_{OG} = H_G + \frac{G_m}{L_m}\frac{H_L}{N_{OG}}\int_{y_2}^{y_1}\frac{(p^{\circ}_{Zn}\,\gamma_{Zn})}{P_T}\,\frac{dy}{y-y_e} \tag{8}$$

As the value of H_{OG} is proportional to the over-all resistance to mass transfer, equation (8) can be considered as a statement of the addition of diffusional resistances of the individual phases. The first term in the R.H.S. of equation (8) is a measure of the resistance to mass transfer in the gas phase and the second term accounts for resistance in the liquid lead phase.

Interpretation of the experimental results in terms of equation (8) was not possible by further experimentation on the high temperature system and hence two room-temperature analogues of the lead–zinc absorption column were constructed. The extension of the data derived from the low temperature models to the absorption of zinc vapour in molten lead required a critical examination of the methods of correlating gas and liquid film mass transfer data. The empirical correlation methods are therefore briefly reviewed in the appendix.

Room temperature absorption model

To develop correlations for estimating the height of a gas film transfer unit and the height of a liquid film transfer unit, ammonia and carbon dioxide were absorbed in water using the same tower packing as used in the zinc absorption experiments. So that conditions in this low temperature model would simulate absorption of zinc vapour by molten lead, the tower walls and packing were made non-wetting, with respect to the irrigating liquid, by treatment with paraffin wax.

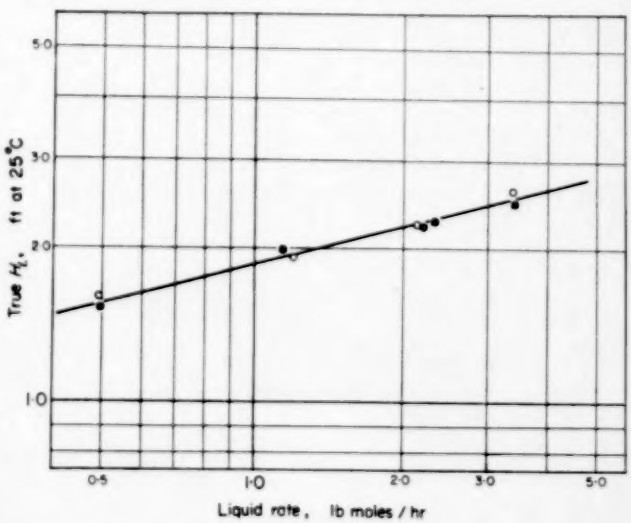

FIG. 5. Carbon dioxide absorption in water. True heights of liquid film transfer units.
● Non-wetting 21 in. bed.
○ Non-wetting 10·5 in. bed.

The experimental techniques used in the room temperature absorption model were the same as used by STEPHENS and MORRIS [2] and TAYLOR and ROBERTS [5] for calibrating a disk column for physical absorption. As these and similar techniques have been used frequently by other investigators, the experimental methods contained no novel features and therefore the end results only are presented in Figs. 5 and 6. The heights of transfer units plotted have been

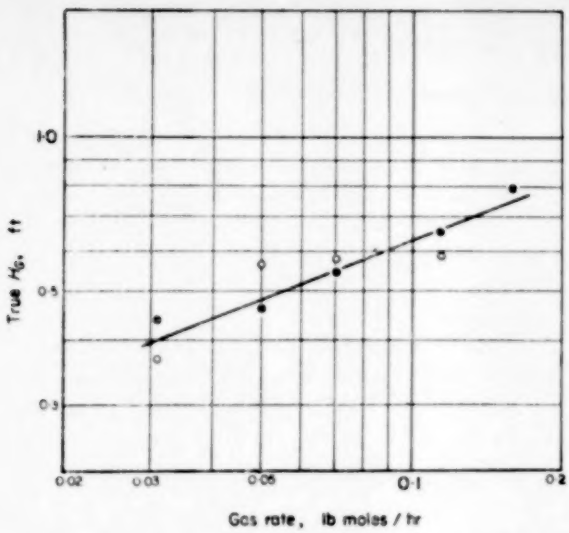

FIG. 6. Ammonia absorption in water. True heights of gas film transfer units.
(Constant water rate = 1·32 lb mole/hr)
● Non-wetting 21 in. bed.
○ Non-wetting 10·5 in. bed.

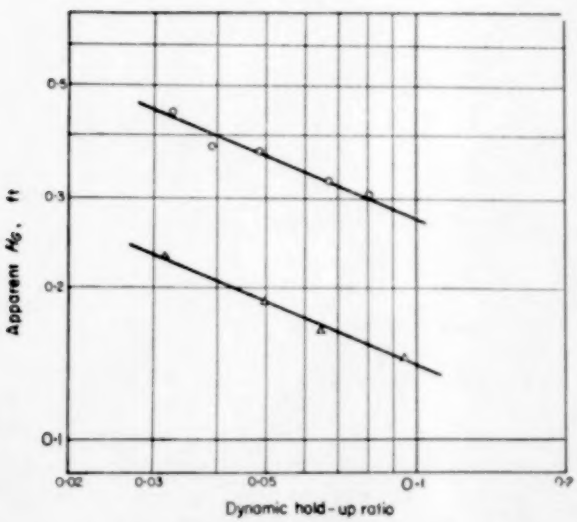

FIG. 7. Ammonia absorption in water. The effect of dynamic hold-up ratio.
(Constant air rate = 0·0705 lb mole/hr)
○ Non-wetting 10·5 in. bed.
Δ Wetting 10·5 in. bed.

corrected for end effects. The same correction of 4·8 in. of additional packed height was required for both absorptions to bring into line data derived from beds of 10·5 and 21 in. packed height.

The effect of liquid rate on the height of a gas film transfer unit is given in Fig. 7, which shows that H_G varies with $H_E^{-0.42}$. The choice of the effective hold-up ratio for studying liquid rate effects in gas phase mass transfer is discussed in the appendix. For the ammonia absorptions the effective hold-up ratio is considered to be the dynamic hold-up.

Estimation of molten lead hold-up and velocity

A second room-temperature analogue of the zinc absorption column, employing mercury as irrigating liquid metal with hydrogen and nitrogen as the countercurrent flowing gas phase, was used to estimate the hold-up and average liquid velocities. The total hold-up of liquid lead under the operating conditions for each zinc absorption run was estimated from the observed pressure drop across the column, the gas mass flow rate and the mean gas temperature and pressure in the bed. The estimation was a trial and error process of selecting values of total hold-up so that the experimental data cross-plotted the empirical correlation developed previously by the author [6] for mercury irrigation of the same bed. The estimated total liquid lead hold-ups for all runs are given in Table 3.

As only the total hold-up of lead could be estimated using this procedure, the dynamic liquid lead hold-up was determined as the difference of the estimated total hold-up under the particular operating conditions and the estimated total hold-up in the absence of irrigation.

The static hold-up of liquid lead in the packing was obtained by observing the pressure drop across the column, the gas mass flow rate and the mean gas temperature and pressure inside the bed immediately after the completion of an experimental run with the lead pump shut off. Examination of the value of hold-up thus obtained revealed that, prior to Run 5A, the hold-up of liquid lead was below "saturation level" and it was only after the high liquid lead rate of Run 5A that the static hold-up sites in the packing were completely occupied by semi-stagnant liquid lead. After Run 4A, the estimated

static hold-ups remained fairly constant at approximately 180 ml of liquid lead.

The average linear velocity of water and mercury flowing under non-wetting conditions in the packing was experimentally determined by recording the time taken for the liquid phase to flow over a measured height of previously "saturated" packing.

As the liquid velocity was required to estimate the gas–liquid relative velocity in the packed bed, the high gas velocities associated with the zinc absorption data enabled the lead velocity to be adequately estimated for the purpose of this investigation by assuming the lead velocity to be equal to the mercury velocity at the same volumetric flow rate.

VOL. 11 959/60

Location of the controlling diffusional resistance

The fraction of the total diffusional resistance which is located in the liquid lead phase can be expressed by rearrangement of equation (8).

Fraction of Total Resistance in Liquid Lead Phase =

$$\frac{(G_m/L_m)(H_L/N_{OG})\int_{y_2}^{y_1}[p^{\circ}_{Zn}\gamma_{Zn}/P_T(y-y_e)]\,dy}{H_{OG}} \qquad (9)$$

As in the evaluation of the number of transfer units, an exponential decrease in the gas phase zinc concentration from the bottom to the top of the column and a linear relationship between lead temperature and position in the column were assumed to evaluate the integral.

The estimation of H_L for zinc absorption in molten lead required the application of the empirical correlation methods, discussed in the appendix, to the data derived from the carbon dioxide absorptions in water. The diffusivity of zinc in molten lead was estimated using the STOKES–EINSTEIN equation with the ionic radius as the size of the diffusing species. The zinc ionic radius was used because the published diffusion data of various metals in mercury support the concept of the movement of metals free of their conductance electrons in the liquid state.

For example in Run 2D:

$$\int_{y_2}^{y_1}\frac{p^{\circ}_{Zn}\gamma_{Zn}\cdot dy}{P_T(y-y_e)} = 1{\cdot}104 \text{ by graphical integration}$$

and $(H_L)_{Zn-Pb} = 0{\cdot}115$ ft

$\therefore$ Fraction of total resistance in liquid lead phase $= 0{\cdot}0041$.

Hence, for Run 2D, only 0·4 per cent of the total resistance to mass transfer is located in the liquid lead phase. Similar calculations on the other runs indicated that the liquid lead phase resistances were negligible, under the conditions of the zinc absorptions carried out in this investigation.

It is important to note that the experimental conditions determine the contribution which the liquid lead phase makes to the over-all mass transfer resistance. Thus, for example, if the experiments were carried out at very high gas rates, very low liquid lead rates and much higher temperatures inspection of the equation (9) indicates that the fractional resistance of the lead phase could then become appreciable.

For the experimental conditions of this investigation, the absorption of zinc vapour in molten lead is clearly controlled by the diffusional resistance in the gas phase, and any resistance in the liquid lead phase can be neglected.

Under these conditions equation (8) reduces to

$$H_{OG} = H_G \qquad (10)$$

COMPARISON OF ZINC AND AMMONIA ABSORPTION

A comparison of the heights of gas film transfer units for zinc vapour absorption in molten lead with those for ammonia absorption in water permitted an evaluation of the gas phase empirical correlation methods for predicting absorption rates of metallic vapours in liquid metals at elevated temperatures, an application far beyond the hitherto restricted range of such correlations.

As a preliminary analysis of the zinc absorption data revealed anomalies when the inlet zinc partial pressure was less than 1 mm Hg, such data are excluded from the correlation of zinc and ammonia

absorptions and the reasons for the omission discussed later.

One packed height was used in the zinc absorption experiments and the results must be considered as apparent values of H_{OG} or H_G. It seems reasonable to assume that the end effects associated with the zinc absorptions are approximately equal to those measured in the room temperature analogue. Therefore, these apparent values were converted to true heights of transfer units by assuming the end effects were equivalent to another 4·8 in. of packed height, before the comparison with the ammonia absorption data was made.

In ammonia absorption, the dynamic hold-up is the effective component of the total liquid in the bed during the absorption. Therefore, as a logical start to the comparison of the two absorption processes the conventional form of correlation given by equation (13) was used, with the dynamic hold-up being considered as the effective component in both cases. The exponent on the effective hold-up ratio was previously determined as $-0{\cdot}42$.

Inspection of the data plotted as $H_G\,Sc^{-0{\cdot}67}\,H_D^{0{\cdot}42}$ vs. $v_g\rho/\mu$ on a log–log graph showed that all the zinc absorption runs up to and including Run 3B fell significantly below the ammonia data, whilst the points for runs after Run 3B were displaced above. The significance of this was not at first realized. It was only after a search of the experimental records, that the cause of the displacement of the data was believed to have been identified. At the conclusion of Run 3B, the stainless steel inlet analysis sampling line broke due to a combination of gross overheating and zinc attack with the result that the static hold-up of liquid lead in the column at the conclusion of Run 3B was exposed to oxidizing conditions for about 15 min and became drossed up. It is not envisaged, however, that the liquid lead was completely converted to dross but merely drossed on the surface. Had the static hold-up been completely drossed, the volume of hold-up would have changed considerably, but hold-up estimations showed that the static hold-up volume was not significantly different after Run 3B than it was in the earlier runs once the packing had all its static hold-up sites occupied (i.e. after Run 4A).

The significant feature, which determines the effectiveness of the semi-stagnant static hold-up in an absorption process, is the rate of movement of this component through the packing. For water irrigation of the packing, the rate of movement is very slow and hence equilibrium in the static hold-up is reached and it is then no longer effective for absorption. However, if the semi-stagnant static hold-up moves through the packing at a rate only slightly less than the recognised flowing component (i.e. dynamic hold-up), then the static hold-up could be equally as effective as the dynamic hold-up.

It is suggested that the rate of movement of a liquid metal or similar dense medium static hold-up in a packed column would be considerably greater than that which has been observed for water. The higher kinetic energy of the flowing component could have the effect of "knocking-on" or displacing the semi-stagnant liquid through the sites of static hold-up, thereby increasing the over-all rate of movement of the so-called static hold-up under irrigated conditions. Evidence of this increased mobility was given previously when the observed effect of liquid rate on static hold-up of mercury was discussed by the author [6], whereas the static hold-up is unaffected by liquid rate when water is the irrigating phase.

It is therefore tentatively proposed, pending further experimentation, that the concept of effective interfacial area for liquid metals irrigating a packing be modified to take into account the increased mobility of the semi-stagnant liquid and the so-called static hold-up considered effective in an absorption process involving the flow of a liquid metal or similar medium. It is likewise considered that the non-wetting flow of the liquid metal also facilitates an increased mobility of the semi-stagnant liquid hold-up. If the free flow of the static hold-up was impaired by dross formation or similar effects, the mobility would be seriously affected and the movement would most likely be completely arrested or slowed down to such an extent that equilibrium would be reached and the surface rendered ineffective for further absorption.

VOL. 11 959/60

A qualitative test was run to check the assumption that dross formation would prevent free movement of the lead retained by the rings. A quantity of steel rings was irrigated with molten lead and then partially oxidized. The rings were then quickly shaken before the lead froze. An examination of the rings, after such treatment, indicated that the drossed lead droplets were retained by the packing. A similar test carried out on clean mercury-irrigated packing showed that the mercury could be readily shaken from the packing.

In view of the preceding discussion, it was therefore assumed that the total hold-up of liquid lead up to and including Run 3B was effective for absorption. After Run 3B only the dynamic hold-up was considered to be effective for absorption, as the movement of the static hold-up would have been arrested by dross formation.

The correlation of the data obtained after making the appropriate amendment to the effective hold-up ratio is shown in Fig. 8.

The displacement of the zinc absorption data above the ammonia data in Fig. 8 could possibly be due to a deficiency in the estimated values of Schmidt number or effective hold-up ratio, but it also suggests that the Reynolds number, based on the gas velocity, is not a good correlating modulus, as the ammonia data of these studies are particularly sensitive to a relative velocity correction.

As a check to see if the gas inertia is the better correlating modulus, as suggested by equation (15), the data were replotted in Fig. 9 using the same ordinate as in Fig. 8 but with $(v_g^2 \rho)^{0.5}$ as the abscissa. The square root of the gas inertia was used in this plot so as to retain the same gas velocity dependency as in the previous graph.

The vertical displacement of the two sets of data has been overcome using this method of correlation, and the data in Fig. 9 can be well represented by a single straight line.

As the newly defined "relative j_D" factor, developed by the author [7] from gas phase mass transfer studies with a disk column, is believed to have general application to all mass transfer studies, the new type of correlation proposed by equation (16), in which the relative interfacial

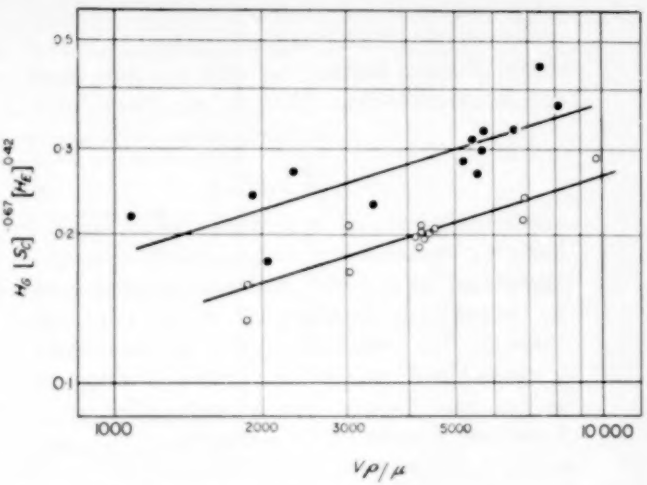

FIG. 8. Correlation of zinc and ammonia absorption data.
● Zinc absorption in lead.
○ Ammonia absorption in water.

velocity is considered the significant velocity term in the transfer process, was applied to the zinc and ammonia absorption data. The relative interfacial velocity used in the correlation of the data shown in Fig. 10 was taken as the sum of the gas and liquid phase average linear velocities.

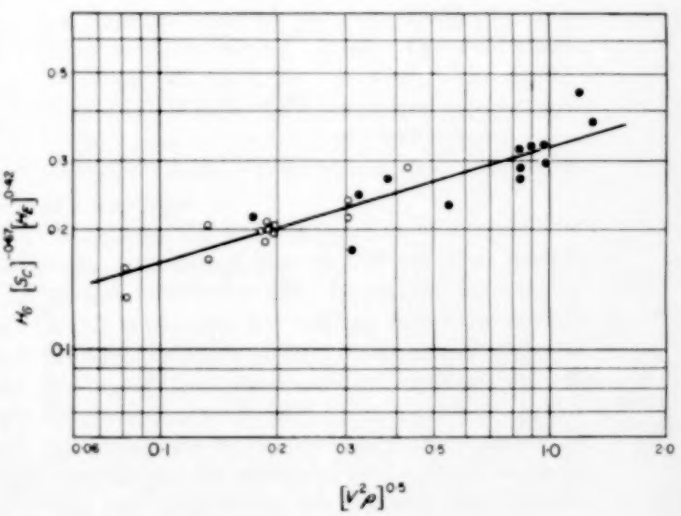

FIG. 9. Correlation of zinc and ammonia absorption data.
● Zinc absorption in lead.
○ Amonnia absorption in water.

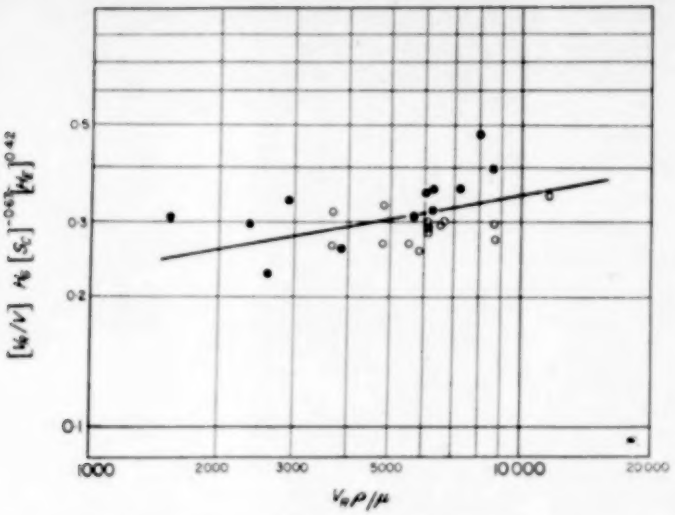

Fig. 10. Correlation of zinc and ammonia absorption data.
● Zinc absorption in lead. ○ Ammonia absorption in water.

Although the experimental points in Fig. 10 exhibit a degree of scatter, the data can be represented by the single full line drawn on the graph. This is in marked contrast to the obvious displacement of the two sets of data obtained for the conventional type of correlation using the gas velocity as the significant velocity term, as can be seen by comparing Fig. 8 with Fig. 10.

As indicated previously, the zinc absorption runs, in which the inlet zinc partial pressure was

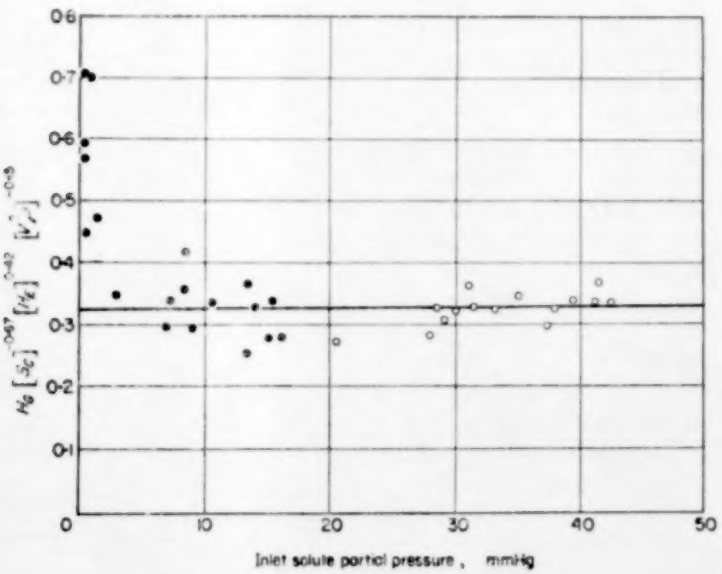

Fig. 11. The effect of inlet solute partial pressure.
● Zinc absorption in lead. ○ Ammonia absorption in water.

VOL 11 1959

less than 1 mm Hg, were excluded from the preceding analysis. The anomalous behaviour of these very low zinc inlet partial pressure runs can be seen by selecting the correlation form, observed as fitting the other data with the least scatter, and replotting the data in such a form as to show the effect of inlet solute partial pressure.

Thus Fig. 11 is a plot of $H_G\,(\mathrm{Sc})^{0\cdot67}\,(H_E)^{0\cdot42}\,(v_g^2\rho)^{-0\cdot15}$ versus solute partial pressure. Theory predicts that there would be no variation of the group plotted with the inlet partial pressure of the diffusing species.

As can be seen from Fig. 11, there is clearly some extraneous factor coming into the analysis, when the zinc inlet partial pressures are less than about 1 mm Hg. At these very low zinc concentrations, errors in the analytical procedures could be expected but these can hardly account for the very pronounced and consistent effect observed. The only feasible explanation appears to be that the low zinc partial pressures were not effective in removing the oxygen and carbon dioxide from the gas circulation system before the runs were commenced.

If there were no leaks in the system, any oxygen contamination would have been eliminated by reaction with zinc vapour well before the runs were commenced, because the nitrogen was recycled. Thereafter, the only oxygen which could enter the system would be in the small commercial grade nitrogen make-up to compensate for leaks in the system, as the entire system was maintained above atmospheric pressure. As this nitrogen passed through a bed of granulated charcoal maintained at 1,000°C before coming into contact with the zinc vapour in the boiler, the effects of oxygen or carbon dioxide contamination could normally be considered as being eliminated.

However, in the low zinc partial pressure runs, it is considered that the quantitative removal of oxygen and the conversion of carbon dioxide to carbon monoxide was not completed before the runs were commenced because of insufficient zinc being present. Under these conditions, part of the zinc entering the absorption column would be as zinc oxide, which would pass through the column in particulate form without being absorbed by the molten lead. As the gas phase analysis methods used in the investigation could not detect any difference between zinc oxide and zinc vapour, the gas phase analyses under these very low inlet zinc partial pressure conditions would not be truly representative of the actual zinc vapour present.

Conclusion

These studies clearly show the absorption of zinc vapour in molten lead to be a diffusion controlled mass transfer operation, which is fundamentally the same as a conventional gas absorption carried out at room temperature with aqueous or organic liquids as the absorbing liquid phase.

The contacting of zinc vapour with molten lead, in such processes as the recently developed zinc blast furnace, should be considered as an absorption not a condensation and the units used should be termed absorbers not condensers. The use of the nomenclature existing at present in metallurgical industry, in which the zinc vapour – molten lead contacting chamber is called a condenser, can lead to erroneous conclusions being drawn with respect to the potential performance of such units. These units may be operated with neither the lead or gas temperatures below the dew point of the zinc vapour as can be seen by noting the temperature conditions of Runs 2D and 6D, for example. In these runs, the lead temperatures were at no stage below the dew point of the inlet zinc vapour. The dew points for Runs 2D and 6D are 573°C and 576°C, respectively, whereas the lowest lead temperature in these runs were 610°C and 635°C, respectively. Such performance obviously could not be expected of a condenser.

The most important effect of lead temperature is in determining the equilibrium zinc partial pressure above the alloy formed by absorption. If this is less than the bulk gas phase zinc partial pressure, diffusion of zinc from the gas phase to the liquid lead phase can be expected and, if sufficient time is allowed, the concentration in the gas phase will be reduced until the equilibrium condition for the particular lead surface composition and temperature are reached, even though the gas is at no stage cooled to the dew point of its zinc vapour content.

Besides the equilibrium restriction in determining the direction of the mass transfer, the other factor which limits the temperature of the lead phase is that increased lead temperatures result in increased vaporization of the liquid lead, although even operation at temperatures approaching 1,000°C, the losses of lead would be very small. (Vapour pressure of lead at 987°C = 1 mm Hg).

Of the types of correlations discussed for gas phase mass transfer, the form based on the gas inertia or the relative interfacial velocity gave the best correlation of the zinc absorption in molten lead and the ammonia absorption in water data. The correlations using the gas inertia appears slightly superior, but the relative merits of the two methods cannot be definitely established until further experimental work is undertaken. Despite the slightly better correlation obtained when the gas inertia is used, it is considered that the form of correlation using the relative interfacial velocity is fundamentally the best approach to the examination of a gas phase mass transfer in a packed column.

The mobility of the semi-stagnant liquid hold-up was of considerable importance in assessing the effective hold-up of liquid lead used in the interpretation of the zinc absorption data. It was suggested that the total liquid lead hold-up was effective prior to the static hold-up becoming partially drossed, and thereafter only the dynamic hold-up was considered effective in the absorption process.

Although the absorptions of zinc vapour in molten lead were controlled by the diffusional resistance of the gas phase under the conditions of this investigation, the contribution of the liquid lead phase to the over-all mass transfer resistance depends entirely on the conditions under which the absorption is carried out, as can be seen by inspection of the fundamental equation derived:

$$H_{OG} = H_G + \frac{G_m H_L}{L_m N_{OG}} \int_{y_2}^{y_1} \frac{\mathring{p}_{Z_n} \gamma_{Z_n}}{P_T (y - y_e)} \cdot dy$$

If the value of the second term on the R.H.S. of the above equation had been significant the interpretation of the zinc absorption data would have been very much more difficult, particularly as the values of H_L should strictly also be included within the integral, because of the variation of liquid phase Schmidt number associated with the different inlet and outlet lead temperatures.

Throughout this investigation the principal interest has been directed towards the analysis of gas phase controlled absorptions. For the absorption of a metallic vapour in a liquid metal at an elevated temperature, in which the principal diffusional resistance is located in the liquid phase, further research is definitely indicated.

The application of room temperature analogues, for investigating experimentally difficult high temperature operations, has been demonstrated in these studies. The zinc absorption in molten lead and the absorption of ammonia in water can be directly compared using appropriate empirical correlations suitably modified to contain the essential parameters of relative performance.

VOL 11 1959

Appendix

Empirical Mass Transfer Correlations

(1) *Correlation of liquid phase data*

Sherwood and Holloway [8] proposed that packed column liquid phase data be correlated according to equation (11):

$$H_L = \alpha \left(\frac{L}{\mu}\right)^n \left(\frac{\mu}{\rho_D}\right)^s \qquad (11)$$

Sherwood and Holloway investigated a wide range of systems, with the result that the exponent (s) on the Schmidt number was found to be 0·33 in equation (11).

The values of the exponent (n) and the constant (α) depend on the size and type of packing, the nature of the surface of the packing and the type of flow, whether wetting or non-wetting, and therefore must be determined experimentally on the type and size of packing and flow for which the correlation is being developed.

(2) *Correlation of gas phase data*

Yoshida [9] chose to correlate his data, for the vaporization of water by a series of gases in a packed column, by a form similar to that used by Sherwood and Holloway for liquid phase data. Equivalent forms in terms of the mass transfer coefficients have been used by many investigators of gas phase mass transfer. Modification of these forms to include the true rather than superficial gas velocity gives equation (12), which may be considered as the conventional method of correlating gas phase data.

$$H_G = \beta L^a \left(\frac{v_g \rho}{\mu}\right)^b \left(\frac{\mu}{\rho_D}\right)^c \qquad (12)$$

The use of the superficial liquid phase mass velocity, to account for the observed effect of liquid rate on gas phase mass transfer, is considered to be the principal weakness of these correlations, when examined from the aspect of application to the zinc absorption studies of this investigation. If the correlation is developed by experimentation with aqueous systems, the extension of the correlation to a system, in which the liquid phase is molten lead, would be extremely questionable. Therefore, rather than using a liquid rate in the correlation, a term indicating the actual volume of liquid present in the packing, which is effective for absorption, should be used in the correlation. It is proposed that the dimensionless quantity "the effective hold-up ratio" H_E be introduced for this purpose. The "effective hold-up ratio" to be defined as the volume of liquid in the packing, which is effective in absorption, divided by the volume of the packed bed. By the introduction of this term, it is considered that a compromise has been reached between the use of effective interfacial area as suggested by SHULMAN *et al.* [10, 11, 12] and the more readily achieved procedure of evaluating transfer rates per unit packed bed volume. Equation (12) can then be modified to the new form given in equation (13).

$$H_G = \beta' \left(\frac{v_g \rho}{\mu}\right)^b \left(\frac{\mu}{\rho D}\right)^c H_E{}^d \qquad (13)$$

LYNCH and WILKE [13] proposed that the rate of mass transfer may be a function of the inertia of the gas stream ($v_g{}^2 \rho$) at high flow rates rather than the Reynolds number. The form of correlation suggested is given in equation 14.

$$H_G = \phi \left[(v_g{}^2 \rho), \left(\frac{\mu}{\rho D}\right) \right] \qquad (14)$$

Equation (14) was proposed tentatively pending further study. Although these workers successfully correlated their data by such a method, their data can also be correlated conventionally, if the effects of interfacial velocity are taken into account, as demonstrated previously by the author [6]. As no real assessment of the merits of equation (14) can be made until further experimental work is undertaken, a modified form involving the newly proposed effective hold-up ratio, as shown in equation (15), was also considered as a possible basis for the correlation of the zinc absorption data.

$$H_G = \beta'' (v_g{}^2 \rho)^e \left(\frac{\mu}{\rho D}\right)^c H_E{}^d \qquad (15)$$

The exponent of the Schmidt number in equations (12) to (15) is considered to be $\frac{1}{3}$. The investigations supporting this exponent are very numerous. Although the recent studies of LYNCH and WILKE [12] and YOSHIDA [8] obtained different exponents on the Schmidt number, these are believed to be due to interfacial velocity effects masking the true effect of the diffusivity, as was proposed previously by the author [6].

The author's gas phase mass transfer studies [6] resulted in the introduction of a newly defined mass transfer factor, "the relative j_D factor," in which the significant velocity term in the mass transfer process is taken to be the relative interfacial velocity, rather than the true gas velocity. As the use of this new approach is considered to have general application, a possible form of correlating the zinc absorption data of this investigation would be an equation derived from the "relative j_D factor" as given by equation (16).

$$H_G \cdot \left(\frac{v_R}{v_g}\right) = \beta''' \left(\frac{v_R \rho}{\mu}\right)^f \left(\frac{\mu}{\rho D}\right)^{2/3} H_E{}^d \qquad (16)$$

Acknowledgements—Sincere thanks are due to Professor J. P. BAXTER, School of Chemical Engineering and Vice-Chancellor, University of New South Wales, for suggesting the research topic and for his continued interest and support throughout the project.

The numerous helpful discussions with Dr. G. H. ROPER, School of Chemical Engineering, are gratefully acknowledged.

Acknowledgement is also made to the Monsanto Chemical Co. (Aust.), for the provision of the research scholarship in 1953, under which the research programme was initiated, and to the Broken Hill Associated Smelters Ltd., who kindly loaned the lead used in the investigation.

NOMENCLATURE

D	= diffusion coefficient	ft²/sec
G_m	= superfical molar mass velocity of the gas phase	lb mole/sec ft²
H_D	= dynamic hold-up ratio	
H_E	= effective hold-up ratio	
H_G	= height of a gas film transfer unit	ft
H_{OG}	= height of an over-all gas phase transfer unit	ft
H_L	= height of a liquid film transfer unit	ft
$K_g a$	= over-all volumetric gas phase coefficient	lb mole/sec ft³ atm
$\kappa_g a$	= volumetric gas film coefficient	lb mole/sec ft³ atm
$k_L a$	= volumetric liquid film coefficient	lb mole/sec ft³ unit ΔC
L	= superficial mass velocity of the liquid phase	lb/sec ft²
L_m	= superficial molar mass velocity of the liquid phase	lb mole/sec ft²
N_{OG}	= number of over-all gas phase transfer units	
P	= total pressure in the system	atm
P_T	= total pressure on system	mm Hg
p°_{Zn}	= equilibrium vapour pressure of pure zinc	mm Hg
p_{Zn}	= partial pressure of zinc in gas phase	mm Hg
Sc	= Schmidt number = $(\mu/\rho D)$	dimensionless
v_g	= true gas velocity	ft/sec

v_R = relative velocity of the gas and liquid streams ft/sec
x = mole fraction of zinc in liquid lead
y = mole fraction of zinc in the gas phase
Z = height of packed section of absorption column ft
a, b, c, d, e, f, n, s = exponents in empirical equations
$\alpha, \beta, \beta', \beta'', \beta'''$ = constants in empirical equations
γ_{Zn} = activity coefficient of zinc in liquid lead–zinc alloy (standard state pure liquid zinc at the same temperature)

ρ = fluid density lb/ft^3
ρ_m = molar density lb mole/ft^3
μ = fluid viscosity lb/ft sec

Subscripts

1 = concentrated end of countercurrent system
2 = dilute end of countercurrent system
e = equilibrium value
L.M. = logarithmic mean

REFERENCES

[1] MORGAN S. W. K. *Trans. Inst. Min. Metall.* 1957 **66** 553.

[2] STEPHENS E. J. and MORRIS G. A. *Chem. Engng. Progr.* 1951 **47** 232.

[3] KELLEY K. K. *Bull. U.S. Bur. Min.* 1935 **383** 109.

[4] LUMSDEN J. *Disc. Faraday Soc.* 1948 No. 4 60.

[5] TAYLOR R. F. and ROBERTS F. *Chem. Engng. Sci.* 1956 **5** 168.

[6] WARNER N. A. *Chem. Engng. Sci.* This issue p. 149.

[7] WARNER N. A. *Chem. Engng. Sci.* 1959 **11** 130.

[8] SHERWOOD, T. K. and HOLLOWAY F. A. L. *Trans. Amer. Inst. Chem. Engrs.* 1940 **36** 39.

[9] YOSHIDA F. *Chem. Engng. Progr.* (Symposium Series, No. 16) 1955 **51** 59.

[10] SHULMAN H. L., ULLRICH C. F., PROULX A. Z. and ZIMMERMAN J. O. *Amer. Inst. Chem. Engrs. J.* 1955 **1** 253.

[11] SHULMAN H. L., ULLRICH C. F. and WELLS N. *Amer. Inst. Chem. Engrs. J.* 1955 **1** 247.

[12] SHULMAN H. L., ULLRICH C. F., WELLS N. and PROULX A. Z. *Amer. Inst. Chem. Engrs. J.* 1955 **1** 259.

[13] LYNCH E. J. and WILKE C. R. *Amer. Inst. Chem. Engrs. J.* 1955 **1** 9.

VOL 11 1959

Chemical Engineering Science, 1959, Vol. 11, pp. 183 to 193. Pergamon Press Ltd., London. Printed in Great Britain

Conserved-property diagrams for rate-process calculations—I

Comparison of known diagrams

D. B. SPALDING
Imperial College, London, S.W.7

(*Received* 2 *January* 1959)

Abstract—The paper compares three known methods of representing the enthalpy and composition of binary mixtures, namely those in which these properties are referred respectively to the mass of mixture, the number of moles of mixture, and the mass of one component of the mixture. The water–steam–air system is used as an example. Each of the diagrams can be used for calculating the rates of simultaneous transfer of heat and matter across a phase boundary. The graphical constructions necessary for determining the rates are described and their convenience discussed.

The paper is primarily an assembly of known facts, prepared as a starting-point for the demonstration, to follow in Part II, that the three charts are members of a much wider family, other members of which may be used with advantage in heat and mass transfer calculations.

Résumé—Ce mémoire compare trois méthodes connues de représentation de l'enthalpie et de la composition des mélanges binaires c'est-à-dire celles où ces propriétés se rapportent respectivement à la masse du mélange, au nombre de moles du mélange et à la masse de l'un des composants du mélange. Le système eau–vapeur–air est utilisé comme exemple. Chacun des diagrammes peut être utilisé pour le calcul des vitesses du transfert simultané de chaleur et de matière à travers la limite des phases. Les constructions graphiques nécessaires à la détermination des vitesses sont décrites et leurs avantages discutés.

Le mémoire compare d'abord un ensemble de faits connus servant de point de départ pour démontrer (à suivre dans la part II), que les trois diagrammes font partie d'une famille très vaste qui peut être utilisée avec avantage dans les calculs de transfert de chaleur et de masse.

Zusammenfassung—Diese Arbeit vergleicht drei bekannte Methoden zur Darstellung der Enthalpie und der Zusammensetzung von Zweistoffgemischen, insbesondere solche, in denen diese Grössen entweder auf die Masse der Mischung, die Molzahl der Mischung oder die Masse einer Komponente der Mischung bezogen sind. Das System Wasser Dampf–Luft wird als Beispiel verwendet. Jedes der Diagramme kann zur Berechnung von gleichzeitigem Wärme - und Stofftransport durch eine Phasengranzfläche verwendet werden. Die graphischen Konstruktionen zur Bestimmung der Übertragungsgeschwindigkeiten werden beschrieben und ihre Vorteile diskutiert.

Die Arbeit teilt im wesentlichen bekannte Tatsachen mit dient als Ausgangspunkt für den folgenden Teil II. Hier wird gezeigt, dass drei Diagramme Glieder einer viel grösseren Schar von Diagrammen sind ; andere Glieder dieser Schar können mit Vorteil für die Berechnungen der Wärme-und Stoffübertragung verwendet werden.

1. INTRODUCTION

1.1 *Representation of Thermodynamic Properties*

THE thermodynamic properties of binary and ternary mixtures are often represented by means of charts, the ordinate and abscissa of which are properties featuring in conservation laws. Examples are:

(a) The enthalpy-composition diagram for binary mixtures. This has been used in one form or another by PONCHON [1], SAVARIT [2], MOLLIER [3], KEENAN [4] and, perhaps most extensively, BOŠNJAKOVIĆ [5].

(b) The triangular diagram for ternary mixtures. This is often used for delineating the phase boundaries, and representing the isotherms, of mixtures encountered in solvent-extraction

processes (see for example SHERWOOD and PIGFORD [6], or TREYBAL [7]).

(c) The ternary mixture data are often re-plotted in the so-called "solvent-free co-ordinates." The charts are then similar in appearance to enthalpy-composition charts of the PONCHON type.

Recently, enthalpy-composition diagrams have been used, by BOŠNJAKOVIĆ [8, 9], POWELL [10], and SPALDING and TYLER [11], to represent the properties of equilibrium mixtures of substances which undergo chemical reaction when the mixture ratio changes. These are particularly important in combustion technology.

The mixing rule

All these diagrams have an important common feature: they obey the "Lever Rule" of mixing. This is illustrated in Fig. 1. It states that where two systems, each being a mixture of the two or three substances in question, are mixed adiabatically and at constant pressure, the state of the resulting mixture is represented by a point, Y, on the property diagram, which lies on the straight line joining the state-points X and Z of the initial systems. Further, Y divides XZ in such a ratio that

$$\frac{XY}{YZ} = \frac{\text{quantity of material in system Z}}{\text{quantity of material in system X}} \quad (1)$$

This means that Y lies at the correct point for the fulcrum of a lever (Fig. 1).

The "Lever Rule" holds because conserved properties (enthalpy, fractional concentration) are used as co-ordinates; it permits calculations involving material balances and the First Law of Thermodynamics to be represented, and indeed carried out, by simple graphical constructions.

The term "quantity of material," in the "Lever Rule," has to be interpreted differently according to the actual co-ordinates used. Sometimes it is measured in mass of mixture, sometimes in moles of mixture, and sometimes it refers to just a single one of the components.

If ternary mixtures are in question, the restriction to adiabatic constant-pressure processes in the "Lever Rule" can be dropped; then however only the composition of the final mixture is determined, not its temperature.

1.2 *Representation of Rate Processes*

Enthalpy-composition charts have also been used for the separate task of calculating the *rate* at which heat and mass transfer will occur when mixtures of different phases, compositions and temperatures are in contact. This was first done, it appears, by BUSEMANN [12]; the method has been extended recently by BOŠNJAKOVIĆ, who has applied it to water–steam–air mixtures [13, 14],

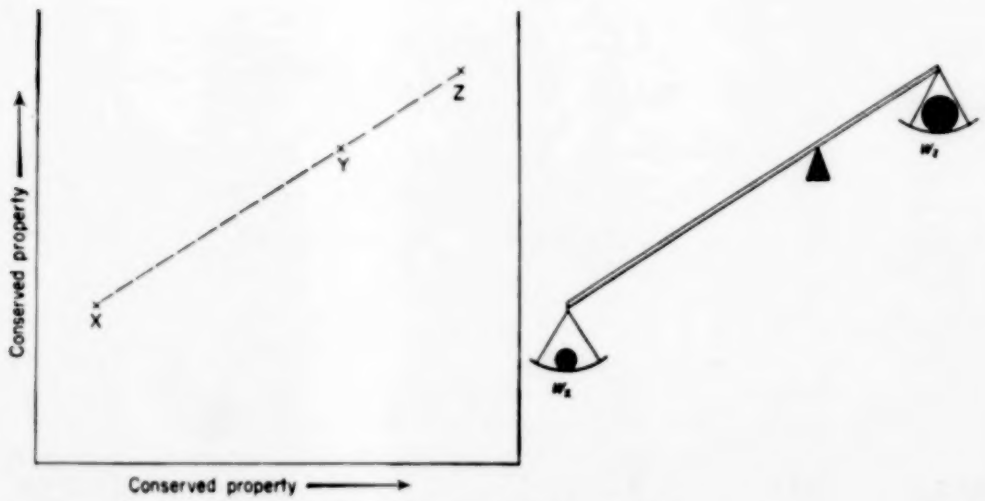

FIG. 1. Illustrating the "Lever Rule."

to chemical reactions catalysed on surfaces [8] and to the industrial gas-producer [9].

The method has the advantage, as compared with purely numerical methods, of introducing the non-linear inter-phase equilibrium relations, which provide boundary conditions in the rate-process calculations, without requiring trial-and-error. Its graphical nature enables calculations to be performed quickly and with little mental effort, and with an accuracy which is quite sufficient in view of the uncertainty in current knowledge of transfer coefficients, and even of interfacial areas, in chemical engineering equipment.

Similar methods have also been developed independently by the present author and applied to water–steam–air mixtures [15] and to the combustion of liquid and solid fuels [11].

VOL. 11 959/60

1.3 *Purpose and Content of the Present Paper*

The methods of BUSEMANN, BOŠNJAKOVIĆ and the present author exhibit both similarities and differences. The differences lie chiefly in the choice of co-ordinate system for the thermodynamic charts and in the details of the graphical calculations; the basic assumptions are very similar however.

The present paper has arisen out of the effort to compare the validity, convenience and accuracy of the various methods. Its main result is to show that a still wider variety of method exists; great freedom of choice of co-ordinate system is available and can be exploited with advantage. This will be discussed in Part II.

For the sake of concreteness, discussion is here restricted to the water–steam–air system, which is familiar from studies of psychrometry, drying, cooling-towers and the like. This means that one co-ordinate of the chart will represent composition and the other enthalpy. However, the theory to be presented is quite general; the substances may react chemically with each other to produce any number of other compounds; the concentration of a third material component may replace enthalpy as one co-ordinate; and indeed it is not even necessary that thermodynamic equilibrium should prevail throughout the whole physical system (though it must do so at certain points).

2. THREE TYPES OF ENTHALPY-COMPOSITION DIAGRAM COMPARED

2.1 *Description of Charts*

(a) "*Mass-of-mixture*" *basis*

Fig. 2(a) shows an enthalpy-composition chart for water–steam–air mixtures at 1 atm pressure. The horizontal co-ordinate, m, is the fractional mass concentration of H_2O (liquid and/or vapour) in the mixture; its units are lb_m H_2O/lb_m mixture; $m = 0$ for pure air, and $m = 1$ for pure water or steam.

The vertical co-ordinate, h, is the enthalpy in B.t.u/lb_m mixture. The enthalpy is defined arbitrarily as having the value zero for pure air at 32°F and for pure water at 32°F. The vapour-phase mixture is supposed to obey Dalton's Law (though this is not necessary for the major part of the subsequent argument). Solubility of air in water is neglected.

The body of the chart is divided into two regions by the curve marked "saturation line": above lies the steam-plus-air (vapour) region; below lies the steam-plus-air-plus-water (mixed-phase) region. The two regions are traversed by a few representative lines of constant temperature (isotherms). The region below 32°F is omitted as being of minor interest.

Charts such as Fig. 2(a) have been used by the present author [15]; in that reference however the $m = 0$ line was on the right of the diagram; here the $m = 0$ line has been placed on the left in order to conform with the two other diagrams which are to be discussed.

(b) "*Mole-of-mixture*" *basis*

Fig. 2(b) shows an enthalpy-composition chart for H_2O – air at 1 atm pressure which differs from Fig. 2(a) in having its enthalpy and composition based on the mole unit. Diagrams of this type have been presented by BOŠNJAKOVIĆ [14]. The abscissa, M, measures the composition as the number of lb moles of H_2O in the mixture divided by the sum of the number of lb moles of H_2O and the number of lb moles of air in the mixture; the units of M are abbreviated to "moles H_2O/moles mixture," for short. One lb mole of H_2O is

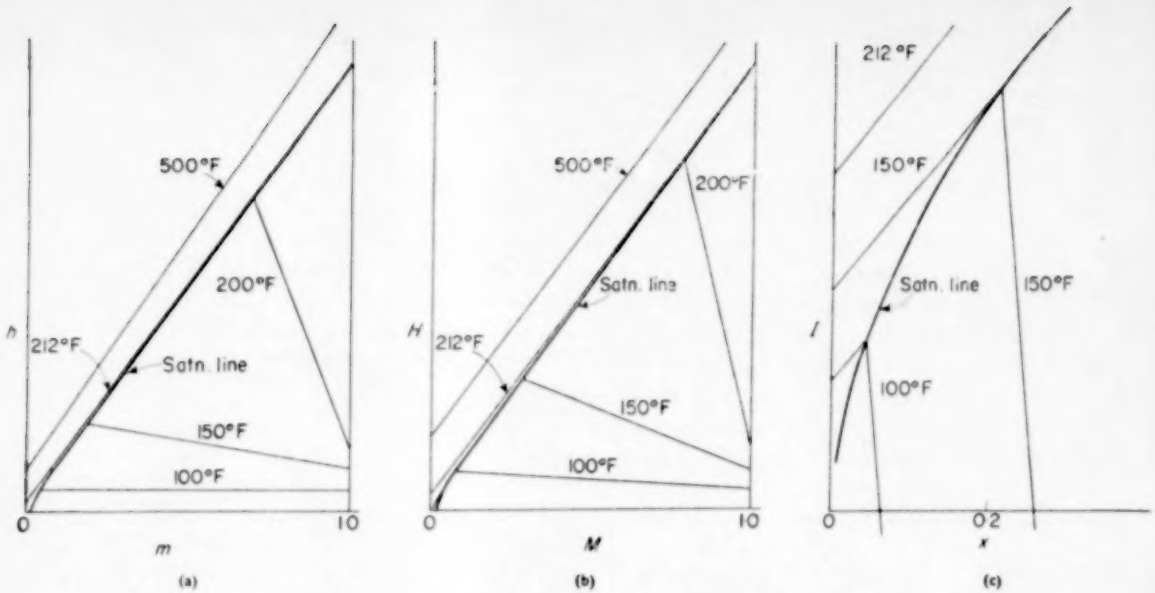

FIG. 2. Enthalpy-composition charts for H_2O – air at 1 atm pressure.

(a) "Mass-of-mixture" basis (b) "Moles-of-mixture" basis (c) "Mass-of-air" basis.

18 lb_m; and one lb mole of air is 29 lb_m. The "molecular weight" of the mixture (mass of mixture divided by sum of numbers of moles of H_2O and air) thus depends on composition (see section 2.2, equation 6). $M = 0$ for pure air and $M = 1$ for pure H_2O.

The vertical co-ordinate, H, is likewise the enthalpy in B.t.u/lb mole mixture. The zero state and other assumptions are the same as for the chart of Fig. 2(a).

The general appearance of the chart is similar to that of Fig. 2(a); but the gas-phase isotherms are rather more nearly parallel, and there are other distortions.

(c) "*Mass-of-air*" *basis*

Fig. 2(c) shows an enthalpy-composition chart, for H_2O – air at 1 atm pressure, of the type introduced by MOLLIER [3]. Its characteristic feature is that the co-ordinate properties are based on unit mass of air. Thus the abscissa, x, measures the composition as the number of lb_m of H_2O in the mixture divided by the number of lb_m of air in the mixture. So $x = 0$ for pure air; and $x = \infty$ for pure steam or water. Only the range $0 \leqslant x \leqslant 0{\cdot}3$ is covered by Fig. 2(c); but whatever the range, no finite diagram of this type can represent mixtures of pure H_2O.

The vertical co-ordinate, I, measures the enthalpy of the mixture in B.t.u/lb_m air. The zero-enthalpy conditions exhibit a difference from the previous cases: $I = 0$ for air at 32°F, as before, but for *steam* (not water) at 32°F. This is why the 32°F gas-phase isotherm is now horizontal.

N.B. MOLLIER, and all subsequent commentators, have used i for enthalpy. i differs from I in having the same zero condition as h and H. Then, in order to obtain a diagram of convenient shape, MOLLIER uses "slanting co-ordinates," i.e. plots i vertically upwards from a base line which is not at right angles to the lines of constant x; the slope of the line is chosen to make the gas-phase isotherm for 32°F horizontal. This practice is therefore essentially the same as the use of I, with rectangular co-ordinates, exhibited by Fig. 2(c); the explicit use of I seems to be the more straightforward practice.

Fig. 2(c) shows the division into two regions by the saturation line which has already appeared in Figs. 2(a) and 2(b). But the three charts are by no means geometrically similar to each other. What is their relationship?

VOL. 11 59/60

2.2 *Relations between the Co-ordinates*

We have now introduced three ways of describing the state of a given H_2O – air mixture: the $h-m$, the $H-M$, and the $I-x$ co-ordinate systems. We shall later want to use the algebraic relations between these quantities which are implied in their definitions. These are easily shown to be:

For composition

$$m = x/(1+x) \tag{2}$$

$$= \frac{M}{(29/18) + \left[1-(29/18)\right]M} \tag{3}$$

together with equivalent relations, such as

$$x = m/(1-m) \tag{4}$$

$$M = \frac{m}{(18/29) + \left[1-(18/29)\right]m}, \text{ etc} \tag{5}$$

while the "molecular weight" of the mixture, μ, is given by

$$\left.\begin{aligned} \mu &= 18M/m \\ &= 29\,(1-M)/(1-m) \\ &= 29 + (18-29)\,M \\ &= 1/\left[\frac{1}{29} + m\left(\frac{1}{18}-\frac{1}{29}\right)\right] \end{aligned}\right\} \tag{6}$$

For enthalpy

$$h = H/\mu \tag{7}$$

$$= i/(1+x) \tag{8}$$

$$= \frac{I + x\,h_{fg}}{1+x} \tag{9}$$

where h_{fg} = latent heat of vaporization of water at 32°F, together with equivalent expressions such as

$$H = h\,\mu \tag{10}$$

$$I = i - x\,h_{fg}$$

$$= \frac{h - m\,h_{fg}}{1-m}, \text{ etc.} \tag{11}$$

2.3 *The "Lever Rule" on the Three Charts*

The conservation-of-matter principle, and the Steady-Flow Energy Equation, can be written for adiabatic constant-pressure mixing processes using any one of the three pairs of properties: $\eta-m$, $H-m$ or $I-x$. Application of these principles to the mixing of systems X and Z to make a mixture Y, as discussed above, readily shows that the "Lever Rule," equation (1), is valid provided "quantity" is interpreted as mass of mixture in case (a) $(h-m)$, as moles of mixture in case (b) $(H-M)$ and as mass of air in case (c) $(I-x)$.

It can then be deduced that the position of the point Y on the line XZ of Fig. 1 is related to the ratio of the mass of system Z, w_z, to that of system Z, w_Z, by:

(a) $(h-m$ chart)

$$\frac{\overline{XY}}{\overline{YZ}} = \frac{w_Z}{w_X} \tag{12}$$

(b) $(H-M$ chart)

$$\frac{\overline{XY}}{\overline{YZ}} = \frac{w_Z}{w_X}\cdot\frac{\mu_X}{\mu_Z} \tag{13}$$

(c) $(I-x$ chart)

$$\frac{\overline{XY}}{\overline{YZ}} = \frac{w_Z}{w_Z}\cdot\frac{(1+x_X)}{(1+x_Z)} \tag{14}$$

where the subscripts X and Z indicate the system for which the properties μ and x should be evaluated.

With these interpretations, each of the charts can be used for the construction of the "polar diagrams" (3, 4, 16, etc.), which so greatly facilitate application of the conservation laws to chemical engineering equipment. These are too well known to be described here.

2.4 *Rate Process Calculations on the Three Charts*

In this section some of the more important graphical constructions will be described which enable simultaneous heat and mass transfer processes to be calculated. We consider an element of the exchange surface as illustrated in Fig. 3; this shows a water film in contact, through a thermal resistance, with a reservoir at temperature t_0; the free surface of the liquid is swept by a steam–air mixture. This might represent conditions in a cooling-tower, in which case the reservoir is the bulk of the water stream at the

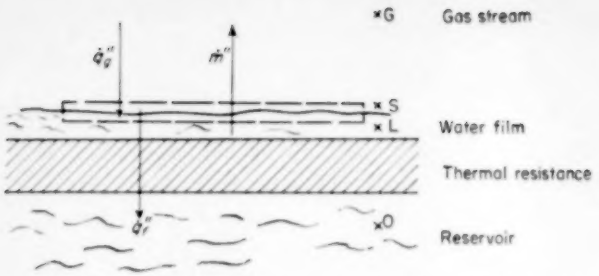

FIG. 3. Element of exchange surface, with heat and mass fluxes.

section in question, and the thermal resistance referred to above is the boundary layer of the water stream. A similar situation arises in condensers, in which case the reservoir is the cooling fluid, while the thermal resistance is made up of the cooling-fluid boundary layer, the tube wall and its adhering scale and the water film on the outside.

For the sake of simplicity, it will be assumed that radiative heat transfer between the water surface and its surroundings is negligible, and that the enthalpy increase of the water flowing in the film can be disregarded. The more general case is dealt with in [15].

We suppose that the state of the gas stream and the temperature of the reservoir are given; in addition the gas-side heat transfer coefficient and the over-all heat transfer coefficient between the water film and the reservoir are supposed known. The problem is to determine, first of all, the temperature of the water surface and so the state of the gas immediately in contact with it; thereafter the rate of mass transfer (condensation or vaporization), the rates of heat transfer from gas to water and from water to reservoir, and the direction of change of the gas state, are all to be determined.

It is assumed that the liquid (L) and the gas (S), in contact at the phase boundary, are in thermodynamic equilibrium.

(a) *On the $h - m$ chart*

The method developed by the present author [15, 11], utilizes the "mass-of-mixture" basis for enthalpy and composition. The following constructions and formulae are extracted from [15]; Their derivations are outlined in Appendix A. They are also valid for mixtures which undergo chemical reactions.

Determination of the interface states L *and* S. (See Fig. 4).

(i) Locate O on the line $m = 1$ corresponding to water at temperature t_O.

(ii) Locate H on the line $m = 1$ such that the vertical distance $\overline{OH}$ (measured upwards, and in enthalpy units) is given by

$$\overline{OH} = \frac{c_f (t_G - t_O)}{1 + [\sigma/(\sigma - 1)](U/g\,c)} \tag{15}$$

(iii) Draw the line $\overline{HG}$ and find A on it such that

$$\frac{\overline{AG}}{\overline{HA}} = \frac{U}{g\,c_f} \cdot \sigma + \frac{c}{c_f}(\sigma - 1) \tag{16}$$

(iv) Locate L and S, which lie at the extremities of the mixed-phase isotherm through A. L lies on the line $m = 1$; S lies on the saturation line.

N.B. When the Lewis Number equals unity, and so $\sigma = 1$ also, the procedure simplifies; for then H coincides with O so that (15) does not have to be evaluated; and the second term of (16) disappears.

Transfer rates (Fig. 4). Drop a vertical line from G to intersect the gas-phase isotherm through S at D. Produce LS to cut DG at C. Plot K on $\overline{DG}$ such that

$$\frac{\overline{DK}}{\overline{DG}} = \sigma \tag{17}$$

N.B. K and G coincide for $\sigma = 1$.

Then the mass transfer rate is given by

$$\frac{\dot{m}''\,\sigma}{g} = \frac{\overline{CS}}{\overline{SL}} \tag{18}$$

the heat transfer rate to the reservoir is given by

$$\frac{\dot{q}''_f\,\sigma}{g} = \overline{CK} \tag{19}$$

and the heat transfer rate from the gas to the liquid surface is given by

$$\frac{\dot{q}''_g}{g} = \overline{DG} \tag{20}$$

VOL 11 1959

Change of gas condition (Fig. 5). Produce $\overline{KS}$ to cut the line $m = 1$ at J. Let T be the intersection of $\overline{GJ}$ with the vertical through S.

Then the state of the gas stream changes, as a result of contact with the liquid, in such a way that the corresponding state-point G moves towards J.

More specifically, if the mass flow rate of the local gas stream is $\dot{m}_G$, the elementary contact area is δa, the state of the gas before contact is represented by G_1 and after contact by G_2, then G_2 lies on the line $\overline{G_1J}$ at a point such that

$$\frac{\overline{G_2G_1}}{\overline{G_2J}} \cdot \frac{\overline{TJ}}{\overline{TG_1}} = \frac{g\,\delta a}{\sigma \dot{m}} = \delta N_{m,g}, \text{ say} \qquad (21)$$

The expression on the right-hand side of (21) is the increment in the number of gas-side mass transfer units.

(b) *On the H–M chart*

Bošnjaković [14] has described graphical procedures permitting the calculation of heat and mass transfer using the "mole-of-mixture" basis; his procedures differ from, and are somewhat more complicated than, the constructions which will now be recommended for use with this chart; but they are based on the same principles and assumptions.

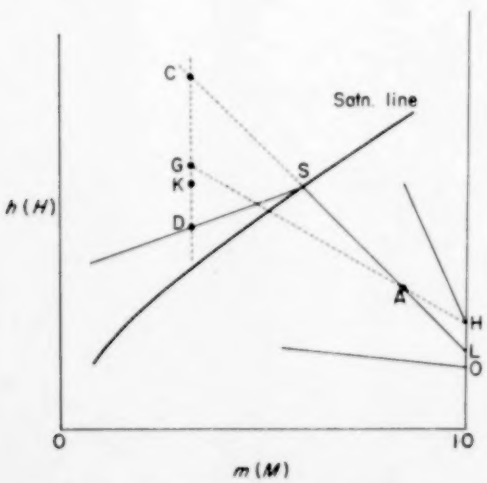

Fig. 4. Rate-process constructions.
(Erratum: DS should be prolonged to intersect OH at V)

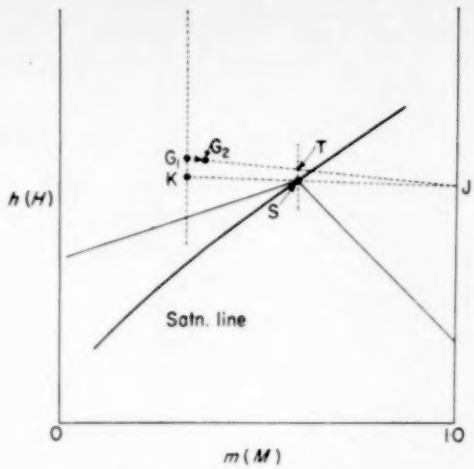

Fig. 5. Change of gas state.

The constructions now to be described do not differ qualitatively from those of Figs. 4 and 5; the same diagrams can therefore be referred to. Proofs will not be given as yet; they involve use of a result to be derived later (Part II, Section 1.3).

Determination of the interface state, L *and* S (Fig. 4).

(i) As for case (a).

(ii) As for case (a), except that the expression on the right-hand side of (15) must be multiplied by 18, the molecular weight of H_2O.

(iii) As for case (a), except that the expression on the right-hand side of (16) must be multiplied by $\mu_G/18$ where μ_G is the "molecular weight" corresponding to state G. It is convenient to provide a horizontal scale for this quantity on the diagram.

(iv) As for case (a).

Transfer rates (Fig. 4). D, C and K are points determined as in case (a). Then the transfer rates are calculated from the following equations, which parallel (18), (19) and (20):

$$\frac{\dot{m}'' \sigma}{g} = \frac{\overline{CS}}{\overline{SL}} \cdot \frac{18}{\mu_G} \qquad (22)$$

$$\frac{\dot{q}''_f \sigma}{g} = \frac{\overline{CK}}{\mu_G} \qquad (23)$$

$$\frac{\dot{q}'' g}{g} = \frac{\overline{DG}}{\mu_G} \qquad (24)$$

Change of gas condition (Fig. 5). The construction and its evaluation are identical with those of case (a): equation (21) still holds.

(c) *On the $I-x$ chart*

The early rate-process constructions developed by BUSEMANN [12] were made on the $I-x$ chart. Much of the work of BOŠNJAKOVIĆ [8, 13], including that on the carbon-air system [9], has also been done with charts of this type. The constructions now to be presented differ somewhat from his in the interests of simplicity and of conformity with those of cases (a) and (b).

Determination of the interface states, L *and* S (Fig. 6). The characteristic feature of the $I-x$ chart is that the pure-H_2O line is at infinity.

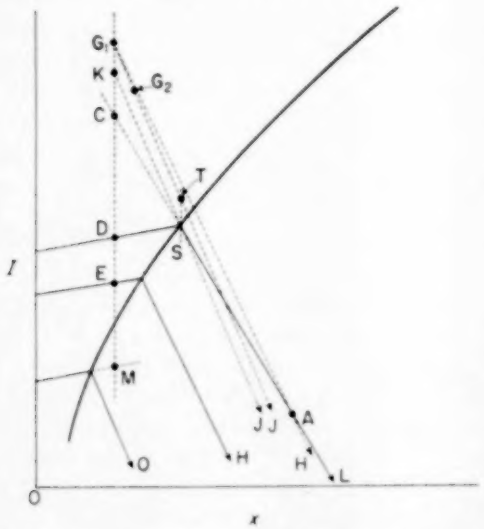

FIG. 6. Rate-process and change of gas state.

O, H, L and J can only be established as directions, not as points. The procedure therefore is:

(i) Note the isotherm, t_O

(ii) Evaluate t_H, from

$$t_H - t_O = \frac{t_G - t_O}{1 + [\sigma/(\sigma-1)](U/g\,c)} \qquad (25)$$

and note the corresponding isotherm.

Two procedures are now possible. We first give one which is similar to those of cases (a) and (b):

(iii) Draw a line through G parallel to the mixed-phase branch of the t_H isotherm. Find the point A on this line such that

$$\frac{x_A - x_G}{1 + x_G} = \frac{U}{g\,c_f} \cdot \sigma + \frac{c}{c_f}(\sigma - 1) \qquad (26)$$

(iv) As for case (a).

This procedure will fail if A lies beyond the right-hand edge of the available chart, as is likely to occur when $U/g\,c_f$ is large. The following alternative procedure may be used:

(iii) Drop a vertical through G to intersect the gas-phase isotherm t_H (produced if necessary) at E.

N.B. $\overline{ME} = \overline{MG} \Big/ \left\{1 + \frac{\sigma}{\sigma-1} \cdot \frac{U}{g\,c}\right\}$, where M is the intersection of the vertical with the gas-phase isotherm t_0, produced if necessary.

(iv) Find S such that

$$\frac{\overline{CG}}{\overline{ED}} = \frac{\sigma\,U}{g\,c} + (\sigma - 1) \qquad (27)$$

where C and D lie on the vertical through G and respectively on the mixed-phase and gas-phase isotherms through S. L, of course, is a point at infinity on the mixed-phase isotherm through S.

The determination of S to satisfy (27) proceeds very quickly by trial-and-error: a point C is guessed; D is immediately located and the ratio $\overline{CG}/\overline{ED}$ evaluated; comparison with the prescribed value of the ratio shows immediately whether C should be moved up or down.

This procedure can also be used, without modification, on the $h-m$ or $H-M$ charts.

Transfer rates (Fig. 6). D and C have already been determined; K can be determined as for case (a). Then the transfer rates are calculated from the following equations, which parallel (18), (19) and (20), and (22), (23) and (24):

$$\frac{\dot{m}''\,\sigma}{g} = \frac{\overline{CS}\,h}{1 + x_G} \qquad (28)$$

$$\frac{\dot{q}''_f\,\sigma}{g} = \frac{\overline{CK}}{1 + x_G} \qquad (29)$$

$$\frac{\dot{q}''_g}{g} = \frac{\overline{DG}}{1 + x_G} \qquad (30)$$

VOL 11 1959

It will be noted that $(1 + x)$ occupies the place taken by μ in the $H - M$ formulation.

Direction of change of gas state. G_2 is related to G_1 as for case (a) except that, since the point J is at infinity, $\overline{G_1G_2}$ is drawn parallel to $\overline{KS}$. For the same reason, equation (21), which is still valid, simplifies to

$$\frac{\overline{G_2G_1}}{\overline{G_2J}} = \frac{g \cdot \delta a}{\sigma \dot{m}_G} \qquad (31)$$

2.5 *Comparison of the Merits of the Three Charts for Rate-Process Calculations*

(a) *The $h - m$ chart*

The "mass-of-mixture" basis provides formally, and in the author's opinion conceptually also, the simplest of the three sets of procedures. No μ_G's or $1 + x_G$'s appear in the equations used for evaluation. Only in respect of the evaluation of $\overline{G_2G_1}$ (via equation 21), does the $h - m$ formulation involve a more complex expression than the $I - x$ formulation.

The reason for the simplicity of equations using the "mass-of-mixture" basis lies essentially in the fact that the fluid-mechanical processes which occur in the boundary layer adjacent the surface are responsive to the mass velocity of the stream rather than to the "mole velocity" or the "mass-of-air" velocity. g can be evaluated without direct reference to molecular weight or composition.

The main disadvantage of the $h - m$ chart is that its scale is often such that intricate constructions have to be performed on a small section of the chart. For H_2O – air the region of the chart covering states near that of the atmosphere is often too small for adequate accuracy of construction.

(b) *The $H - M$ chart*

The "mole-of-mixture" basis introduces the position-dependent quantity μ_G into a number of formulae connected with the graphical constructions and their interpretation. This makes the significance of lines and ratios on the chart somewhat harder to grasp.

There is a slight enlargement, as compared with the $h - m$ chart, of the important atmospheric region for H_2O – air. But this is not usually sufficient, in the author's opinion, to compensate for the greater conceptual difficulty. The use of $H - M$ co-ordinates does not therefore seem advisable.

However it will later be shown that the important feature of the mole basis is that different mass units are used for the two components. We shall see that there can be great advantage in using two different mass units, but that there is no reason why these units should be related to the molecular weights of the substances.

(c) *The $I - x$ chart*

In addition to having the position-dependent quantity $(1 + x_G)$ in many of the formulae, the meanings of the constructions on this chart are rendered difficult to grasp by the fact that all pure-H_2O points lie at infinity. This absence of the $m = 1$ line sometimes requires the use of slightly more involved constructions for determining the interface state (either Bošnjaković's, or those presented above) than are needed for the $h - m$ method. This is true not only of the rate-process constructions which are chiefly in question here, but also of the polar diagrams representing mass and energy balances.

Not only is the $m = 1$ line absent, but the I–x chart is incapable of representing mixtures which have an appreciable proportion of H_2O in them. Heat and mass transfer in condensers, to name an important practical example, cannot be studied on the $I - x$ chart.

However the I–x chart has the great advantage that it can easily be drawn to a suitable scale for the solution of problems involving relatively small moisture contents, such as occur in heating-and-ventilating practice and in cooling-towers. A minor advantage is that the formula for the change of gas condition, equation (31), is simpler than the corresponding one for the $h - m$ and $H - M$ charts.

2.6 *Summarizing Remarks*

It appears that there are striking similarities between the three charts discussed. Each has its own advantages and disadvantages, and which

is the best to use depends on the problem to be solved, whether it involves high or low moisture contents for example.

Before trying to decide which chart is best used in various circumstances, we should inquire whether these three bases for the mixture quantity are the only ones which can be used. This is the subject of Part II.

APPENDIX A.

Derivation of Rate-Process Constructions

A.1 *Determination of interface states* L *and* S

From the theory of heat and mass transfer (17), we have

$$\dot{m}'' = g \cdot \frac{h_G - h_{GS}}{(\dot{q}''_f/\dot{m}'') + h_{fg}} \tag{A.1}$$

and

$$\dot{m}'' = \frac{g}{\sigma} \cdot \frac{m_G - m_S}{m_S - 1} \tag{A.2}$$

Consideration of similar triangles in Fig. 4 shows that (A.2) can take the form :

$$\dot{m}'' = \frac{g}{\sigma} \cdot \frac{\overline{DC}}{\overline{LV}} \tag{A.3}$$

From Fig. 4 and the fact that $h_{fg} = \overline{LV}$, (A.1) becomes :

$$\dot{m}'' = g \cdot \frac{\overline{DG}}{(\dot{q}''_f/\dot{m}) + \overline{LV}} \tag{A.4}$$

where V is the intersection of DS produced and the line $m = 1$.

From (A.4) and the definition of U, viz.

$$\begin{aligned} \dot{q}''_f &= U\,(t_L - t_O) \\ &= (U/c_f)\,\overline{OL} \end{aligned} \tag{A.5}$$

we deduce :

$$\dot{m}'' = \frac{\dot{q}''\overline{DG} - (U/c_f)\,\overline{OL}}{\overline{LV}} \tag{A.6}$$

Eliminating $\dot{m}''$ from (A.3) and (A.6), we find :

$$\overline{CG} = (U\sigma/c_f g)\,\overline{OL} - (\sigma - 1)\,\overline{DG} \tag{A.7}$$

Introducing into (A.7) the definition of point H (equation 15) in the form :

$$\overline{OH} = \frac{(c_f/c)\,\overline{DG} + \overline{OL}}{1 + [\sigma/(\sigma - 1)] \cdot (U/g\,c)} \tag{A.8}$$

we obtain :

$$\frac{\overline{CG}}{\overline{HL}} = \frac{\sigma\,U}{g\,c_f} + (\sigma - 1)\,\frac{c}{c_f} \tag{A.9}$$

But, from similar triangles in Fig. 4,

$$\frac{\overline{CG}}{\overline{HL}} = \frac{\overline{AG}}{\overline{HA}} \tag{A.10}$$

from which the required result (16) follows immediately.

Transfer rates

Equation (18) follows from (A.2) by similar triangles. Equation (19) follows from (A.4), (18), the definition (17) and similar triangles.
Equation (20) may be regarded as a definition of $\dot{q}''_g$.

Change of gas condition

From (18), (19) and similar triangles,

$$\overline{LJ} = \dot{q}''_f/\dot{m}'' \tag{A.11}$$

Therefore the actual heat and mass fluxes through the surface are equivalent to a mass flux without heat flux with the material entering at state J. It follows from the Lever Rule that the gas state moves towards J and that

$$\frac{\overline{G_1G_2}}{\overline{G_2J}} = \frac{\dot{m}'' \cdot \delta a}{\dot{m}_G} \tag{A.13}$$

Introduction of (A.2) and similar triangles thereupon lead directly to the required result (21).

NOTATIONS

- G = State-point of gas stream
- L = State-point of liquid surface
- S = State-point of gas in contact with liquid surface
- G_S = Composition of G and temperature of S
- O = State-point of water at reservoir temperature t_O
- U = Over-all heat transfer coefficient from liquid surface to reservoir
- g = Gas-side heat transfer coefficient divided by c (g = Stanton Number times mass velocity in gas stream ; its units are $lb_m/ft^2\,hr$)
- c = Specific heat of mixture G at constant pressure
- c_f = Specific heat of water at constant pressure
- $\dot{m}''$ = Mass transfer rate from liquid to gas phase $lb_m/ft^2\,hr$
- $\dot{q}''_f$ = Heat transfer rate to reservoir (across lower surface of dotted control volume in Fig. 3) (across upper surface of dotted control volume in Fig. 3)
- σ = Function of Lewis Number (Le ≡ diffusion coefficient of steam in air divided by thermal diffusivity of gas mixture) appearing in Chilton–Colburn analogy between heat and mass transfer, where it is assumed $\sigma = (Le)^{-n}$ when n is between (1/2) and (2/3) [15].

VOL 11 1959/

References

[1] Ponchon *Tech. mod.* 1921 **13** 21.

[2] Savarit *Arts et Mét.* 1922 **65** 142, 178, 241, 266, 307.

[3] Mollier R. Z. *Ver. dtsch. Ing.* 1923 **67** 869 ; 1929 **73** 1009.

[4] Keenan J. H. *Thermodynamics.* John Wiley, New York 1941.

[5] Bošnjaković F. *Technische Thermodynamik.* Steinkopf, Dresden 1937.

[6] Sherwood T. K. and Pigford R. L. *Absorption and Extraction.* McGraw Hill, New York 1952.

[7] Treybal R. E. *Mass Transfer Operations.* McGraw Hill, New York 1955.

[8] Bošnjaković F. *Chem. Ing. Tech.* 1957 **29** 187.

[9] Bošnjaković F. *Waermediagramme fuer Vergasung, Verbrennung und Russbildung.* Springer Verlag, Berlin 1956.

[10] Powell H. N. *Amer. Soc. Mech. Engrs.* Paper 56-SA-68 (1956).

[11] Spalding D. B. and Tyler R. D. *Int. Un. Pure Appl. Chem.* and *Inst. Mech. Engrs.* (*Joint Conf.*) 1957, Paper 1, Session 4.

[12] Busemann A. *Der Waerme und Stoffaustausch, dargestellt in Mollierschen Zustandsdiagramm für zweistoffgemische.* Berlin, 1933.

[13] Bošnjaković F. *Jb. Kältetech.* 1957 **9** 309.

[14] Bošnjaković F. *Kyltekn. Tidskr.* 1957 No. 3 142.

[15] Spalding D. B. *Proc. Inst. Mech. Engrs.* 1958 **172** No. 28.

[16] Matz W. *Die Thermodynamik des Waerme-und Stoffaustausches in der Verfahrenstechnik.* Steinkopf, Frankfurt 1949.

[17] Spalding D. B. *Proc. Inst. Mech. Engrs.* 1954 **168** 545.

VOL. 11 959/60

Chemical Engineering Science, 1959, Vol. 11, pp. 194 to 198. Pergamon Press Ltd., London. Printed in Great Britain

The longitudinal diffusion coefficient in flow through a tube with stagnant pockets

R. Aris

Department of Chemical Engineering, University of Minnesota, Minneapolis 14, Minnesota

(*Received* 1 *April* 1959)

Abstract—In Turner's ' Model I ' flow structure a fluid is assumed to flow through a tube whose wall leads to pockets of varying lengths. It is here shown that the presence of these pockets influences the Taylor diffusion coefficient for flow in the tube and a general method for calculating this is given.

Résume—Dans le système d'écoulement présenté par Turner dans son " Modèle I," un fluide est supposé s'écouler à travers un tube dont la paroi aboutit à des poches de longueurs variables. L'auteur montre ici que la présence de ces poches influe sur le coefficient de diffusion de Taylor pour l'écoulement dans le tube et il donne une méthode générale pour calculer ce coefficient.

Zusammenfassung—Das Verhalten einer Strömung nach dem " Modell I " von Turner kommt durch eine Flüssigkeit zustande, die durch ein Rohr strömt, dessen Wände Taschen verschiedener Länge besitzen. Es wird hier gezeigt, dass die Anwesenheit dieser Taschen den Diffusionskoeffizienten für die Rohrströmung nach Taylor beeinflusst; zu seiner Berechnung wird eine allgemeine Methode angegeben.

Turner [1] has proposed a model of flow systems in which there are stagnant pockets of various depths opening on the flow channels. The diffusion coefficient in these pockets is the molecular diffusion D whilst in the flowing channel a longitudinal diffusion coefficient $\bar{D}$ is assumed. Neither in Turner's work nor in a later paper [2] on the same model is a value ascribed to $\bar{D}$ and one might be inclined to write for it the apparent longitudinal diffusion coefficient $D + \kappa U^2 a^2/D$ found by Taylor [3] (U = mean velocity, a = radius of circle having the same area, κ is a shape factor, $\kappa = 1/48$ for circular cross-section). This however is not correct and it is our purpose of this note to show how κ depends not only on the cross-section and flow profile, as in Taylor's analysis, but also on β. The result is related to the behaviour of the tubular chromatographic column, which has been treated more generally elsewhere [4, 5], but cannot be immediately deduced from it. The result will be deduced from a comparison of two methods used to find the apparent diffusion coefficient, the one for Taylor's analysis [6] and the other for Turner's model [7].

1. Two Methods of Determining Apparent Diffusion Coefficients

To see this comparison unencumbered consider a tube of length L through which a fluid is flowing with uniform speed U and in which a solute is diffusing with diffusion coefficient D^*. If c be the concentration of solute it satisfies the equation

$$\frac{\partial c}{\partial t} = D^* \frac{\partial^2 c}{\partial x^2} = U \frac{\partial c}{\partial x} \tag{1}$$

where x is distance along the tube and t the time. In the first method it is subject to the conditions

$$\left.\begin{aligned} c(x, o) &= 0 \\ -D^* \frac{\partial c}{\partial x} + Uc &= U c_0(t), \quad x = 0, \\ \frac{\partial c}{\partial x} &= 0, \quad x = L, \end{aligned}\right\} \tag{2}$$

and we take the inlet concentration to be a unit amount of solute introduced at zero time, i.e.

$c_0(t) = \delta(t)$. The emergent concentration as a function of time $c(L, t)$ will be a peak representing the probability of a molecule having residence time t and can be used to define a mean $\bar{t}$ and variance σ^2, where

$$\bar{t} = \int_0^\infty t\, c(L, t)\, dt$$

$$\sigma^2 = \int_0^\infty (t - \bar{t})^2\, c(L, t)\, dt$$

Van der Laan [7] has shown how these quantities may be calculated from the Laplace transform of the solution of (1) and (2) without inversion. In this case

$$\bar{t} = \frac{L}{U}, \quad \sigma^2 = 2D^* \frac{L}{U^3} + 0(L^{-1})$$

whence

$$D^* = \frac{1}{2} UL \frac{\sigma^2}{\bar{t}^2}.$$

Using this method on Turner's model it is shown elsewhere that, with a diffusion coefficient D in the channel and a distribution of pockets such that $\beta(l)\, dl$ is the volume of pocket of length between l and $l + dl$ per unit volume of channel, the apparent diffusion coefficient is

$$D^* = D + \frac{U^2}{3D(1 + \beta)^2} \int_0^\infty \beta(l)\, l^2\, dl \qquad (3)$$

There is however another way of looking at equation (1). Consider a very long tube $-\infty < x < \infty$ and suppose that at time $t = 0$ a unit amount of solute is concentrated on the plane $x = 0$. We may ask how the solute distributes itself as time goes on and regard the solution $c(x, t)$ as a probability distribution giving the probability density of a molecule reaching a point x in time t. From this viewpoint we would study the spatial moments

$$m_1(t) = \int_{-\infty}^\infty x\, c(x, t)\, dx$$

$$m_2(t) = \int_{-\infty}^\infty (x - m_1)^2\, c(x, t)\, dx$$

To do this it is convenient to take a moving origin coincident with $x = 0$ at $t = 0$ and travelling with speed V, which will be later chosen to be the speed of centre of mass of the solute. Let $z = x - Vt$ then

$$\frac{\partial c}{\partial t} = D^* \frac{\partial^2 c}{\partial z^2} - (U - V) \frac{\partial c}{\partial z} \qquad (4)$$

$$c(z, o) = \delta(z)$$

Now let

$$c^{(p)}(t) = \int_{-\infty}^\infty z^p\, c(z, t)\, dz$$

so $c^{(0)}(o) = 1$, $c^{(p)}(o) = 0$, $p = 1, 2, \ldots$. Then multiplying equation (4) by z^p and integrating gives

$$\frac{dc^{(p)}}{dt} = D^* p(p - 1)\, c^{(p-2)} + (U - V)\, p\, c^{(p-1)}$$

As we should expect $dc^{(0)}/dt = 0$ showing that the total amount of solute is constant.

$$\frac{dc^{(1)}}{dt} = U - V$$

and if $V = U$, $c^{(1)}$ is constant $= 0$. Thus the centre of mass travels with the uniform velocity of the stream. Finally putting $p = 2$

$$\frac{dc^{(2)}}{dt} = 2D^* \quad \text{or} \quad c^{(2)} = 2D^* t$$

Thus

$$m_1 = Vt = Ut, \quad m_2 = 2D^* t$$

and

$$D^* = U m_2 / 2 m_1. \qquad (5)$$

This technique has been applied to Taylor's problem of simultaneous diffusion and convection by a non-uniform velocity, and will now be applied to Turner's model to obtain a formula which on comparison with (3) gives D.

2. Application to Turner's Model

We will consider circular channels of radius a but the method can be modified for any other cross-section without difficulty. On the wall of

this tube there open the mouths of the stagnant pores or pockets and it is assumed that the distribution of these does not vary along the length of the tube.

Let

$\beta(l)\,dl$ = volume of pockets of lengths between l and $l + dl$ per unit volume of channel

$\beta = \int_0^\infty \beta(l)\,dl$ = total volume of stagnant pocket per unit volume of channel

$c_l(x, y, t)$ = concentration of solute at depth y in a pocket of length l at position x along the channel and time t

$c(r, x, t)$ = concentration of solute in flowing channel at radius r, distance x and time t

$U\phi(r)$ = velocity of stream at radius r, U = mean velocity.

Then since the total area of pockets of lengths between l and $l + dl$ is $\alpha(l) = \beta(l)/l$ per unit volume of channel we can, by attributing the wall area which is not a pocket mouth to pockets of length zero, ensure that

$$\int_0^\infty \alpha(l)\,dl = \int_0^\infty \beta(l) l^{-1}\,dl = 2/a$$

without changing the value of β. The equations satisfied by c_l and c are thus

$$\frac{\partial c_l}{\partial t} = D\frac{\partial^2 c_l}{\partial y^2} \tag{6}$$

$$c_l(x, o, t) = c(a, x, t) \tag{7}$$

$$\frac{\partial c_l}{\partial y} = 0, \quad y = l \tag{8}$$

$$\frac{\partial c_l}{\partial t} = \frac{D}{r}\frac{\partial}{\partial r}\left(r\frac{\partial c}{\partial r}\right) + D\frac{\partial^2 c}{\partial x^2} - U\phi(r)\frac{\partial c}{\partial x} \tag{9}$$

$$\frac{\partial c}{\partial r} = 0, \quad r = 0 \tag{10}$$

$$\frac{\partial c}{\partial r} = \frac{a}{2}\int_0^\infty \alpha(l)\left(\frac{\partial c_l}{\partial y}\right)_0 dl, \quad r = a \tag{11}$$

If the moving co-ordinate system is introduced by $z = x - Vt$ equations (6) and (9) become

$$\frac{\partial c_l}{\partial t} = D\frac{\partial^2 c_l}{\partial y^2} + V\frac{\partial c_l}{\partial z} \tag{12}$$

$$\frac{\partial c}{\partial t} = \frac{D}{r}\frac{\partial}{\partial r}\left(r\frac{\partial c}{\partial r}\right) + D\frac{\partial^2 c}{\partial z^2} - (U\phi(r) - V)\frac{\partial c}{\partial z} \tag{13}$$

Now define the moments

$$c^{(p)} = \int_{-\infty}^{\infty} z^p\, c(z, r, t)\,dz = c^{(p)}(r, t)$$

$$c_l^{(p)} = \int_{-\infty}^{\infty} z^p\, c_l(y, z, t)\,dz = c_l^{(p)}(y, t)$$

$$\mu^{(p)}(t) = \frac{1}{a^2}\int_{-\infty}^{\infty} 2r\, c^{(p)}(r, t)\,dr + \int_0^\infty \alpha(l)\int_0^l c^{(p)}(y, t)\,dy$$

Then multiplying through equations (12) and (13) and conditions (7), (8), (10), (11) by z^p and integrating we have

$$\frac{\partial c^{(p)}}{\partial t} = \frac{D}{r}\frac{\partial}{\partial r}\left(r\frac{\partial c^{(p)}}{\partial r}\right) + Dp(p-1)c^{(p-2)} + p(U\phi - V)c^{(p-1)} \tag{14}$$

$$\frac{\partial c^{(p)}}{\partial r} = 0, \quad r = 0 \tag{15}$$

$$\frac{\partial c^{(p)}}{\partial r} = \frac{a}{2}\int_0^\infty \alpha(l)\left(\frac{\partial c_l^{(p)}}{\partial y}\right)_0 dl, \quad r = a \tag{16}$$

$$\frac{\partial c_l^{(p)}}{\partial t} = D\frac{\partial^2 c_l^{(p)}}{\partial y^2} - pV c_l^{(p-1)} \tag{17}$$

$$c_l^{(p)} = c^{(p)}(a) \quad y = 0 \tag{18}$$

$$\frac{\partial c_l^{(p)}}{\partial y} = 0 \qquad y = l \tag{19}$$

Finally integrating with respect to r and y and using the boundary conditions (15), (16), (18) and (19)

$$\frac{d\mu^{(p)}}{dt} = D\,p\,(p-1)\,\frac{1}{a^2}\int_0^a 2r\,c^{(p-2)}\,dr + \\ + \frac{pU}{a^2}\int_0^a 2r\,\phi\,(r)\,c^{(p-1)}\,dr - p\,V\,\mu^{(p-1)} \quad (20)$$

Initially the solute is concentrated in the plane $z = 0$ so $c^{(0)} = c_l^{(0)} = (1+\beta)^{-1}$, $\mu^{(0)} = 1$ and $c^{(p)} = c_l^{(p)} = \mu^{(p)} = 0$, $p > 0$, at $t = 0$. Putting $p = 0$ in (20) gives $d\mu^{(0)}/dt = 0$ so $\mu^{(0)}$ is constant, which is to be expected since it is the total amount of solute present. Also equations (14)–(19) are satisfied if $c^{(0)}$ and $c_l^{(0)}$ are constant. Thus for all t

$$c^{(0)} = c_l^{(0)} = \frac{1}{1+\beta}, \quad \mu^{(0)} = 1 \quad (21)$$

For $p = 1$ equation (20) gives

$$\frac{d\mu^{(1)}}{dt} = \frac{U}{(1+\beta)\,a^2}\int_0^a 2r\,\phi\,(r)\,dr - V \\ = \frac{U}{1+\beta} - V$$

since the mean value of ϕ is 1. Thus if $V = U/(1+\beta)$ the centre of mass is stationary in the moving co-ordinate system, being in fact at the moving origin.

In seeking solutions for $c^{(1)}$ and $c_l^{(1)}$ it has been shown [6] that we need only concern ourselves with the part of the solution independent of time. The time dependent will ultimately grow to a small constant in the expression for $\mu^{(2)}$, but since $\mu^{(2)}$ is increasing linearly with time such a constant is ultimately negligible. For the time independent part of the solution $c_l^{(1)}$ equations (17)–(19) give

$$\frac{\partial c_l^{(1)}}{\partial y} = -\frac{V}{D}\frac{l-y}{1+\beta}$$

$$c_l^{(1)} = c^{(1)}\,(a) - \frac{V}{D\,(1+\beta)}\left(ly - \frac{1}{2}y^2\right) \quad (22)$$

$$\int_0^\infty \alpha\,(l)\int_0^l c_l^{(1)}\,dy\,dl = \beta\,c^{(1)}\,(a) - \\ - \frac{V}{3D\,(1+\beta)}\int_0^\infty \beta\,(l)\,l^2\,dl$$

Also the time independent part of $c^{(1)}$ satisfies

$$\frac{D}{r}\frac{\partial}{\partial r}\left(r\,\frac{\partial c^{(1)}}{\partial r}\right) + \frac{U}{1+\beta}\left(\phi\,(r) - \frac{1}{1+\beta}\right) = 0$$

$$\frac{\partial c^{(1)}}{\partial r} = 0, \quad r = 0$$

$$\frac{\partial c^{(1)}}{\partial r} = -\frac{a}{2}\int_0^\infty \alpha\,(l)\,\frac{V}{D\,(1+\beta)}\,dl = \\ -\frac{Va}{2D}\frac{\beta}{1+\beta}, \quad r = a \quad (23)$$

If

$$\Phi\,(r) = \frac{1}{a^2}\int_0^r 2r\,\phi\,(r)\,dr \quad (24)$$

so that

$$\Phi\,(o) = 0, \quad \Phi\,(a) = 1$$

and

$$\frac{\partial c^{(1)}}{\partial r} = -\frac{Ua^2}{2D\,(1+\beta)}\,\frac{1}{r}\,\Phi\,(r) + \frac{U}{2D\,(1+\beta)^2}\,r$$

Since $\Phi\,(r) = 0\,(r^2)$ at $r = o$, $\partial c^{(1)}/\partial r$ vanishes at $r = 0$ and the condition (23) is identically satisfied at $r = a$. Integrating again

$$c^{(1)}\,(r) = c^{(1)}\,(a) + \frac{U\,a^2}{2D\,(1+\beta)}\int_r^a \frac{1}{r}\,\Phi\,(r)\,d\zeta + \\ + \frac{U}{4D\,(1+\beta)^2}\,(r^2 - a^2)$$

and $c^{(1)}\,(a)$ can be determined by the condition $\mu^{(1)} = 0$

$$c^{(1)}\,(a) = \frac{U}{3D\,(1+\beta)^3}\int_0^\infty \beta\,(l)\,l^2\,dl + \\ + \frac{U\,a^2}{8D\,(1+\beta)^2} - \frac{U}{2D\,(1+\beta)^2}\int_0^a r\,\Phi\,(r)\,dr \quad (25)$$

Let $p = 2$ in equation (20) and substituting from (22) and (24)

$$\frac{d\mu^{(2)}}{dt} = \frac{2D}{1+\beta} + \frac{2\,\kappa\,U^2\,a^2}{D\,(1+\beta)} + \\ + \frac{2U^2}{3D\,(1+\beta)^3}\int_0^\infty \beta\,(l)\,l^2\,d \quad (26)$$

where

$$\kappa = \frac{1}{2}\int_0^1 \Phi^2(\rho)\,\frac{d\rho}{\rho} - \frac{1}{2(1+\beta)}\int_0^1 2\rho\,\Phi(\rho)\,d\rho + \frac{1}{8(1+\beta)^2} \quad (27)$$

and $\rho = r/a$. Thus

$$m_1 = Ut/(1+\beta)$$

$$m_2 = 2Kt$$

where $2K$ is an abbreviation for the right-hand side of (26). Then by (3)

$$D^* = \frac{Um_2}{2m_1} = D + \kappa\frac{U^2a^2}{D} + \frac{U^2}{3D(1+\beta)^2}\int_0^\infty \beta(l)\,l^2\,dl \quad (28)$$

Comparing (28) with (3) we see that the correct value for $\bar{D}$, the effective longitudinal diffusion coefficient in TURNER's model,

$$\bar{D} = D + \kappa\,U^2a^2/D \quad (29)$$

where κ is a constant depending not only on $\phi(r)$ but also on β.

For the parabolic profile $\phi(r) = 2(1 - r^2/a^2)$

$$\kappa = \frac{1 + 6\beta + 11\beta^2}{48(1+\beta)^2}$$

This reduces to TAYLOR's value when $\beta = 0$ but rises to eleven times this value when β is large. This is physically reasonable for the longitudinal dispersion is caused by the solute spending time in slowly moving regions. Thus if there is a large region of zero speed, i.e. β is large, the longitudinal diffusion is enhanced.

NOTATION

a = radius of circular channel
c = concentration in channel
c_l = concentration in pocket of length l
$c^{(p)} = p^{\text{th}}$ moment of $c = \int_0^\infty z^p\,c\,dz$
D = molecular diffusion coefficient
D^* = apparent diffusion coefficient in a flow system
$\bar{D}$ = longitudinal diffusion coefficient in TURNER's model
l = length of pocket
L = length of channel
$m_i = i^{\text{th}}$ spatial moment of concentration distribution
t = time
$\bar{t}$ = mean residence time
U = mean flow velocity
V = velocity of centre of mass of solute
x = length along channel
y = depth into pocket
$z = x - Vt$
$\alpha(l) = \beta(l)/l$
$\beta(l)$ = probability density of pockets of length l
$\delta(t)$ = Dirac's delta function
κ = shape factor
$\mu^{(p)} = p^{\text{th}}$ moment of total solute
σ^2 = variance of residence time
$\phi(r)$ = ratio of velocity at r to mean velocity
$\Phi(r) = \frac{1}{a^2}\int_0^r 2r\,\phi(r)\,dr$

REFERENCES

[1] TURNER G. A. *Chem. Engng. Sci.* 1958 **7** 156.
[2] VAN DER LAAN E. T. *Chem. Engng. Sci.* 1958 **7** 187.
[3] TAYLOR G. I. *Proc. Roy. Soc.* 1953 **A219** 186.
[4] ARIS R. *Proc. Roy. Soc.* In press.
[5] GOLAY M. J. E. Contribution to the Gas Chromatography Symposium, Amsterdam, 1958.
[6] ARIS R. *Proc. Roy. Soc.* 1956 **A235** 67.
[7] ARIS R. *Chem. Engng. Sci.* 1959 **10** 80.

Chemical Engineering Science, 1959, Vol. 11, pp. 199 to 206. Pergamon Press Ltd., London. Printed in Great Britain

An analysis of chemical reactor stability and control—IV.

Mixed derivative and proportional control

D. J. Nemanic and J. W. Tierney
Remington Rand Univac St. Paul
and
R. Aris and N. R. Amundson
Department of Chemical Engineering, University of Minnesota, Minneapolis 14, Minnesota

(*Received* 7 *April* 1959)

VOL. 11 959/60

Abstract—The previous analysis of reactor stability and control is here extended to show the new features which arise when a derivative mode is added to the proportional controller. It is found that more care is needed to ensure full control of the whole phase plane, for the possibility of partial control is greater than in the previous example. It is also necessary to consider the effect of delay in the controller. These phenomena emphasize the care that must be taken in a satisfactory stability analysis.

Résumé—L'étude précédente sur la stabilité et le contrôle d'un réacteur est poursuivie pour montrer les nouveaux caractères qui se présentent quand une action dérivée est ajoutée à l'action proportionnelle du contrôleur. Les auteurs ont trouvé que pour assurer un contrôle total du palier de stabilité, il faut apporter plus de soin, la possibilité d'un contrôle partiel étant plus grande que dans l'exemple précédent. L'effet de retard du contrôleur est aussi à considérer. Le phénomène souligne les précautions à prendre pour une analyse de stabilité satisfaisante.

Zusammenfassung—Eine frühere Untersuchung über die Stabilität und Regelung eines Reaktors ist hier für den Fall erweitert, dass dem Proportionalregler ein Vorhalt gegeben wird. Es zeigt sich, dass man in diesem Falle stärker auf die volle Regelung im ganzen Phasenbereich achten muss, weil die Möglichkeit einer Teilregelung grösser ist als im früheren Beispiel. Auch die Verzögerung in dem Regler muss in Betracht gezogen werden. Auf alle diese Erscheinungen ist bei einer ausreichenden Stabilitätsuntersuchung zu achten.

The preceding papers of this series [1] have outlined the methods of analysing the stability and control of a single stirred tank reactor. The possibility of control by a mixture of proportional and derivative control was established (Part I, Section 4), but the evolution of the system only fully described for proportional control. This paper will show the new features which arise when a measure of derivative control is added to the proportional controller. As might be expected from the very responsive nature of derivative control the possibility of hard oscillations is greater. It is also found necessary to consider the effect of a small delay in the controller, for however small this may be it imposes on the derivative control gain constant a restriction that could not otherwise have been anticipated. A second-order reaction is used in this discussion and a slightly different reduction to dimensionless variables adopted.

1. The System

The system to be considered is a single stirred tank reactor of volume V in which a second-order irreversible reaction is taking place. If A is the concentration of the reactant which is being used at a rate kA^2 per unit volume a mass balance gives

$$V\frac{dA}{d\theta} = Q(A_0 - A) - kVA^2 \qquad (1.1)$$

where θ is the time, Q the flow rate and A_0 the inlet concentration. k is the reaction rate constant, a function of temperature $k = k_1 \exp(-E/RT)$.

If the temperature is controlled by a cooling coil through which a coolant flows at a rate Q_c

entering at temperature T_c and leaving at $T_c + \Delta T_c$, a heat balance gives the equation

$$Vc\rho \frac{dT}{d\theta} = Qc\rho (T_0 - T) + (-\Delta H) kVA^2 - Q_c \rho_c c_c \Delta T_c \quad (1.2)$$

where c, c_c are specific heats of reactants and coolant, and

ρ, ρ_c are densities of reactants and coolant respectively,

T_0 is the inlet reactant temperature,

$-\Delta H$ is the heat evolved for each mole of A destroyed.

Since the mean temperature of the coolant is $T_c + (1/2)\Delta T_c$ a heat balance on the cooling coil gives

$$Q_c \rho_c c_c \Delta T_c = h A_h (T - T_c - (1/2)\Delta T_c) \quad (1.3)$$

where A_h is the area of cooling coil and h the heat transfer coefficient. By solving (1.3) for ΔT_c and substituting into the last term of (1.2) we have

$$Q_c \rho_c c_c \Delta T_c = \frac{F}{1+F} h A_h (T - T_c) = U(T - T_c) \quad (1.4)$$

where

$$F = 2 Q_c \rho_c c_c / h A_h.$$

If h were constant F would be proportional to Q_c. This would be the case if the resistance to heat transfer were wholly on the reactor side, for the value of h would then be set by the level of agitation. If the resistance were wholly on the inside of the cooling tube we should expect h to vary with Q_c, a popular correlation gives $h = h_1 Q_c^{4/5}$. The combined effect of these will give

$$\frac{1}{h} = \frac{1}{h_1 Q_c^{4/5}} + \frac{1}{h_2}$$

whence

$$F = \frac{2 \rho_c c_c}{A_h} \left(\frac{Q_c^{1/5}}{h_1} + \frac{Q_c}{h_2} \right) \quad (1.5)$$

then

$$U(Q_c) = 2 Q_c \rho_c c_c \left[1 + \frac{2 \rho_c c_c}{A_h} \left(\frac{Q_c^{1/5}}{h_1} + \frac{Q_c}{h_2} \right) \right]^{-1} \quad (1.5)$$

Thus F is a function of Q_c and gives a dimensionless form of the flow rate, and eliminating Q_c between these two equations U can be expressed as a function of h. The heat balance equation can then be written

$$Vc\rho \frac{dT}{d\theta} = Qc\rho (T_0 - T) + (-\Delta H) kVA^2 - U(F)(T - T_c) \quad (1.7)$$

The controller varies the coolant flow rate in response to measured deviations of the temperature from the desired value T_s and to the derivative of the temperature variation. For reasons given earlier (Part II, section 9, [1]), T_s is chosen to be a natural steady state of the system. Thus the controller equation can be written

$$F = F_s + c_1 (T - T_s) + c_2 \frac{d}{d\theta} (T - T_s)$$

It is this equation together with (1.1) and (1.7) which have been integrated to show the behaviour of the system, the interest again being in whether the naturally unstable steady state can be controlled. The values of the physical constants, which have been chosen to simulate a realistic situation, are given in Table 1.

Table 1. *Physical constants*

Constant	*Value*	*Units*	*Constant*	*Value*	*Units*
A_0	1·000	lb moles/ft^3	A_h	500	ft^2
T_0	650	°R	h_1	0	B.t.u/ft^2 hr °R
Q	0·3	ft^3/sec	h_2	100	B.t.u/ft^2 hr °R
ρ	60·0	lb/ft^3	$-\Delta H$	20,000	B.t.u/lb mole
ρ_c	62·5	lb/ft^3	k_1	$2{\cdot}7 \times 10^{11}$	ft^3/lb mole sec
c	1·0	B.t.u/lb °R	T_c	520	°R
c_c	1·0	B.t.u/lb °R	E	44,700	B.t.u/lb mole
V	100	ft^3	R	1·11	B.t.u/lb mole °R

Table 2. Dimensionless parameters

$$\alpha = 2\,V k_s A_s/Q \qquad \gamma = \frac{V k_s A_s}{Q}\frac{E}{RT_s}\frac{(-\Delta H)A_s}{c\rho\,T_s}$$

$$\beta = \frac{U_s}{Qc\rho} - \frac{F_s}{1+F_s}\frac{h\,A_h}{Qc\rho} \qquad \delta = \frac{T_s - T_c}{T_s}\frac{1}{Qc\rho}\left(\frac{\partial U}{\partial F}\right)_s$$

$$\left(\frac{\partial U}{\partial F}\right)_s = \frac{A_h h_2}{(1+F_s)^2}\,\frac{1 + 8\,(Q_c\,\rho_c\,c_c/A_h\,h_2)\,(h_2/5h_1\,Q^{1/5})}{[1 + (h_2/5h_1\,Q_c^{4/5})]}$$

$$\kappa = (-\Delta H)\,A_s/c\rho\,T_s$$

A steady state has concentration $A = A_s$ and temperature $T = T_s$ satisfying the equations

$$Q(A_0 - A_s) - k_s V A_s^2 = 0 \qquad (1.8)$$

$$Qc\rho\,(T_0 - T_s) + (-\Delta H)\,k_s V A_s^2 - U_s(T_0 - T_c) = 0 \qquad (1.9)$$

where $k_s = k_1 \exp(-E/RT_s)$ and $U_s = U(F_s)$. For the numerical values of Table 1 the unstable steady state we wish to control is at

$$A_s = 0{\cdot}61912 \text{ lb moles/ft}^3, \quad T_s = 700{\cdot}00\ ^\circ\text{R}$$

with $$Q_{cs} = 0{\cdot}13810 \text{ ft}^3/\text{sec}.$$

It is convenient to introduce dimensionless quantities by the substitutions

$$\tau = Q\,\theta/V,\ a = (A - A_s)/A_s,$$
$$t = (T - T_s)/T_s,\ f = F - F_s$$

With these substitutions equations (1.1) and (1.7) can be linearized in the usual way, and become

$$\frac{da}{d\tau} = -(1+\alpha)\,a - \kappa^{-1}\gamma\,t \qquad (1.10)$$

$$\frac{dt}{d\tau} = \kappa\,\alpha\,a - (1 + \beta - \gamma)\,t - \delta f \qquad (1.11)$$

where the dimensionless constants are defined in Table 2 α, β, γ and δ play the same role as in Part 1, section 3, though they differ in detail because of the different definition of the dimensionless quantities. With this linearization we can discuss the stability of the steady states.

2. Stability Under Control

The form of control we wish to investigate is that in which the departure of the coolant flow rate Q_c from its set point is proportional to a linear combination of the departure of the reactor temperature T from its set point T_s and the derivative of the temperature. In terms of the dimensionless co-ordinates introduced we put

$$\delta f = \lambda t + \mu\frac{dt}{d\tau} \qquad (2.1)$$

where λ and μ are the two proportionality constants. Equations (1.10) and (1.11) then become

$$\frac{da}{d\tau} = -(1+\alpha)\,a - \kappa^{-1}\gamma\,t \qquad (2.2)$$

$$\frac{dt}{d\tau} = \frac{\kappa\alpha}{1+\mu}\,a - \frac{1+\beta-\gamma-\lambda}{1+\mu}\,t \qquad (2.3)$$

Proceeding exactly as in Part I, section 4 we have to examine the roots of the quadratic

$$\Delta(p) \equiv \begin{vmatrix} p + 1 + \alpha & \kappa^{-1}\gamma \\ -\dfrac{\kappa\alpha}{1+\mu} & p + \dfrac{1+\beta-\gamma+\lambda}{1+\mu} \end{vmatrix} = 0$$

This may be written

$$\left.\begin{aligned} &(1+\mu)\,p^2 + d_e' + d_f' = 0 \\ \text{where } &d_e' = (1+\alpha)(1+\mu) + 1 + \beta - \gamma + \lambda \\ &d_f' = (1+\alpha)(1+\beta) - \gamma + \lambda(1+\alpha) \end{aligned}\right\} \qquad (2.4)$$

and the condition for stability is that $(1+\mu)$, d_e and d_f should all be of the same sign. In the absence of control this means that

$$d_e \equiv 1 + \alpha + 1 + \beta - \gamma > 0 \text{ and}$$
$$d_f = (1+\alpha)(1+\beta) - \gamma > 0$$

the criteria obtained in Part I, section 3 equations (3.5) and (3.6) [1].

We are interested however in controlling a naturally unstable state in which not both d_e and d_f are positive. The constants λ and μ therefore have to make the three quantities

$$1 + \mu, \quad d_e' = d_e + \lambda + (1 + \alpha)\,\mu,$$
$$d_f' = d_f + (1 + \alpha)\,\lambda$$

all of the same sign. It is intuitively evident that no good can come of large negative λ and μ, for this would mean that the cooling rate would be decreased when the temperature increased, just the opposite of what is required. It would be a mistake however simply to require all three to be positive and dispose of the analytical possibility of all being negative with a flurry of intuitive arm-waving, for in the proper resolution of this difficulty we shall find that not only is $\mu > -1$ (making all quantities positive) but also $\mu < 1$, a restriction that could not otherwise have been anticipated. This will be the burden of the next paragraph; we will conclude this one by seeing what features of the reactor's behaviour can be predicted before the actual calculations are made.

The values of the proportionality constants λ and μ may be taken as co-ordinates of a point in a plane. The region of stability defined by $1 + \mu > 0$, $d_e' > 0$, $d_f' > 0$ is thus the region above and to the right of the three lines AB, BC and CD in Fig. 1. The roots of quadratic $\Delta(p) = 0$ are complex if the point λ, μ is within the parabola $d_e'^2 = 4(1 + \mu)\,d_f'$. This parabola touches AB at B and CD at C and immediately shows the character of the steady state at any point, as shown in Fig. 1. Fig. 1 is drawn for the given system and the numerical results are

$$\lambda + 2{\cdot}2300\,\mu > 2{\cdot}1695, \qquad \lambda > 1{\cdot}1855$$

Since the steady states are defined by setting the derivative equal to zero it is evident that their position is independent of μ. For a given value of λ the position of all the critical points can be obtained by solving equations (1.8) and (1.9) for A_s and T_s. Moreover since λ does not appear in equation (1.8) all critical points lie on the curve in the A, T plane defined by equation (1.8). The method of solution is exactly the same as in Part II, section 9 [1] and need not be repeated here. The result of the calculation is shown in Fig. 2 where the numerical values are for the example given. As in the previous example it is found that the two other steady states coalesce and disappear at a value of λ (1·46) less than that at which stability of the controlled steady state is assured. We may thus expect a region where there is a stable limit cycle surrounding the still unstable control point.

A more interesting situation however, which was uncovered in the previous work, may be expected here, namely the presence of an unstable limit cycle surrounding the control point even after this has been made stable. This means that the control is really only exercised over a small

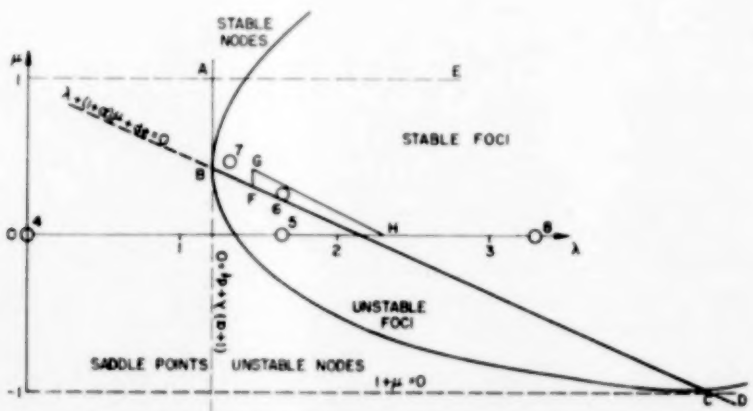

Fig. 1. Stability for control parameters λ and μ.
[Numbered circles refer to figure number of phase portraits].

region of the phase plane and that any excitation that takes the system beyond this will lead to a steady oscillation round a stable limit cycle. This phenomenon is discussed in detail in Part II, section 10 [1], but in the example there given was very transitory. In the present case we might expect a zone lying to the right and above the transition line BC such that values of λ and μ lying there would give rise to this effect. Such is the case and the part of its boundary which has been determined is the line FGH in Fig. 1.

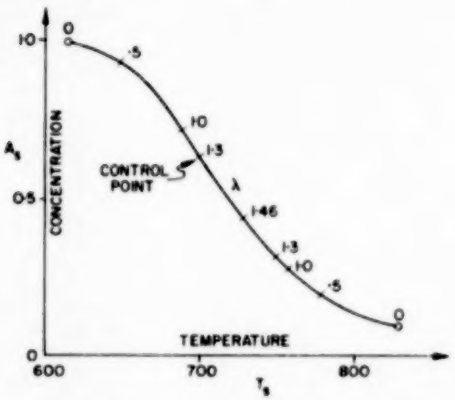

FIG. 2. Position of steady state for varying λ.

3. Stability with Delayed Control

If the controlling system has a small delay ϵ in transmitting the signal the values of T and $dT/d\theta$ actuating the value for the coolant flow rate Q_c at time θ will be $T(\theta - \epsilon)$ and $(dT/d\theta)_{\theta-\epsilon}$. Thus the transform of δf will not now be

$$\delta\bar{f} = \lambda\bar{t} + \mu\left[p\bar{t} - t(0)\right] \text{ but}$$

$$\delta\bar{f} = \exp(-\epsilon p)\left\{\lambda\bar{t} + \mu\left[p\bar{t} - t(0)\right]\right\} \qquad (3.1)$$

If this is inserted in the Laplace transformation of equations (1.10) and (1.11) and these are solved for $\bar{t}$ we have,

$$\bar{t} = \left\{\kappa\,\alpha\,a(0) + (p + 1 + \alpha) \times \left[1 + \mu\exp(-\epsilon p)\right] t(0)\right\}/\Delta'(p)$$

where

$$\Delta'(p) = (p^2 + d_e\,p + d_f) + \exp(-\epsilon p) \times (p + 1 + \alpha)(\mu p + \lambda) \qquad (3.2)$$

The stability will now depend on the sign of the real part of the zeros of $\Delta'(p)$, the system being stable if these are all negative.

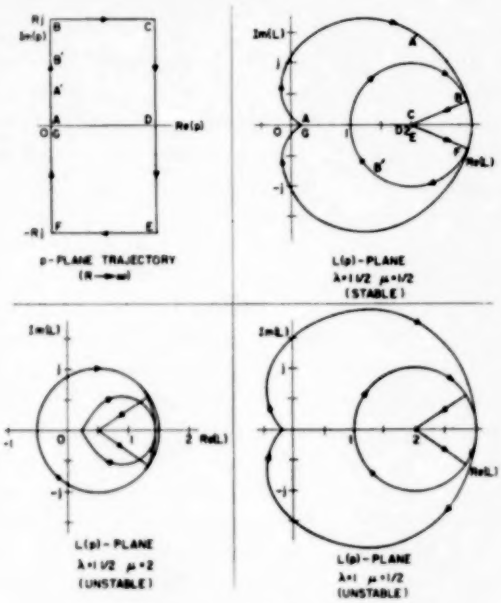

FIG. 3. Nyquist diagrams.

The existence of roots with positive real part may be shown by the Nyquist diagram. Consider the function

$$L(p) = \exp(-\epsilon p) + \frac{p^2 + d_e\,p + d_f}{(p + 1 + \alpha)(\mu p + \lambda)} \qquad (3.3)$$

This will map the p contour of Fig. 3 into a curve in the L plane such as is shown in the other diagrams of this figure. The imaginary axis $p = i\omega$ maps on the curve AA′ B′ B which goes from the point A on the real axis of the L plane and goes rapidly into the circle $L = \exp(-i\epsilon\omega) + \mu^{-1}$ for when ω, and so $|p|$, is large the quotient of quadratics is close to μ^{-1}. The point B on the imaginary axis of p will correspond to some point B on the circle of argument ω_B. Now as the imaginary part of p is held constant and Re (p) increases the quotient of quadratics will remain close to μ^{-1} since $|p|$ is large and arg $\exp(-\epsilon p)$ will remain constant $(= \omega_B)$ but the modulus of $\exp(-\epsilon p)$ will tend to zero. The image of BC in the p-plane is thus the radius BC of the circle in

L plane. As p traverses CDE the image point will describe an arbitrarily small curve about the point $L = \mu^{-1}$. The rest of the curve is a mirror image of the earlier part in the real axis of the L plane.

Now the value of ϵ affects the approach to the circle and the number of times it is traversed, but however small ϵ may be the circle will have unit radius and centre μ^{-1}. Thus whatever the behaviour of the rest of the curve the circle will certainly contain the origin if $-1 < \mu^{-1} < 1$ i.e. $|\mu| > 1$. We have then a further condition for stability $-1 < \mu < 1$. The first inequality disposes of the paradoxical region $\mu < 1$ $\lambda < d_f/(1 + \alpha)$, the second is a new restriction not anticipated by simple linearization.

The third and fourth sections of Fig. 3 show two cases of instability. In (iii) it is due to the delay term, it being the circle that encloses the origin; in (iv) the conditions are unstable even without delay. The curves are drawn for the constants of the given system and for $\epsilon = 0{\cdot}01$, but would scarcely be different for any other sufficiently small value of $\epsilon > 0$.

It will be observed that a restriction of this kind will apply in the general case discussed in Part I, section 5 [1] where

$$\delta\bar{f} = K\,G(p)\,\bar{l}$$

and $G(p) = M(p)/N(p)$ is a rational function of degree m in the numerator and n in the denominator, if $m = n + 1$. Physically this transfer function defines an imperfect form of derivative and proportional control. If in addition it has a delay ϵ then the function whose zeros must be examined is

$$L(p) = \exp(-\epsilon p) + \frac{1}{K}\,\frac{p^2 + d_e\,p + d_f}{(p + 1 + \alpha)\,G(p)}$$

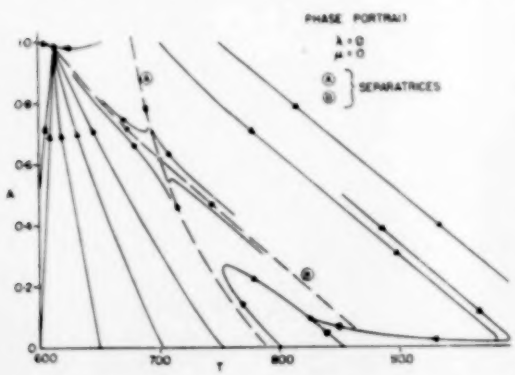

FIG. 4. $\lambda = 0$, $\mu = 0$ Phase portrait.

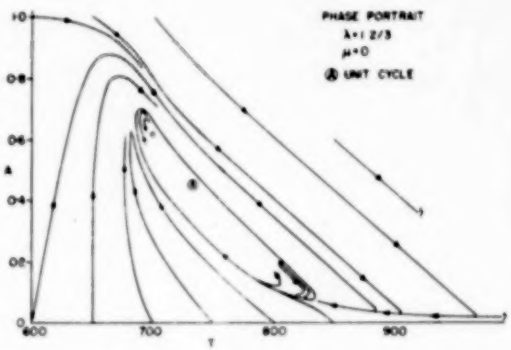

FIG. 5. $\lambda = 1{\cdot}66$, $\mu = 0$, Phase portrait.

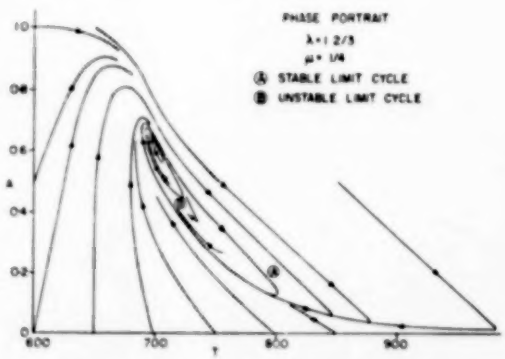

FIG. 6. $\lambda = 1{\cdot}6,6$ $\mu = 0{\cdot}25$ Phase portrait.

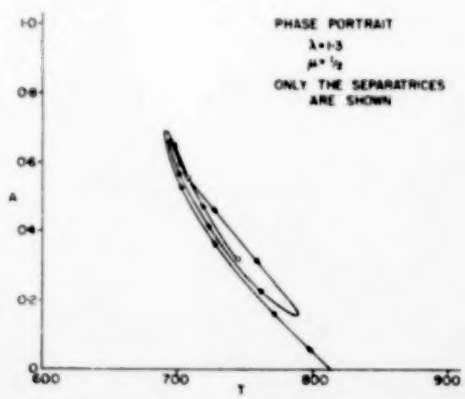

FIG. 7. $\lambda = 1{\cdot}3$, $\mu = 0{\cdot}5$ Phase portrait.

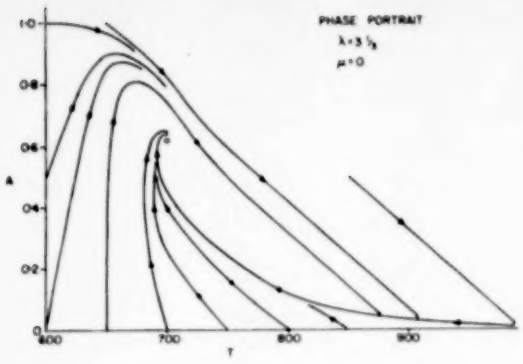

FIG. 8. $\lambda = 3{\cdot}33$, $\mu = 0$ Phase portrait.

VOL. 11 959/60

Since $m = n + 1$ the second term is the quotient of two polynomials each of degree $n + 2$ and so when $|p|$ is very large $L(p) = \exp(-\epsilon p) + K^{-1}$. Again we must require $|K| < 1$.

4. Results

As in the earlier parts of the paper the behaviour of the reactor has been studied by integrating the non-linear equations (1.1) and (1.7) numerically. The Univac Scientific Computer, Model 1103, was again used and the Gill modification of the Runge-Kutta numerical integration scheme. The general structure of the programme has been described in Part III.12 [1] and need not be repeated. The value of the derivative for control purposes was taken to be the value at the previous time increment. Thus the slight delay ϵ was simulated and the conclusion regarding instability for $|\mu| > 1$ was checked. That this delay had no effect on the calculation of curves in the phase plane was established by decreasing it to 1/32 of its value; with this decrease the curves were reproduced accurately.

Of the phase portraits calculated Figs. 4–8 will suffice to show the general behaviour of the system. Their disposition relative to the boundaries of stability is shown in Fig. 1. Fig. 4 is the natural face of the reactor, showing the way it behaves without control. This is entirely similar to the system previously discussed (Part II, Fig. 11). The naturally unstable steady state at $T = 700°$R, $A = 0{\cdot}61912$ moles/cu. ft is the one we wish to control. In Fig. 5 $\lambda = 1{\cdot}66$, $\mu = 0$ and there is sufficient control to have removed the other states, but the control state is still unstable and surrounded by a stable limit cycle. Fig. 6 ($\lambda = 1{\cdot}66$, $\mu = 0{\cdot}25$) shows the condition of partial control in which the stable control point is surrounded by an unstable limit cycle and this again by a stable cycle. The unstable limit cycle was accurately located by reversing the direction of time. This reverses the stabilities and by starting a trajectory very close to the control point, which is now unstable, the solution spirals outwards to the now stable limit cycle. By a careful search using this technique the boundary FGH (see Fig. 1) of the region of the λ, μ plane in which such unstable limit cycles exist was determined. The sharp vertical boundary FG seems to correspond to the value of λ above which only one steady exists. This is confirmed by Fig. 7 with $\lambda = 1{\cdot}3$ $\mu = 0{\cdot}5$; although this is very close to the threshold of stability there is no limit cycle but two unstable and one stable critical point. For clarity only the separatrices are shown in this figure. Finally Fig. 8 with $\lambda = 3{\cdot}33$ and $\mu = 0$ shows the whole phase plane under full control.

Notation

A = concentration of reactant
A_0 = inlet concentration
A_s = steady state concentration
A_h = area of cooling coil
E = activation energy
$F = 2Q_c \rho_c c_c / h A_h$ = dimensionless flow rate
F_s = steady state value of F
$G(p) = M(p)/N(p)$ = transfer function for imperfect control
$-\Delta H$ = heat of reaction
K = proportionality constant
$L(p)$ = complex variable of Nyquist plots
$M(p)$ = numerator of $G(p)$
$N(p)$ = denominator of $G(p)$
Q = flow rate through reactor
Q_c = flow rate of coolant
T = temperature
T_c = inlet coolant temperature
T_0 = inlet temperature
T_s = steady state temperature
U = heat transfer coefficient
U_s = steady state heat transfer coefficient
V = volume of reactor
$a = (A - A_s)/A_s$

c = specific heat of reactant
c_c = specific heat of coolant
$d_e = 1 + \alpha + 1 + \beta - \gamma$
$d_f = (1 + \alpha)(1 + \beta) - \gamma$
$d_e' = d_e + (1 + \alpha)\mu + \lambda$
$d_f' = d_f + (1 + \alpha)\lambda$
$f = F - F_s$
h, h_1, h_2 = heat transfer coefficients for cooling coil
k = reaction rate constant $= k_1 \exp(-E/RT)$
k_s = steady state value of k
p = Laplace transform variable
$t = (T - T_s)/T_s$
ϵ = time delay in system
θ = time
λ = proportional control constant
μ = derivative control constant
ρ = density of reactants
ρ_c = density of coolant
$\tau = Q\theta/V$
ω = imaginary part of p

Reference

[1] Aris R. and Amundson N. R. *Chem. Engng. Sci.* 1958 **7** 121.

VOL
11
1959

Chemical Engineering Science, 1959, Vol. 11, pp. 207 to 211. Pergamon Press Ltd., London. Printed in Great Britain

The hydrodynamics of flow between horizontal concentric cylinders—II.

Generalized criteria and correlation of heat transfer data

A. H. Nissan and F. C. Haas

Department of Chemical Engineering, Rensselaer Polytechnic Institute, Troy, New York

(*Received* 16 *May* 1959)

Abstract—The neutral stability criteria for the generalized case of flow due to circumferential pumping and rotation of the inner cylinder are reviewed. The neutral stability is defined by the parameter, P, as used by Brewster *et al.* Heat transfer data taken from the literature have been recalculated. The parameter P is found to be useful in correlating the data.

Résumé—Les auteurs ont examiné les critères de stabilité indifférente pour le cas généralisé d'un écoulement dû à un pompage circulaire et à une rotation d'un cylindre intérieur. La stabilité indifférente est définie par le paramètre P, tel qu'il a été utilisé par Brewster *et al.* Les données du transfert thermique prises dans la littérature ont été calculées à nouveau. Il a été constaté que le paramètre P a son utilité dans la corrélation des données.

Zusammenfassung—Verfasser teilen das neutrale Stabilitätskriterium mit für eine Strömung, die unter dem Einfluss einer Zwangskraft in Umfangsrichtung bei Rotation des inneren Zylinders zustande kommt. Die neutrale Stabilität wird durch den Parameter P nach Brewster *et al.* definiert. Wärmeübertragungswerte der Literatur werden von neuem berechnet. Hierbei erweist sich der Parameter P als zweckmässig, um die Daten zu korrelieren.

Introduction

In an earlier paper Brewster and Nissan [1] have discussed the fluid motion between concentric cylinders when the flow was due to rotation of the inner cylinder. The secondary flow patterns discussed included those that occurred when the primary flow was either fully or partially reversed. It is the purpose of this paper to review the case where the flow may be due to a circumferential pressure gradient and/or rotation of the inner cylinder and to show that a generalized parameter may be used to correlate heat transfer data.

Review of Generalized Criteria

Dean [2] has shown theoretically and Brewster *et al.* [3] have shown experimentally that when a fluid is pumped circumferentially around an annulus, a vortex instability occurs in the outer section of the annulus. The instability is similar to the vortex motion predicted and shown by Taylor [4] in his classical paper on hydrodynamics of fluids contained between concentric rotating cylinders.

The problem of simultaneous circumferential pumping and rotation of the inner cylinder has been treated theoretically and experimentally by Nissan *et al.* [3] and theoretically by Di Prima [5]. It is observed that all possible combinations of secondary flow can be obtained by suitably adjusting the variables in this generalized case. To allow for the combined rotation and pumping, the parameter N is defined:

$$N = \frac{\Omega_1 a d t}{2 Q} \tag{1}$$

It may be noted from the definition of N that a value of zero corresponds to the problem Dean [2] considered and that a value of one corresponds to the problem considered by Taylor [4].

Nissan *et al.* [3] have considered the case of $N = \pm \infty$. Applying the Rayleigh instability criteria for inviscid fluids (shown by Synge [6] also to be applicable to viscous fluids) to this case, it is found that actually two regions of potential instability occur in the annulus. One region occurs adjacent to the inner cylinder wall,

while the other occurs adjacent to the outer cylinder wall. It is further shown that the region adjacent to the inner cylinder will become unstable first and this is considered to be the point of neutral stability for the system. The criteria for neutral stability for the three cases $N = 0$, 1, and $\pm \infty$ are listed in Table 1.

If the unstable region, δ, is bounded by a streamline of zero velocity, the width is easily calculated by considering the radius of the zero velocity streamline as derived from the Couette flow equation:

$$\Omega = \frac{\Omega_1 (1 - \mu)}{1 - (a/b)^2} \left(\frac{a}{r}\right)^2 + \frac{\Omega_1 (1 - \mu)(b/a)^2)}{1 - (b/a)^2} \qquad (2)$$

If $d/a \to 0$, then δ/d may be defined as follows:

$$\delta/d = \frac{1}{1 - \mu}$$

Nissan *et al.* [3] define a parameter, P, which describes the stability for all values of N as applied to the case of simultaneous circumferential pumping and rotation of the inner cylinder.

$$P = \frac{V \delta}{\nu} \sqrt{\frac{\delta}{a}} \qquad (3)$$

The values of P which define the condition of neutral stability are given as:

$$0 < \delta/d < 2/3 \qquad P_c = 12$$

$$2/3 < \delta/d \leqslant 1{\cdot}0 \qquad P_c = 20{\cdot}7\,(\delta/d)^{5/2} \times \frac{\sqrt{[2\,(\delta/d) - 1]}}{\sqrt{\{[2\,(\delta/d) - 1]^2 + 0{\cdot}01\}}} \qquad (4)$$

Heat Transfer Data

Although only a small amount of data is available in the literature for heat transfer through a fluid contained between concentric rotating cylinders, it is evident that the heat transfer rate is dependent upon the annulus size and the ratio of angular velocities of the cylinders. Bjorklund and Kays [7] present the only extensive set of data at the present time. Their data indicate that the Nusselt number is constant and dependent only on geometry until the critical angular velocity is reached. When the critical angular velocity is exceeded, the Nusselt number steadily increases. The data indicate, as is to be expected, that each combination of d/a and μ presents an individual critical Taylor number. The authors use the following empirical equation to correlate their data:

$$\frac{\mathrm{Nu}}{\mathrm{Nu}_{\mathrm{cond.}}} = 1{\cdot}1 \left\{\frac{\mathrm{Ta} - [\mathrm{Ta}_{c\mu} - \mathrm{Ta}_{c\mu=0}]\,[1 - 3{\cdot}5\,(d/a)]}{41{\cdot}4 + [\mathrm{Ta}_{c\mu} - {}_{c\mu}\mathrm{Ta}_{=0}]\,[3{\cdot}5\,(d/a)]}\right\}^{1/2} \qquad (5)$$

Gazley [8] considers the problem of heat transfer in electric motors and presents a limited amount of heat transfer data for smooth concentric rotating cylinders.

Correlation of heat transfer data

The data of Bjorklund and Kays [7] and Becker [9] have been recalculated using the parameter P. Since there was no circumferential

Table 1. *Criteria for neutral stability*

N	*Defining equation*	*Width of unstable region*	*Author*
0	$\frac{V_c d}{\nu}\sqrt{\frac{d}{a}} = 36$	$d/2$	Dean [2]
1	$\frac{\Omega_{ic} a d}{\nu}\sqrt{\frac{d}{a}} = 41{\cdot}4$	d	Taylor [4]
$\pm \infty$	$\frac{\Omega_{ic} a d}{\nu}\sqrt{\frac{d}{a}} = 140$	$d/3$	Nissan *et al.* [3]

pumping involved, the parameter may be defined as:

$$P = \frac{\Omega_1 a \delta}{2\nu}\sqrt{(\delta/a)} \qquad (6)$$

or more conveniently for this case:

$$P = 1/2\,(\delta/d)^{1/2}\,\mathrm{Ta}_0$$

where Ta_0 is the Taylor number which has been corrected for the finite gap width by the use of a geometric factor, F_g, as suggested by KAYE and ELGAR [10]. The geometric factor modifies the Taylor number when the gap width is large, i.e., when d/a does not approach zero.

$$\mathrm{Ta} = \mathrm{Ta}_0 F_g$$

where F_g is defined by

$$F_g = \frac{\pi^2}{41{\cdot}4}\left(1 - \frac{b}{2r_m}\right)^{-1} Z^{-1/2} \qquad (7)$$

$$Z = 0{\cdot}0571\left[1 - 0{\cdot}652\left(\frac{b/r_m}{1 - b/2r_m}\right) + \right.$$
$$\left. + 0{\cdot}0056\left[1 - 0{\cdot}652\left(\frac{(b/r_m)}{1 - b/2r_m}\right)\right]^{-1}\right.$$

For counter-rotation of the two cylinders, δ was calculated by considering radii of zero streamline velocity through use of the Couette flow equation.

$$r_0^2 = \frac{(\mu - 1)(a^2 - b^2)}{[1 - (a/b)^2][1 - \mu\,(b/a)^2]}$$

For co-rotation of the two cylinders the unstable region extends over the entire gap width. Following the suggestion of DIPRIMA [11] the angular velocity was approximated by a constant, the arithmetic mean velocity, and the parameter was defined as:

$$P = \frac{\mathrm{Ta}_0(1 + \mu)}{4}$$

The points of neutral stability defined by P_c as determined from the data are listed in Table 2. It is noteworthy that the values for $\delta/d < 2/3$ and $\delta/d = 1$ are quite constant and agree well with the theoretical values previously cited. The data have been plotted using the parameter P/P_c to represent the hydrodynamic situation (Fig. 1). The following equations may be said to represent the data.

Table 2. Critical values of P as determined from heat transfer data

d/a	μ	δ/d	P_c	*Reference*
0·054	− 0·99	0·488	11·6	[7]
0·084	− 0·56	0·620	12·0	[7]
0·084	− 0·99	0·476	11·9	[7]
0·084	− 1·96	0·310	11·5	[7]
0·128	− 0·55	0·625	12·6	[7]
0·128	− 0·96	0·470	11·5	[7]
0·128	− 1·96	0·320	11·8	[7]
0·246	− 0·55	0·568	12·0	[7]
0·246	− 0·96	0·446	11·2	[7]
0·246	− 1·95	0·284	10·7	[7]
		$\bar{P}_c =$	11·7	
0·054	0	1·0	20·2	[7]
0·084	0	1·0	19·8	[7]
0·084	+ 0·65	1·0	22·8	[7]
0·128	0	1·0	20·7	[7]
0·128	+ 0·62	1·0	22·1	[7]
0·246	0	1·0	20·9	[7]
0·243	0	1·0	21·3	[9]
		$\bar{P}_c =$	21·1	

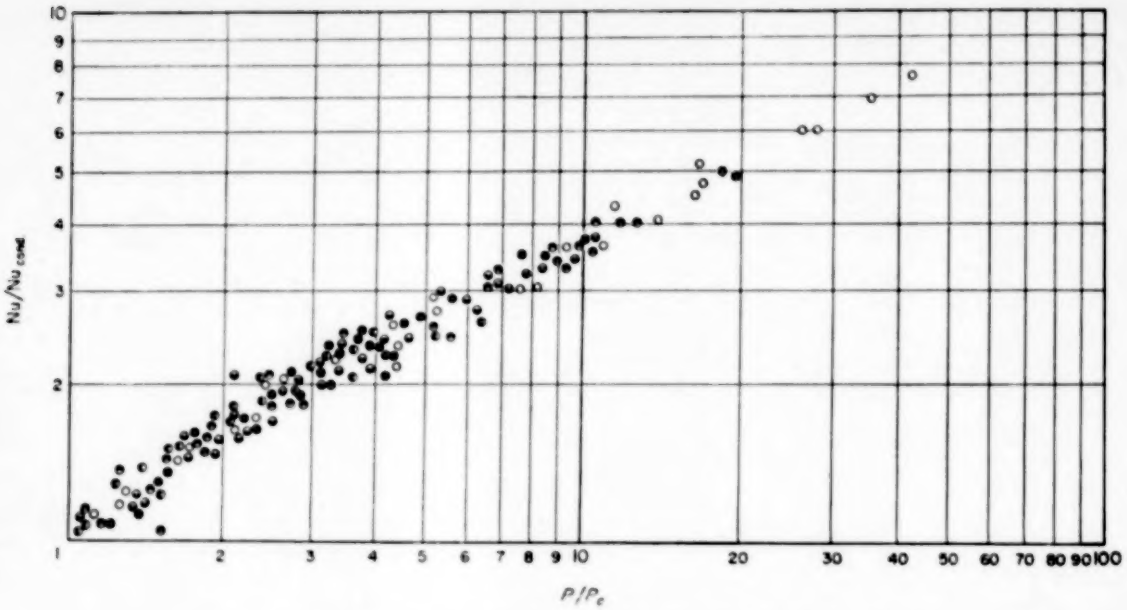

Fig. 1. Correlation of heat transfer data using the parameter P/P_c

	d/R_1	*Author*
○	0·246	Bjorklund and Kays
◓	0·128	Bjorklund and Kays
◒	0·084	Bjorklund and Kays
◐	0·054	Bjorklund and Kays
●	0·243	Becker

$$1 < \frac{P}{P_c} < 3 \quad \frac{Nu}{Nu_{cond.}} = \left(\frac{P}{P_c}\right)^{0.7}$$

$$3 < \frac{P}{P_c} < 40 \quad \frac{Nu}{Nu_{cond.}} = 0.5 + \left(\frac{P}{P_c}\right)^{0.5} \qquad (8)$$

All experimental points lie within $\pm$ 15 per cent of the lines defined by the above equations.

Within the limits of present knowledge (all data available is for one fluid-air) the above correlation allows one to predict the heat transfer characteristics of a system of concentric rotating cylinders if the geometry and cylinder rotational speeds are specified. The value of P_c is given directly by a knowledge of δ which may be evaluated from the geometry and μ. P is evaluated from knowledge of the cylinder rotational speed, and with these values, the convection heat transfer coefficient may be evaluated.

It would be desirable to know the effects of Prandtl number and circumferential pumping on the above correlation, but such data are not available at present.

Conclusion

It has been established that the parameter P is useful in correlating heat transfer data for a fluid contained between concentric rotating cylinders. A study of data taken from the literature has indicated that the convection heat transfer coefficient may be predicted if the geometry and cylinder angular velocities are established.

Acknowledgements—The authors wish to thank the Procter and Gamble Company for their Fellowship support to F. C. Haas, and the authors also wish to record their indebtedness to Professor Joseph Kaye of Massachusetts Institute of Technology for permitting use of the data listed under Reference [9].

Notation

a = radius of inner cylinder
b = radius of outer cylinder
d = width of annulus
F_g = geometric factor defined by equation (7)
h = convection heat transfer coefficient
k = thermal conductivity
N = dimensionless number defined by equation (1)
$\mathrm{Nu} = 2hd/k$ = Nusselt Number
$\mathrm{Nu}_{\mathrm{cond.}} = \dfrac{2\,(d/a)}{\ln[(d/a)+1]} \simeq 2$ Nusselt number for conduction
$\mathrm{Ta} = (\Omega_1\, ad)/\nu\sqrt{(d/a)}$ = Taylor number
P = dimensionless number defined by equation (3)
Q = volumetric flow rate through pump
r = radius
r_0 = radius of zero velocity streamlines
l = axial length of annular space
$\bar{V}$ = average velocity in unstable region
δ = width of unstable flow region
μ = ratio of angular velocity of outer and inner cylinders
ν = kinematic viscosity
Ω = angular velocity

Subscripts

0 = denotes $d/a \to 0$
1 = denotes inner cylinder
c = denotes condition of neutral stability
m = arithmetic mean
μ = denotes cylinder speed ratio

References

[1] Brewster D. B. and Nissan A. H. *Chem. Engng. Sci.* 1958 **7** 215.
[2] Dean W. R. *Proc. Roy. Soc.* 1928 **A121** 402.
[3] Brewster D. B., Grosberg P. and Nissan A. H. *Proc. Roy. Soc.* 1959 **A251** 76.
[4] Taylor G. I. *Phil. Trans.* 1922 **A223** 289.
[5] DiPrima R. C. *J. Fluid Mech.* 1959 in press.
[6] Synge J. L. *Proc. Roy. Soc.* 1938 **A167** 250.
[7] Bjorklund I. S. and Kays W. M. *Trans. Amer. Soc. Mech. Engrs.* 1959 **81** 175.
[8] Gazley C. Jr., *Trans. Amer. Soc.* Mech. *Engrs.* 1958 **80** 79.
[9] Becker K. M. Sc.D.Thesis, Massachusetts Institute of Technology 1957
[10] Kaye J. and Elgar E. C. *Trans. Amer. Soc. Mech. Engrs.* 1958 **80** 753.
[11] DiPrima R. C. *Quart. J. Appl. Math.* 1955 **13** 55.

VOL. 11 959/60

Chemical Engineering Science, 1959, Vol. 11, pp. 212 to 220. Pergamon Press Ltd., London. Printed in Great Britain

Heat transfer in two-phase flow

H. Grootthuis and W. P. Hendal

Koninklijke/Shell-Laboratorium, Amsterdam
(Shell Internationale Research Maatschappij N.V.)

(*Received* 22 *May* 1959)

Abstract—Heat transfer measurements for the two-phase flow of water/air and gas-oil/air mixtures in a vertical tube are described.

Much attention has been given to the contribution of the heat-transfer section of the tube and the thermocouples for measurements of its wall temperatures so as to obtain accurate results.

The results of the measurements are compared with those for pure liquid flow. It is shown that especially the first amount of gas added to the liquid raises the heat transfer coefficient considerably. The results for the two-phase systems can be represented by simple correlations between the Nusselt and Reynolds numbers of the systems.

At higher gas/liquid ratios a maximum in the heat transfer coefficient is observed. An attempt is made to characterize its position by a dimensionless quantity.

Résumé—On a fait des mesures du transfert de la chaleur dans le cas d'écoulement de systèmes à deux phases, à savoir eau/air et gas-oil/air, dans un tube vertical.

Pour obtenir des résultats exacts, une grande attention a été dévouée à la construction de la section du tube où le transfert de chaleur se déroule, et aux thermocouples servant à mesurer les températures à la paroi.

Les résultats obtenus ont été comparés avec ceux pour l'écoulement d'un liquide normal. Il a été démontré que c'est surtout la première quantité de gaz ajoutée au liquide qui donne lieu à une forte augmentation du coefficient de transfert de la chaleur. Les résultats pour les systèmes à deux phases peuvent être représentés par de simples corrélations entre les nombres de Nusselt et de Reynolds des systèmes.

A des taux gaz/liquide plus élevés on observe un maximum dans le coefficient de transfert de chaleur. On a fait un effort de caractériser la position de ce maximum à l'aide d'une quantité sans dimensions.

Zusammenfassung—Die Verfasser beschreiben Wärmeübergangsmessungen für die Zweiphasenströmung von Wasser/Luft und Gas-Öl/Luft in einem senkrechten Rohr.

Auf die Konstruktion der Messstrecke des Rohres und der Thermoelemente zur Messung der Wandtemperatur wurde besondere Sorgfalt verwendet.

Die Messergebnisse werden mit denen für reine Flüssigkeitsströmung verglichen. Es zeigt sich, dass besonders die erste Gasmenge, die der Flüssigkeit zugefügt wird, den Wärmeübergangskoeffizienten beträchtlich erhöht. Die Ergebnisse für das Zweiphasensystem können durch eine einfache Beziehung zwischen den Nusselt- und den Reynolds-Zahlen des Systems dargestellt werden.

Bei höheren Verhältnissen Gas/Flüssigkeit wird ein Maximum des Wärmeübergangskoeffizienten beobachtet. Seine Lage wird versuchsweise durch eine dimensionslose Grösse charakterisiert.

VOL. 11
959/60

1. Introduction

In 1951, Stemerding and Verschoor [1] published results of measurements on heat transfer to water/air mixtures flowing concurrently through a vertical tube. Their immediate purpose was to obtain data for the simultaneous heating of a liquid and a permanent gas, to be used for the design of a heat exchanger for heating up a liquid/gas mixture to reaction temperature. They varied the liquid mass-velocity and the air-to-liquid ratio and found that over a wide range the coefficient of heat transfer increases with increasing values of these quantities.

After the publication of their results on the system water/air, the work in this laboratory was continued with measurements on gas-oil/air mixtures. It then appeared that in some cases the measurements of wall temperatures were not sufficiently accurate. An analysis of this difficulty resulted in the construction of a new measuring tube of considerably increased wall thickness and with improved mounting of the thermocouples.

In this article the considerations which led to the improved construction are presented as well as the results obtained, both with water/air and gas-oil/air mixtures. In a general way these confirm the trends observed by the previous authors.

2. Design of apparatus

The heat transfer coefficient from a heated tube wall to a liquid flowing inside is given by the well-known equation:

$$\phi_w = \alpha\,(t_w - t_b) \qquad (1)$$

ϕ_w = heat transferred per unit time and unit area,
α = heat transfer coefficient
t_w = wall temperature
t_b = bulk temperature of liquid.

Of the variables in this equation only t_w, the temperature of the wall where it is in contact with the fluid to be heated, is difficult to measure.

For a correct determination of the average wall temperature two conditions must be fulfilled. In the first place the insertion of the sensing element, in this case a thermocouple, in the wall must be such that the heat flow through the wall is not perceptibly disturbed. Otherwise the temperature at the measuring point can adjust itself to a value differing from that in undisturbed surroundings. In a thin-walled tube this condition cannot practically be fulfilled. Secondly, the temperature distribution along the wall should be as uniform as possible. However, when saturated steam is used as a heating medium, considerable local temperature differences occur on the heated side. For, owing to differences in wettability of the wall the condensate runs down in bands and the rest of the wall remains dry. Thus the dry and the wetted spots will develop temperature differences which are of the same order of magnitude as the temperature drop across the condensate film. Under certain conditions the latter was sometimes 20 °C in our experiments. In a thin-walled tube these differences are only partly levelled out by conduction and the result is an irregular temperature distribution on the side where the coefficient of heat transfer is measured. Consequently the average temperature on that side cannot be determined accurately.

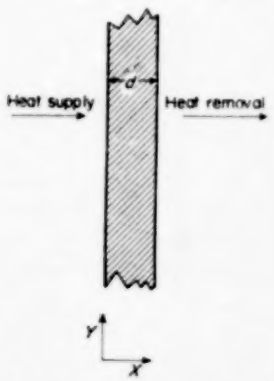

Fig. 1. Heat transport through a thick wall.

In order to obtain an impression of the wall-thickness required to smooth out these temperature differences sufficiently, a calculation was made for the following simplified model: (see Fig. 1).

An infinitely long wall of thickness d is heated on the side $x = 0$. On that side the temperature

shows a sinusoidal disturbance in the y-direction (parallel to the wall), so:

$$t(0, y) = t_0 + \Delta t \cos 2\pi \frac{y}{l} \qquad (2)$$

Δt is the amplitude of the disturbance, l the distance between two temperature maxima.

At $x = d$ the heat is transferred in accordance with equation (1), so that:

$$-\lambda \frac{\partial t}{\partial x}(d, y) = \alpha \left[t(d, y) - t_b\right] \qquad (3)$$

λ stands for the coefficient of heat conductivity of the wall material. For the stationary case we have:

$$\frac{\partial^2 t}{\partial x^2} + \frac{\partial^2 t}{\partial y^2} = 0. \qquad (4)$$

Substituting $x = d$ in the solution of this set of equations the following expression is found for the temperature distribution at the side of the wall where heat is removed ($x = d$):

$$t(d, y) = t_0 - \frac{(t_0 - t_b)\,\alpha\, d/\lambda}{\left[1 + (\alpha d/\lambda)\right]} + \\ + \frac{2\pi\, d/l}{\left[(\alpha\, d/\lambda) + (2\pi\, d/l)\sinh 2\pi\, d/l\right]} + \\ \Delta t \cos 2\pi\, y/l \qquad (5)$$

$$= t_0 - N + R\,\Delta t \cos 2\pi\, y/l$$

In this equation N represents the temperature drop across the wall in the absence of a disturbance and R denotes the fraction of the disturbance amplitude Δt remaining on the opposite side of the wall. In Fig. 2 R has been plotted against l/d (ratio of distance between two maxima to wall thickness) with $\lambda/\alpha d$ (ratio of resistance in liquid film to resistance in tube wall) as parameter.

It is seen from this Fig. that in order to reduce a disturbance of 20 °C at the heated side to a value of 2° C at the liquid side of the tube, a value of 2 for l/d is the maximum allowed. The distance l is difficult to estimate, but for a tube of 14 mm internal diameter, 10 mm seemed reasonable in view of visual observations in a similar, transparent tube and this leads to a wall thickness of 5 mm. The material of the wall is not important in this respect, since $\lambda/\alpha d$ has little influence on R. The choice fell on copper in order to keep down the temperature gradient in the radial direction. In connexion with the location of thermocouples the wall was made slightly thicker, namely 6 mm.

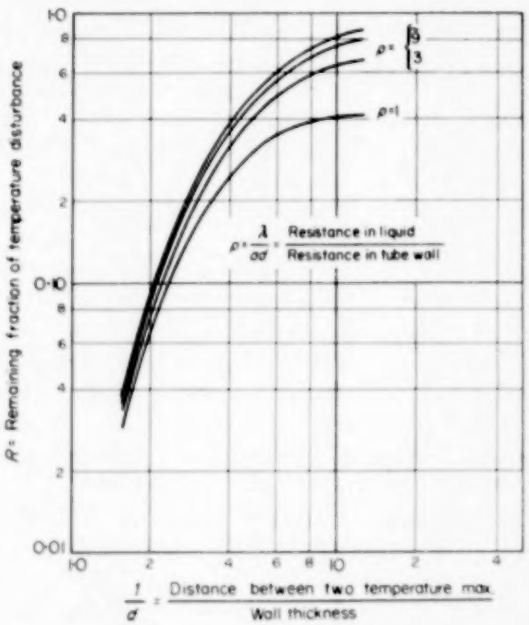

FIG. 2. Smoothing-out of temperature disturbances in wall of heat transfer tube.

A correct insertion of the thermocouples is greatly facilitated by this considerable wall thickness. Two constructions were used, which are shown in Figs. 3(a) and 3(b).

In case (a) a hole of 2 mm diameter was drilled in the wall, reaching to 1·5 mm from the inner wall. A 0·25 mm constantan wire was attached to a thin conical copper disk 2 mm in diameter. This was placed in the hole and subsequently pressed flat, thus ensuring a good contact with the bottom. The rest of the hole was then filled with close-fitting copper rings with a bore of 1 mm, leaving space to insulate the wire with a porcelain tube. In (b) a 1 mm hole was drilled in the wall and the porcelain-insulated constantan wire was introduced into it. Perpendicular to this hole a second one was drilled, into which a close-fitting copper cylinder was driven to fix the wire.

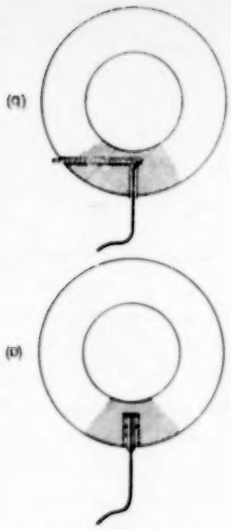

FIG. 3. Methods of attaching thermocouples in tube wall.

In both cases the constantan wire forms, together with the tube material, a copper–constantan thermocouple with a well-defined junction, which does not perceptibly interfere with the heat flow through the wall. Four couples of each type were installed along the tube wall, two of different types at the same height in each case. The couples were calibrated at two fixed temperatures.

During the experiments the readings of the couples at the same height differed by not more than 0·5 °C, while the temperature profile in the axial direction was very regular. It may, therefore, be assumed that with this combination of wall thickness and thermocouple design the average wall temperature is measured with an accuracy better than 1 °C.

The measuring tube itself had a length of 20 cm, internal diameter 1·4 cm and was placed in a double-walled steam jacket, as shown in Fig. 4. Steam was introduced at three places (A) in the outer jacket and reached the measuring section through an annular opening at the bottom of the inner jacket. The condensate formed on the measuring tube was removed through B and its quantity and temperature were measured. Condensate on the outer jacket was removed through C, whilst the amount of steam supplied was so adjusted that a small excess escaped at D.

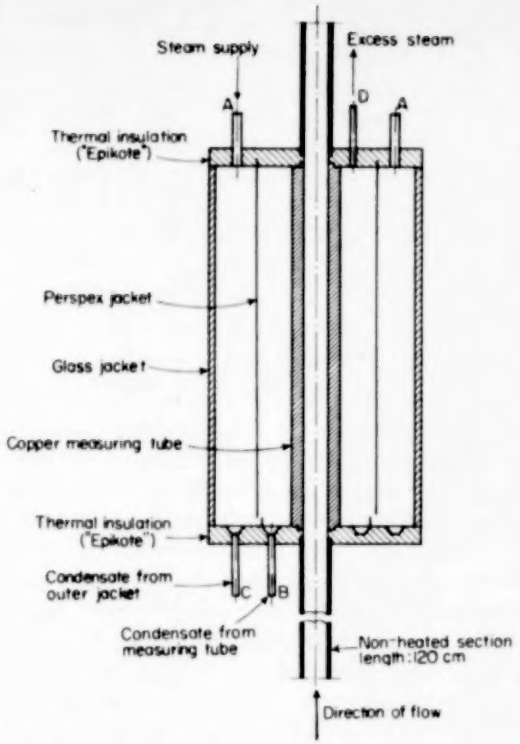

FIG. 4. Apparatus for measuring coefficients of heat transfer.

In order to avoid heat losses in the axial direction of the tube, which would be considerable at the wall-thickness applied, Epikote synthetic resin plates of 22 mm thickness provided with a hole exactly 14 mm in diameter were placed between the measuring tube and the inlet and outlet tubes. The non-heated section of the tube was 120 cm long.

The following quantities were measured: temperature of liquid entering and leaving the tube (after separation of gas), the temperature and volume of the condensate formed during a certain period and the wall temperature at 8 points. The difference in wall temperature between top and bottom of the measuring tube never exceeded 8 °C; as this difference is small with respect to $(t_w - t_b)$, the arithmetical mean of these 8 temperatures could be used in the calculations. By parallel connexion of the thermocouples, all of which had the same internal resistance, this mean

was read from a Brown self-balancing potentiometer. It was then corrected for the temperature gradient in the radial direction in the tube wall, calculated from the total heat flow, the surface area and the thermal conductivity of the material. This correction never exceeded 1·5 °C. The values of α were calculated with formula (1), in which t_b could be taken as the arithmetical mean of liquid inlet and outlet temperature.

3. Results of Measurements for Water and Gas-Oil Without Air

The apparatus was tested by carrying out measurements on water and gas-oil and comparing the results with relationships known from literature. In order to prevent the formation of air bubbles on the tube wall the liquids were deaerated, and recycled in a practically closed system. This included a cooler and was connected with the atmosphere through a narrow, liquid-filled tube. The deposition of scale on the heated section was prevented by the use of distilled water, while 0·2% wt of potassium bichromate was added to prevent corrosion in the iron part of the test installation.

The results of the measurements are given in Fig. 5, where

$$\log \frac{\mathbf{Nu}}{\mathbf{Pr}^{1/3}\,(\eta_b/\eta_w)^{0.14}}$$

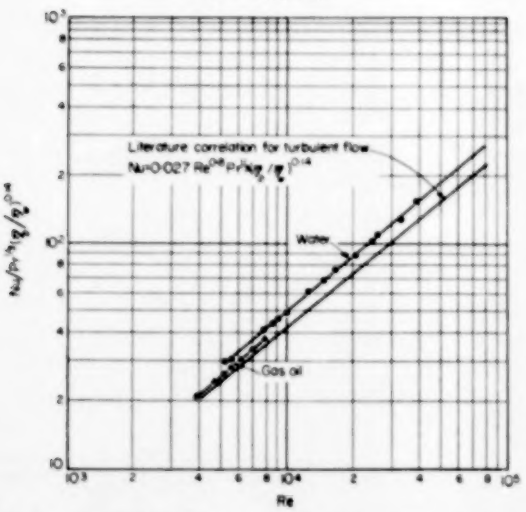

Fig. 5. Correlation of heat transfer data for water and gas-oil in single-phase flow.

has been plotted against log Re. Here η_b is the viscosity of the bulk of the liquid, η_w the viscosity at the wall temperature. For $\mathrm{Re} > 5000$, the experimental points for water lie on a straight line, representing the relation:

$$\mathbf{Nu} = 0{\cdot}030\ \mathbf{Re}^{0.81}\ \mathbf{Pr}^{1/3}\,(\eta_b/\eta_w)^{0.14}$$

For gas-oil the points (provided $\mathrm{Re} > 4000$) lie on a straight line having the same slope, but the coefficient in this case is 0·028. This difference has little significance, because there is a possible error of 10% in the values for the thermal conductivity and the specific heat of the gas oil. It is seen from Fig. 5 that the experimental values of the Nu numbers for water are about 20% higher than predicted by the equation of Sieder and Tate [2]:

$$\mathbf{Nu} = 0{\cdot}027\ \mathbf{Re}^{0.8}\ \mathbf{Pr}^{1/3}\,(\eta_b/\eta_w)^{0.14}$$

This can be partly explained by the relatively small length-to-diameter ratio of the test-section. Theoretical considerations by Deissler [3] which were experimentally confirmed by Hartnett [4] have shown that over approximately the first five diameters' length of a heat-transfer tube the thermal boundary layer is not yet fully developed and this results in high values for the heat transfer coefficients. For our experimental conditions an increase of 10% above the asymptotic value of the Nu numbers obtained in a long tube is in agreement with these considerations.

The repeatability of the measurements amounted to about 3%. The scatter of the experimental data is smaller than that of most literature data. From this fact and from the correlation observed it was concluded that the results obtained with this apparatus are reliable.

4. Measurements on Air/Water and Air/Gas-Oil Mixtures

(a) *Air/water*

Air and water were supplied separately through needle valves mounted at the bottom of the unheated section of the tube at angles of 45° to its axis. To eliminate the effect of pressure pulsations in the tube on pump capacity and flow measuring instruments, a gear pump was used for the water supply and a large pressure

VOL 11 1959/

drop was allowed across the valves. With these provisions the flows became very regular.

The mass velocity M of the water was varied from about 20 to about 80 g cm^{-2} sec^{-1}, the volumetric air/water-ratio (V_g/V_l) from one to beyond the value where the coefficient of heat transfer reaches a maximum. Because it was found that the wall temperature influenced the results—the value of α rising by an average of 5% for a temperature rise of 10 °C—all the coefficients of heat transfer have been recalculated for a wall temperature of 60 °C. The pressure drop over the water inlet valve was not kept constant in these experiments, but no differences were found between duplicate measurements. The repeatability was better than 10%. The results of the experiments have been plotted in Fig. 6.

It appears from Fig. 6 that for each value of M there is an unmistakable maximum in the value of α. As M increases, the value of V_g/V_l at which the maximum occurs decreases.

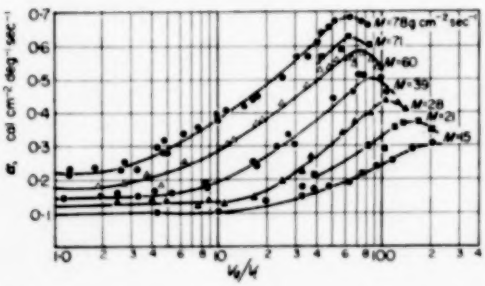

Fig. 6. Heat transfer measurements on water/air mixtures.

(*b*) *Air/gas-oil*

Fig. 7 gives the results of the measurements on this system for mass velocities of 22, 31 and 42 g cm^{-2} sec^{-1} (properties of the gas-oil:

$\rho = 0{\cdot}83$ g cm^{-3}
$\gamma = 23$ dyn cm^{-1} at 97 °C
$\eta = 2{\cdot}40$ *cP* at 15 °C
$0{\cdot}84$ *cP* at 97 °C).

The shape of the α versus V_g/V_l curves is almost equal to that for water/air. Again for each value of M a maximum value of α is found, though at considerable lower air/liquid ratios than with the system water/air.

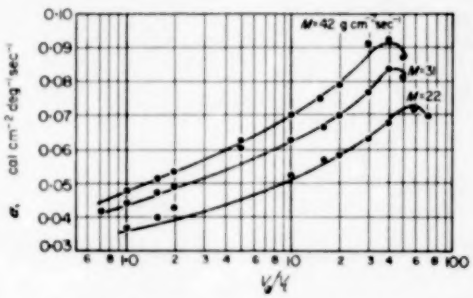

Fig. 7. Heat transfer measurements on gas-oil/air mixtures.

In this case it appeared that the value of α is influenced by the pressure drop over the gas-oil inlet valve, especially at low gas/liquid ratios. Raising the initial pressure from 1 to 2 atg. caused an increase in α values of 24% for the experiments with $V_g/V_l = 1$, of 10% when $V_g/V_l = 5$, while the effect was negligible for a gas/liquid ratio of 20. Photographs showed that the effect is due to the better and finer mixing of gas and liquid at the higher pressure. A $V_g/V_l = 20$ a very fine dispersion is already obtained, caused by the mixing action of the air and the effect is consequently small at this ratio. In view of this effect the initial pressure was kept constant at 1·6 atg in all gas-oil/air experiments. The wall temperature also was constant at ~ 95 °C, making temperature corrections unnecessary.

5. Correlation of Experimental Results

To obtain a better impression of the influence of air addition on the coefficient of heat transfer, the quotient α_2/α_1 was plotted against the air-to-liquid ratio V_g/V_l for the conditions below the maximum in the heat transfer coefficient (Fig. 8). Here α_2 is the coefficient of heat transfer for the two-phase systems, α_1 that for the liquids in single flow at the same values of the mass velocity M.

For α_1 the experimental values have been used. Only for the gas-oil measurements at Re > 3000, α_1 was calculated by means of the relation deduced

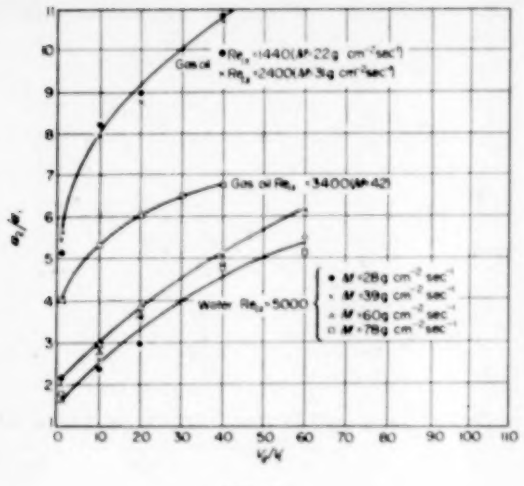

FIG. 8.

Ratio $\frac{\alpha_2}{\alpha_1} = \frac{\text{coefficient of heat transfer in 2-phase system}}{\text{coefficient of heat transfer in single liquid flow}}$ (at the same mass velocity) as a function of air/liquid ratio.

by SIEDER and TATE [2] for viscous substances in the range of laminar flow:

$$\mathrm{Nu} = 1{\cdot}86 \left[\mathrm{Re}\,\mathrm{Pr}\,\frac{d}{l}\right]^{1/3} \times \left(\frac{\eta_b}{\eta_w}\right)^{0{\cdot}14} \qquad (6)$$

where d = diameter and l = length of the tube.

It is evident from Fig. 8 that the first amount of air causes a rapid increase in the coefficient of heat transfer, but that for a further rise a very large quantity is required. Further it is clear that the influence of air is most pronounced at the lowest Re numbers. As the resistance against heat transfer is mainly due to the presence of a viscous sub-layer at the wall, this can be readily explained by the fact that the eddies, present in the wake of the rising air bubbles, penetrate into this viscous sub-layer and reduce its effective thickness. The thicker the original laminar layer, i.e. the lower the Re number, the more pronounced will be the effect which can be expected from this extra source of turbulence.

For each of the systems used, a satisfactory correlation could be obtained by inter-relating the Nusselt, Prandtl and Reynolds numbers for the two-phase systems. In this correlation the Nu and Pr numbers were based on the physical properties of the liquid, because the heat transfer will be determined by the properties of the liquid, at least as long as it covers the wall. For the Re number a volumetric mean Re_2 was used for the two-phase systems, defined by:

$$\mathrm{Re}_2 = h\,\frac{\rho_l\, v_l\, D}{\eta_l} + (1-h)\,\frac{\rho_g\, v_g\, D}{\eta_g} \qquad (7)$$

where h is the fractional hold-up of liquid, v_l and v_g the actual mean velocities of liquid and gas. As the actual velocity is equal to the superficial velocity (subscript: s) divided by the fractional hold-up, equation (7) can be written as:

$$\mathrm{Re}_2 = \frac{\rho_l\, v_{ls}\, D}{\eta_l} + \frac{\rho_g\, v_{gs}\, D}{\eta_g} = \mathrm{Re}_{ls} + \mathrm{Re}_{gs}. \qquad (8)$$

In consequence Re_2 is obtained by adding the liquid and gas Reynolds numbers, both based on superficial velocities. This definition of Re_2 fulfills the condition that for the extreme values of V_g/V_l (0 and ∞) the flow properties are determined by respectively liquid and gas alone.

In Fig. 9 the data for the two-phase systems (for $V_g/V_l > 1$) have been plotted in the same way as indicated in Fig. 5 for single-phase flow.

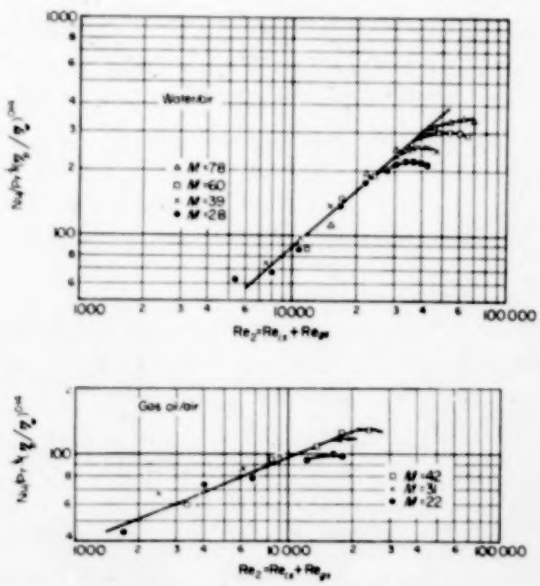

FIG. 9. Correlation of heat transfer data for the two-phase systems water/air and gas oil/air.

VOL 11 1959

Up to just below the maximum value of Nu all measurements for water/air satisfy to within 15% the correlation:

$$Nu = 0{\cdot}029\ Re_2^{0{\cdot}87}\ Pr^{1/3}\ (\eta_b/\eta_w)^{0{\cdot}14} \qquad (9)$$

and for gas-oil/air:

$$Nu = 2{\cdot}6\ Re_2^{0{\cdot}39}\ Pr^{1/3}\ (\eta_b/\eta_w)^{0{\cdot}14} \qquad (10)$$

For all values of the liquid mass velocity Re_{gs} covered a range from about zero to a multiple of Re_{ls}.

In the gas-oil/air measurements the Re number for the liquid alone (Re_{ls}) varied from 1400 to 3500, for water/air it was invariably above 5000. It is remarkable that for the two-phase measurements with gas-oil/air the exponent of Re_2 is close to the value of 0·33 for laminar single-phase flow (equation 6), whilst for water/air it is of the same order of magnitude as with turbulent flow of a liquid alone. This agreement of the exponent with that of single-phase flow, which is illustrated in Fig. 10, might indicate that the gas-oil in this case is still in a "laminar" condition.

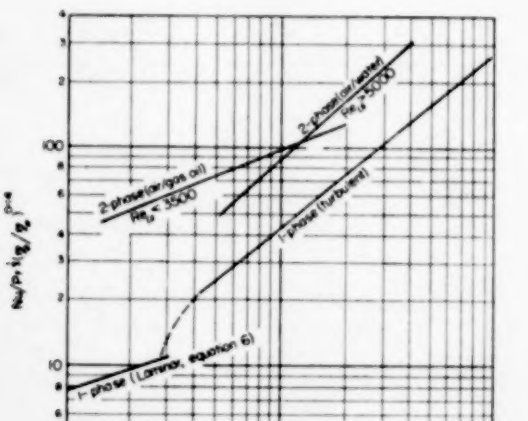

Fig. 10. Comparison between heat transfer data for single- and two-phase flow.

6. Maxima in the Coefficient of Heat Transfer

Description of the maximum in the coefficient of heat transfer is difficult without exact information about the flow pattern, which could not be observed in the present apparatus. An obvious explanation would be to connect this maximum with the transition of froth or slug flow into mist-annular flow. Now it was observed that beyond the above maximum the outlet temperature of the gas was higher than that of the liquid. This experimental fact suggests that the maximum in the heat transfer coefficient might coincide with the flow condition at which, owing to the highly turbulent motion of the gas-liquid mixture with increasing amount of gas, randomly disturbed "dry" spots appear at the walls. The heat transfer beyond the maximum will then no longer be controlled by the heat transfer from wall to turbulently flowing liquid alone, but also by the transfer from wall to gas at the dry spots.

On the basis of this hypothesis a criterion was derived for the flow conditions at which the liquid film on the wall is partly and temporarily disintegrated by the shearing stresses exerted by the flow†. This was assumed to happen if the Weber number exceeds a certain value; therefore:

$$\frac{\rho_g\, v_g^2\, \delta}{\gamma} = \text{constant at the maxima}$$

δ represents the thickness of the viscous film and follows from:

$$\frac{\rho_m\, u^*\, \delta}{\eta_l} = \text{constant} \qquad u^* = \text{the shearing velocity}$$

δ and u^* can be eliminated from these equations by means of the relations:

$$u^* = \sqrt{\frac{\tau_w}{\rho_m}} \qquad \tau_w = \text{shearing stress at the wall}$$

$$\tau_w = \tfrac{1}{2} f\, \rho_m\, v_m^2 \qquad f = \text{friction factor}$$

and

$$4f = C\,(\rho_m\, v_m\, D/\eta_l)^{-1/4} \quad \text{(Blasius equation)}$$

Index m indicates properties of the gas/liquid mixture

†The authors are indebted to Professor J. O. Hinze for ths helpful suggestions.

If our assumption is correct, the maxima can thus be characterized by the dimensionless criterion:

$$\frac{\rho_g v_g^2 \eta_l}{M_t \gamma}\left(\frac{M_t D}{\eta_l}\right)^{1/8} = \text{constant.}$$

M_t = total mass velocity of gas and liquid

The numerical values of this dimensionless quantity at the maxima are listed in the Table below.

The average wall temperature at the maxima was 60 °C for the water/air experiments, 97 °C for the gas-oil/air system.

The result is fairly satisfactory but it should be kept in mind that it is obtained from observations on two liquids only and that a number of properties, e.g. the density of the gas, were not varied. Moreover the influence of the heat flux on the stability of the wall-film was neglected. This result, therefore, should be considered with some reserve as long as no further experimental evidence is available to confirm the hypothesis underlying the criterion.

M (g cm^{-2} sec^{-1})	v_s *liquid* (cm/sec)	V_g/V_l *at the max.*	v_s *air* (cm/sec)	$\frac{\rho_g v_g^2 \eta_l}{M_t \gamma}\left(\frac{M_t D}{\eta_l}\right)^{1/8}$	
20	20	155	3100	$10{\cdot}1 \times 10^{-2}$	
30	30	108	3240	$8{\cdot}1 \times 10^{-2}$	
40	40	90	3600	$7{\cdot}9 \times 10^{-2}$	
50	50	78	3900	$7{\cdot}7 \times 10^{-2}$	water/air measurements
60	60	72	4320	$8{\cdot}1 \times 10^{-2}$	
70	70	65	4550	$7{\cdot}9 \times 10^{-2}$	
80	80	60	4800	$7{\cdot}8 \times 10^{-2}$	
22	27	55	1510	$10{\cdot}8 \times 10^{-2}$	
31	39	45	1750	$10{\cdot}6 \times 10^{-2}$	gas-oil/air measurements
42	52	40	2100	$11{\cdot}8 \times 10^{-2}$	

Notation

Nu = Nusselt number $\left(\frac{\alpha d}{\lambda}\right)$

Pr = Prandtl number $\left(\frac{c_p \eta}{\lambda}\right)$

Re = Reynolds number $\left(\frac{\rho v D}{\eta}\right)$

Re_{ls}, Re_{gs}, Re_2 = Reynolds numbers defined by equations (7) and (8)

c_p = specific heat — cal g^{-1} deg^{-1}

d = wall thickness — cm

D = tube diameter — cm

M = mass velocity — g cm^{-2} sec^{-1}

M_t = total mass velocity of gas and liquid — g cm^{-2} sec^{-1}

t = temperature — °C

v = linear velocity — cm sec^{-1}

v_s = superficial velocity — cm sec^{-1}

V_g/V_l = volumetric gas/liquid ratio

α = coefficient of heat transfer — cal cm^{-2} deg^{-1} sec^{-1}

γ = surface tension — dyn cm^{-1}

η = dynamic viscosity — g cm^{-1} sec^{-1}

λ = coefficient of heat conductivity — cal cm^{-1} deg^{-1} sec^{-1}

ρ = density — g cm^{-3}

Subscripts:

g and l are used for gas and liquid respectively

w and b are used for wall and bulk (temperature and viscosity) respectively.

References

[1] Stemerding S. and Verschoor H. *Proc. Gen. Disc. Heat Transfer, London*, 11-13 *September* 1951. Institution of Mechanical Engineers and the American Society of Mechanical Engineers.

[2] Sieder E. N. and Tate G. E. *Industr. Engng. Chem.* 1936 **28** 1429.

[3] Deissler R. G. *Trans. Amer. Soc. Mech. Engrs.* 1955 **77** 1221.

[4] Hartnett J. P. *Trans. Amer. Soc. Mech. Engrs.* 1955 **77** 1211.

Book Reviews

1958 Heat Transfer and Fluid Mechanics Institute. Preprints of Papers held at University of California, Berkeley, California, June 19, 20, 21, 1958. Stanford University Press, Standford and Oxford University Press, London. viii + 264 pp. £3 $8.50.

The Heat Transfer and Fluid Mechanics Institute is "a nonprofit-making organization whose primary purposes are to promote the preparation of, and provide facilities for, the presentation of scientific and technical work of a fundamental nature in thermodynamics, fluid mechanics and related fields of scientific endeavour." The Institute was formed in 1948 and has since met once yearly for a three-day Symposium at one of its sponsoring Californian Universities for the presentation of selected papers in the above fields. These papers are made available as bound collections of "Preprints," and judging by the steady increase in size of these volumes, the first decade of the Institute's existence has been eminently successful.

The volume under review is the eleventh in the series and, printed on a somewhat reduced format, has been offered at a slightly lower price than in the previous year. Twenty-one papers are included; they cover a wide range of topics and are broadly classified under the headings of Fluid Dynamics, Dynamics of Reactive Fluids, Heat Transfer, Magneto-hydrodynamics and Hypersonics, plus two survey articles on Theoretical Aerothermodynamics and Magnetohydrodynamics. It is not possible to review them in detail here but to make some general remarks instead.

Attention is directed to the statements in the preface that the preprints should not be considered a formal publication and that "the preprints are made available only as a *basis for discussion* and not as contributions in final form to the permanent literature." The Institute has, therefore, issued its warning, although it is difficult not to consider a book costing sixty shillings, and generally available, a formal publication. For those attending the Symposium the preprints obviously serve their purpose. To most others the volume will appear sometime later as a library copy and will be regarded as a work of reference containing papers dealing with the early development of a wide assortment of lines of research.

If it were possible to do so, the publication would benefit from the inclusion of a couple of introductory review articles giving a general picture of recent developments in heat transfer and fluid mechanics, in preference to the existing two surveys which are essentially statements of general principles in their respective fields. Preprints or otherwise, it is reasonable to expect all mathematical equations either to be typewritten or to be handwritten more neatly than appear for example on pp. 2 and 109. A glance at pp. 46 and 32 in the 1956 and 1957 issues respectively will indicate an acceptable standard of handwriting.

J. O. Wilkes

Books Received

Annual Reports of the Progress of Chemistry Vol. 55 1958. The Chemical Society, London 1959.

T. A. Geissman: Principles of Organic Chemistry. Freeman, London and San Francisco 1959.

SELECTION OF CURRENT PAPERS OF INTEREST TO CHEMICAL ENGINEERS

S. Goldstein and J. D. Murray: On the mathematics of exchange processes in fixed columns (ion exchange, heat exchange – fixed beds, adsorption). III. The solution for general entry conditions, and a method of obtaining asymtotic expressions. *Proc. Roy. Soc.* 1959 A **252** 334–347. IV. Limiting values and correction terms for the kinetic-theory solution with general entry conditions. *Ibid.* 348–359. V. The equilibrium theory and peturbation solutions, and their connexion with kinetic-theory solutions, for general entry conditions. *Ibid.* 360–375. (See also S. Goldstein: *Proc. Roy. Soc.* 1953 A **219** 151, 171).

G. M. Sreekantath, N. Rajaram and C. K. Ponnappan: Simple method for finding the ratio of surface tension to viscosity of a liquid. *J. Sci. Instrum.* 1959 **36** 378–380.

A. D. Maude: Theoretical evaluation of capillary viscometers for the measurement of the viscosity of suspensions of spheres. *Brit. J. Appl. Phys.* 1959 **10** 371–376.

F. H. Garner and P. Mina: Surface ageing at liquid–liquid interfaces. Part I. Calibration of contracting jet method (for measuring interfacial tension during short time intervals). Part II. Effect of chain length and structure of organic compounds in water (on variation of interfacial tension with time). Appendix (with V. G. Jenson). Velocity distribution inside liquid–liquid jets. *Trans. Faraday Soc.* 1959 **55** 1607–1630.

F. H. Garner and P. J. Haycock: Circulation in liquid drops. *Proc. Roy. Soc.* 1959 A**252** 457–475.

R. Aris: On the dispersion of a solute by diffusion, convection and exchange between phases (transfer between two coaxial annular phases). *Proc. Roy. Soc.* 1959 A**252** 538–550.

P. G. Saffman: A theory of dispersion in a porous medium (dispersion of a dynamically neutral material in a fluid flowing through an assemblage of randomly oriented straight pores). *J. Fluid Mech.* 1959 **6** 321–349.

N. O. Young, J. S. Goldstein and M. J. Block: The motion of bubbles in a vertical temperature gradient (affected by the thermal variation of surface tension). *J. Fluid Mech.* 1959 **6** 350–356.

D. C. Collis and M. J. Williams: Two-dimensional convection from heated wires at low Reynolds' numbers. *J. Fluid Mech.* 1959 **6** 357–384.

T. H. Ellison and J. S. Turner: Turbulent entrainment in stratified flows. *J. Fluid Mech.* 1959 **6** 423–448.

H. R. Bailey: Heat conduction from a cylindrical source with increasing radius. *Quart. Appl. Math.* 1959 **17** 255–262.

S. C. R. Dennis, A. McD. Mercer and G. Poots: Forced heat convection in laminar flow through rectangular ducts. *Quart. Appl. Math.* 1959 **17** 285–297.

J. Yarwood: Summarized proceedings of a symposium on current developments in the production of high vacua – London, April 1959. *Brit. J. Appl. Phys.* 1959 **10** 383–391.

B. C. Lindley: Pressure loss data for crimped metal strip lattices. *J. Roy. Aer. Soc.* 1959 **63** 597–602.

S. K. Friedlander and M. Litt: Rapid chemical reaction in a laminar boundary layer. *Appl. Sci. Res.* 1959 A**8** 403–412.

J. Ponstein: Instability of rotating cylindrical jets. *Appl. Sci. Res.* 1959 A**8** 425–456.

F. Kreith and D. Margolis: Heat transfer and friction in turbulent vortex flow (swirling flow in a pipe). *Appl. Sci. Res.* 1959 A**8** 457–473.

C. C. Harris: Sedimentation rates, fluidization and flow through porous media. *Nature, Lond.* 1959 **184** 716.

C. Ramshaw and J. D. Thornton: Droplet circulation and interfacial disturbances in gas–liquid systems. *Nature, Lond.* 1959 **184** 719.

SELECTION OF CURRENT SOVIET PAPERS OF INTEREST TO CHEMICAL ENGINEERS*

G. S. Sedelnikov: Industrial production of natural sodium carbonate. *Zh. prikl. Khim.* 1959 **32** 1658–1664.

B. A. Chertkov: Kinetics of auto-decomposition of ammonium sulphite–bisulphite solutions. *Zh. prikl. Khim.* 1959 **32** 1695–1707.

B. A. Chertkov: Auto-decomposition of ammonium sulphite–bisulphite solutions under industrial conditions. *Zh. prikl. Khim.* 1959 **32** 1707–1711.

M. L. Varlamov and Ya. I. Staroselski: Absorption of nitrogen oxides by sodium carbonate solutions in a gas-lift apparatus. *Zh. prikl. Khim.* 1959 **32** 1716–1723.

G. L. Antipenko and E. S. Beletskaya: Temperature dependence of viscosity of nitric acid. *Zh. prikl. Khim.* 1959 **32** 1723–1729.

I. B. Rapaport and I. Par: Preparation of nickel catalyst by decomposition of organic salts. *Zh. prikl. Khim.* 1959 **32** 1744–1750.

I. N. Bushmakin and N. P. Kuznetsov: Vapour–liquid equilibrium of the system methyl*cyclo*hexane – *n*-pentane. *Zh. prikl. Khim.* 1959 **32** 1751–1755.

A. A. Komarovski and V. V. Streltsov: On the hydraulic resistance of a bed of granular material. *Zh. prikl. Khim.* 1959 **32** 1755–1763.

A. G. Evstafev, D. D. Zykov and N. M. Karabaev: Comparison of equations of material balance for a column of plate-type. *Zh. prikl. Khim.* 1959 **32** 1771–1774. Comparison of material-balance equations across a differential section of a plate proposed by various authors.

O. S. Vladirchuk, P. M. Kochergin, K. E. Novikova, L. L. Bespalova, R. M. Titkova, A. M. Tsyganova, G. D. Krasnozhen and A. M. Grigorovski: Fractional distillation of mixtures of nitroethylbenzenes. *Zh. prikl. Khim.* 1959 **32** 1830–1834.

M. K. Shchennikova and I. A. Korshunov: Determination of carbon dioxide content in solutions of monoethanolamine and in acidic solutions of sulphates of sodium and of monoethanolamine. *Zh. prikl. Khim.* 1959 **32** 1870–1872.

A. I. Fedoseev: Retardation of gas-bubble motion by surface active substances at moderate Reynolds numbers. *Zh. fiz. Khim.* 1959 **33** 1681–1686.

V. B. Sandomirski and Sh. M. Kogan: Calculation of the adsorption isotherm in the electronic theory of chemisorption. *Zh. fiz. Khim.* 1959 **33** 1709–1714.

V. G. Manzheli and B. I. Verkin: Investigation into the phenomenon of diffusion in liquified gases. *Zh. fiz. Khim.* 1959 **33** 1758–1761.

N. E. Khazanova and L. P. Linshits: Critical phenomena in the system hexamethyleneimine – water—II. Some physico-chemical properties of the system hexamethyleneimine – water. *Zh. fiz. Khim.* 1959 **33** 1811–1812.

B. N. Vetrov, I. I. Petrenko and O. M. Todes: Non-steady flow of gas and transmission of pressure through a porous medium. *Zh. tekh. Fiz.* **29** 1021–1031.

P. E. Suetin, G. T. Shchegovev and R. A. Klestov: Measurement of mutual diffusion coefficients of gases by optical means. *Zh. tekh. Fiz.* 1959 **29** 1058–1064.

S. S. Kutateladze and V. N. Moskvicheva: On the relation between the hydrodynamics of a two-component layer and the theory of crisis in the mechanism of boiling. *Zh. fiz. Khim.* 1959 **29** 1135–1139.

*To assist readers, translations of any article appearing in the above list can be obtained at a reasonable charge. All orders should be addressed to the Administrative Secretary of the Pergamon Institute at either Headington Hill Hall, Oxford or 1403 New York Avenue N.W., Washington 5, D.C. whichever is more convenient.

P. N. KUBANSKI: On the coagulation of aerosols by free streams of gas. *Zh. fiz. Khim.* 1959 **29** 1140–1141.

V. V. RACHINSKAYA: On the problem of hydrodynamic properties of ion-exchange resins. *Zh. fiz. Khim.* 1959 **29** 1159–1161.

L. M. GINDIN, P. I. BOBIKOV and A. M. ROSEN: Some physico-chemical features of exchange extraction. *Dokl. Akad. Nauk SSSR* 1959 **128** 295–298.

V. A. KIRILIN and S. A. OULIBIN: Experimental determination of specific volume of steam at high temperatures and pressures. *Teploenergetika* 1959 **6** (8) 71–73.

V. A. LOKSHIN and A. L. SHVARTS: Calculation of driving heads and hydraulic resistances in vertical risers during flow of steam–water mixtures. *Teploenergetika* 1959 **6** (8) 73–77.

V. A. KIRILIN and S. A. OULIBIN: Precision analysis and combined table of experimental values of specific volumes of water and steam obtained in the Moscow Power Institute. *Teploenergetika* 1959 **6** (9) 3–7.

A. M. SYROTA and B. K. MALTSEV: Experimental investigation into heat capacity of water at temperatures from 10 to 500 °C and pressures up to 500 kg/cm². *Teploenergetika* 1959 **6** (9) 7–13.

N. B. VARGAITIK and A. A. TARZHIMANOV: Experimental investigation into heat conduction of steam at high parameters. *Teploenergetika* 1959 **6** (9) 15–21.

A. S. SHIFRIN: Viscosity of steam under atmospheric pressure. *Teploenergetika* 1959 **6** (9) 22–27.

VOL
11
1959/